



UNIVERSITY OF IOANNINA

FACULTY OF NATURAL SCIENCES

DEPARTMENT OF CHEMISTRY

*Polypropylene hollow fiber – supported NH<sub>2</sub>-MIL-88B MOF, as a novel microextraction mode for selected nitrophenols, parabens and benzophenones and their subsequent determination by HPLC*

**MASTER'S DEGREE THESIS**

TZIMAS ALKIVIADIS

CHEMIST

IOANNINA, 2023

© 2023 Tzimas Alkiviadis

The approval of the thesis by the Department of Chemistry of the Faculty of Sciences of the University of Ioannina does not imply acceptance of the author's views (Law 5343/32 article.202 par.2).

# Master's degree Diploma thesis

Tzimas Alkiviadis

Student Registration Number.: 01409

## **SUPERVISING PROFESSOR:**

Stalikas Konstantinos, Professor of the Department of Chemistry, University of Ioannina

## **THREE-MEMBER COMMITTEE OF INQUIRY:**

Stalikas Konstantinos, Professor of the Department of Chemistry, University of Ioannina

Mamantos Prodromidis, Professor of the Department of Chemistry, University of Ioannina

Sakkas Vasileios, Associate Professor of the Department of Chemistry, University of Ioannina





Dedicated to my family and loved ones for their support.

## ACKNOWLEDGEMENTS

The present postgraduate research project was carried out at the Laboratory of Analytical Chemistry of the Department of Chemistry of the University of Ioannina in the framework of the postgraduate program of the Department of Chemistry, with the direction "Analytical Chemistry, Chemistry and Technology of Environment and Food", under the supervision of Professor Konstantinos Stalikas during the period 2021-2023.

I would like to start by thanking some of the people who played a catalytic role in the realization of this effort through their valuable collaboration and contributions. I would especially like to thank my supervisor, Konstantinos Stalikas. For the trust he showed me by accepting me to join his research team in the development of my thesis topic and for his continuous help. His insightful observations provided the impetus for the development of my thesis. Next, I would like to thank Dr. Theodoros Chatzimitakos for providing me with continuous practical help, training and information whenever I requested it.

I would also like to thank all the faculty members of the Department of Analytical Chemistry of the University of Ioannina and especially Professor Mamantos Prodromidis for the harmonious coexistence in the laboratory environment. Also, to Professor Sakkas Vasileios, Dr. Florou Angeliki and Dr. Christina Piperidi for our excellent cooperation during my assistantship.

I would also like to thank all the other members of the lab for their positive energy, smooth interactions and the help when it was needed. Finally, I would like to thank my family and my loved ones, without the support of whom I would not be able to achieve what I have.

## Contents

Chapter 1 Introduction.....	17
1.1 Benzophenones, nitrophenols and parabens.....	17
1.2 Methods of detection.....	22
1.2.1 Non-chromatographic methods.....	22
1.2.2 Chromatographic methods and sample pretreatment .....	24
1.2.3 Microextraction.....	25
1.2.4 On-fiber solid phase microextraction.....	27
1.3 Metal-Organic Frameworks .....	29
1.3.1 Introduction to metal-organic frameworks .....	29
1.3.2 MOF in analytical chemistry .....	32
1.3.3 Factors governing MOF stability .....	38
1.3.4 MOF Stability in water .....	43
1.3.5 MOF iso-reticular design .....	46
1.3.6 Post synthetic modification .....	48
1.3.7 MOFs in extraction of analytes and mechanisms of interaction .....	49
1.3.8 MOFs in Microextraction .....	50
1.3.9 Materials institute Lavoisier (MIL).....	52
1.4 Aim of the work.....	55
Chapter 2 Experimental.....	55
2.1 Chemicals and reagents .....	55
2.2 Instrumentation .....	56
2.3 NH <sub>2</sub> -MIL-88B synthesis .....	58
2.4 Characterization of the material.....	58
2.5 Loading of NH <sub>2</sub> -MIL88B on fibers .....	59
2.6 Extraction procedure.....	60
2.7 Elution process.....	60
2.8 Chromatographic analysis .....	61
2.9 Real samples.....	61
2.10 Multivariate experiments.....	61
Chapter 3 Results and discussion .....	63

3.1	Preliminary experiments .....	63
3.1.1	Loading of NH <sub>2</sub> MIL-88B on the fibers.....	63
3.2	Characterization of the material .....	63
3.2.1	Infrared spectroscopy (IR) .....	64
3.2.2	X-ray diffraction spectroscopy (XRD) .....	65
3.2.3	Scanning electron microscope (SEM) .....	66
3.2.4	Energy-dispersive X-ray spectrum.....	71
3.2.5	Dynamic light scattering (DLS).....	73
3.3	Chromatographic conditions .....	74
3.4	Optimization of extraction .....	76
3.3.1	Effect of Salinity / Ionic strength.....	76
3.3.2	Effect of Humic Acids.....	77
3.3.3	Effect of pH .....	77
3.3.4	Effect of temperature .....	79
3.3.5	Effect of the eluting solvent .....	80
3.3.6	Multivariate experiment .....	80
3.5	Calibration curves.....	96
3.6	Real sample analysis .....	102
3.7	Other figures of merit.....	105
3.8	Conclusions .....	106

REFERENCES 106



## Directory of images

<b>Figure 1</b> : Common ligands and their anionic forms.....	31
<b>Figure 2</b> : MOF water stability.....	46
<b>Figure 3</b> : 3D depiction of the NH <sub>2</sub> -MIL-88B structure. The elements are depicted as colored bars and balls: carbon (grey), nitrogen(blue), oxygen(red), iron(orange), hydrogen(green). .....	54
<b>Figure 4</b> : NH <sub>2</sub> -MIL88B synthesis as proposed by (Li et al. 2021). ....	58
<b>Figure 5</b> : The PPHF modification procedure.....	59
<b>Figure 6</b> : Extraction procedure using 70 mL sample (left) and 25 mL sample (right).....	60
<b>Figure 7</b> : Infrared spectrum of NH <sub>2</sub> -MIL-88B.....	64
<b>Figure 8</b> : XRD Spectra of NH <sub>2</sub> -MIL-88B.....	65
<b>Figure 9</b> : SEM image of NH <sub>2</sub> -MIL-88B.....	66
<b>Figure 10</b> : SEM image of NH <sub>2</sub> -MIL-88B.....	67
<b>Figure 11</b> : SEM image of the unmodified PPHF.....	67
<b>Figure 12</b> : SEM image of the unmodified PPHF.....	68
<b>Figure 13</b> : SEM image of the unmodified PPHF.....	68
<b>Figure 14</b> : SEM image of the NH <sub>2</sub> -MIL-88B-modified PPHF.....	69
<b>Figure 15</b> : SEM image of the NH <sub>2</sub> -MIL-88B-modified PPHF.....	69
<b>Figure 16</b> : SEM image of the adsorbedNH <sub>2</sub> -MIL-88B of the surface of the PPHF.....	70
<b>Figure 17</b> : SEM image of the adsorbed NH <sub>2</sub> -MIL-88B of the surface of the PPHF.....	70
<b>Figure 18</b> : Combined elemental map of the NH <sub>2</sub> -MIL-88B depicting the distribution of carbon (blue), Nitrogen (yellow), oxygen (green), iron (red), 5µm.....	71
<b>Figure 19</b> : EDX results for NH <sub>2</sub> -MIL-88B (150 233 counts in 0:02:09 (1 164 c/s)).....	72
<b>Figure 20</b> : The coordination of the NH <sub>2</sub> -H <sub>2</sub> BDC ligands with the iron cluster, to form the NH <sub>2</sub> -MIL-88B structure. 3D representation (left), 2D structure (right). The colored balls in the left figure represent carbon(grey), nitrogen (blue), iron (orange), oxygen (red), and hydrogen (green).....	73
<b>Figure 21</b> : Zeta potential of NH <sub>2</sub> -MIL-88B.....	74
<b>Figure 22</b> : Average particle size of the NH <sub>2</sub> -MIL-88B crystals.....	74
<b>Figure 23</b> : A typical chromatogram depicting the response in 254 nm (black) and 285 nm (pink). Ethyl-paraben ( <b>Eth-PB</b> ), butyl-paraben ( <b>Bu-PB</b> ), propyl-paraben ( <b>Pr-PB</b> ), 2-nitrophenol ( <b>2NP</b> ), 3-methyl-4-nitrophenol ( <b>3Me-4NP</b> ), benzophenone-2 ( <b>BP2</b> ), benzophenone-3 ( <b>BP3</b> ), 4-hydroxybenzophenone ( <b>4OH-BP</b> ), benzophenone-6 ( <b>BP6</b> ) and benzophenone-8 ( <b>BP8</b> ).....	75
<b>Figure 24</b> : Effect of the salinity in the extraction process, the concentration of all the analytes was 0.25 µg/mL.....	76
<b>Figure 25</b> : Effect of the initial pH on the extraction of analytes, the concentration of all the analytes was 0.25 µg/mL.....	78
<b>Figure 26</b> : Comparison of the IR spectra of NH <sub>2</sub> -MIL-88B in acidic and alkaline solution. The yellow line represents the untreated material, while the pink, blue and green lines represent measurements for the alkali-treated material, in gradually more alkaline environments.....	78
<b>Figure 27</b> : The effect of temperature in the extraction of analytes, the concentration of all the analytes was 0.25 µg/mL.....	79

<b>Figure 28:</b> <i>Effect of the interdependent four variables on the extraction efficiency of nitrophenols.....</i>	<b>84</b>
<b>Figure 29:</b> <i>Effect of the interdependent four variables on the extraction efficiency of parabens.....</i>	<b>86</b>
<b>Figure 30:</b> <i>Effect of the interdependent four variables on the extraction efficiency of benzophenones.....</i>	<b>88</b>
<b>Figure 31:</b> <i>Plot of stirring time- volume.....</i>	<b>90</b>
<b>Figure 32:</b> <i>Plot of stirring rate- volume.....</i>	<b>91</b>
<b>Figure 33:</b> <i>Plot of the number of fibers – volume .....</i>	<b>92</b>
<b>Figure 34:</b> <i>Plot of stirring rate- stirring time.....</i>	<b>93</b>
<b>Figure 35:</b> <i>Plot of number of fibers- stirring time.....</i>	<b>94</b>
<b>Figure 36:</b> <i>Plot of number of fibers- stirring rate.....</i>	<b>95</b>
<b>Figure 37:</b> <i>Calibration curve for 2NP. The chromatographic areas were received at 285 nm.....</i>	<b>97</b>
<b>Figure 38:</b> <i>Calibration curve for 3Me-4NP. The chromatographic areas were received at 315 nm.....</i>	<b>97</b>
<b>Figure 39:</b> <i>Calibration curve for BP2. The chromatographic areas were received at 285 nm.....</i>	<b>98</b>
<b>Figure 40:</b> <i>Calibration curve for Eth-PB. The chromatographic areas were received at 254 nm.....</i>	<b>98</b>
<b>Figure 41:</b> <i>Calibration curve for 4OH-BP. The chromatographic areas were received at 285 nm.....</i>	<b>99</b>
<b>Figure 42:</b> <i>Calibration curve for Pr-PB. The chromatographic areas were received at 254 nm.....</i>	<b>99</b>
<b>Figure 43:</b> <i>Calibration curve for BP8. The chromatographic areas were received at 285 nm.....</i>	<b>100</b>
<b>Figure 44:</b> <i>Calibration curve for Bu-PB. The chromatographic areas were received at 254 nm.....</i>	<b>100</b>
<b>Figure 45:</b> <i>Calibration curve for BP6. The chromatographic areas were received at 285 nm.....</i>	<b>101</b>
<b>Figure 46:</b> <i>Calibration curve for BP. The chromatographic areas were received at 285 nm.....</i>	<b>101</b>
<b>Figure 47:</b> <i>Chromatograms of treated lakewater (blue), seawater (grey), and wastewater (brown) at 285 nm superimposed on each other and compared with a blank (pink) and a spiked sample (purple) for reference. ....</i>	<b>102</b>
<b>Figure 48:</b> <i>Chromatograms of treated lake-water (mustard), seawater (green), and wastewater (blue) at 254 nm superimposed on each other, and compared with a blank (black) and a spiked sample (teal) for reference. ....</i>	<b>103</b>

## Directory of tables

<b>Table 1:</b> Benzophenones (The $pK_a$ and $\text{Log}P_{ow}$ values were taken from PubChem except when differently noted).....	20
<b>Table 2:</b> Parabens (The $pK_a$ and $\text{Log}P_{ow}$ values were taken from PubChem except when differently noted).....	21
<b>Table 3:</b> Nitrophenols: (The $pK_a$ and $\text{Log}P_{ow}$ values were taken from PubChem except when differently noted).....	22
<b>Table 4:</b> Some examples of stable MOFs, their metal node and ligand, and softness-hardness.....	43
<b>Table 5:</b> Common MIL MOFs, as reviewed by (Zhang et al. 2022a).....	53
<b>Table 6:</b> Information about the elemental mapping, and the corresponding color of each element.....	72
<b>Table 7:</b> Retention times of the chosen compounds under the applied chromatographic conditions.....	75
<b>Table 8:</b> Multivariate experiments, their conditions and responses. The separate responses were the chromatographic peak areas, and the total response was received from the separate responses after normalization.....	82
<b>Table 9:</b> ANOVA for response surface for the Quadratic model Analysis of variance (partial sum of squares – type III) – <b>Nitrophenols</b> .....	83
<b>Table 10:</b> ANOVA for response surface for the Quadratic model Analysis of variance (partial sum of squares – type III) - <b>Parabens</b> .....	85
<b>Table 11:</b> ANOVA for response surface for the Quadratic model Analysis of variance (partial sum of squares – type III) - <b>Benzophenones</b> .....	87
<b>Table 12:</b> ANOVA for response surface for the Quadratic model Analysis of variance (partial sum of squares – type III) – <b>Total response</b> .....	89
<b>Table 13:</b> Spiking-recovery tests on the lake-water, seawater, and treated wastewater matrices at two different spiking levels.....	104
<b>Table 14:</b> The enrichment factors, calculated as the ratios of the concentrations of the analytes in the condensed extract (160 $\mu$ L) to the concentration of the initial sample.....	104
<b>Table 15:</b> Limits of detection and limits of quantification in $\mu\text{g}/\text{mL}$ .....	105
<b>Table 16:</b> Repeatability and reproducibility.....	105

### *Abbreviations*

<b>2NP</b>	2-nitrophenol
<b>3Me-4NP</b>	3-methyl-4-nitrophenol
<b>BP2</b>	Benzophenone-2
<b>4OH-BP</b>	4-hydroxy- benzophenone
<b>BP8</b>	Benzophenone-8
<b>BP6</b>	Benzophenone-6
<b>BP3</b>	Benzophenone-3
<b>Me-PB</b>	Methylparaben
<b>Eth-PB</b>	Ethylparaben
<b>Pr-PB</b>	Propylparaben
<b>BuPB</b>	Butylparaben
<b>MIL-88B</b>	Material of the institute Lavoisier 88B
<b>NH<sub>2</sub>-MIL-88B</b>	NH <sub>2</sub> modified MIL-88B
<b>MOF</b>	Metal-organic framework
<b>HPLC</b>	High-performance liquid chromatography
<b>MS</b>	Mass spectroscopy
<b>UV</b>	Ultra-violet
<b>BPs</b>	Benzophenones
<b>NPs</b>	Nitrophenols
<b>PBs</b>	Parabens
<b>PPHF</b>	Polypropylene hollow fibers
<b>SERS</b>	Surface-enhanced Raman spectroscopy
<b>H<sub>2</sub>BDC</b>	Terephthalic acid
<b>MIL</b>	Material of Institute Lavoisier
<b>PCN</b>	coordination network frameworks
<b>ZIF</b>	Zeolitic Imidazolate Framework
<b>UiO</b>	University of Oslo
<b>IRMOF</b>	Iso-reticular metal-organic framework
<b>PDA</b>	Photodiode array





# Chapter 1 Introduction

## 1.1 Benzophenones, nitrophenols and parabens

The lifestyle of modern societies is now more than ever put into question, as the adverse effects of many compounds are brought into the light of day. Most notably, emerging pollutants and their transformation products, pose human and ecological threat but are lacking any regulation (Sanganyado and Kajau 2022)(Tang et al. 2019). The European aquatic environment's list of emerging pollutants and their transformation products and metabolites contains more than 700 substances ([www.norman-network.net](http://www.norman-network.net)). Benzophenones(**BPs**), Nitrophenols (**NPs**) and parabens (**PBs**) are characterized as emerging pollutants . Personal care products food additives, plasticizers disinfectants and pesticides, are some of the main sources of emerging pollutants such as BPs, NPs and PBs and greatly contribute to their release into the environment over the years. While improving the standard of living, persistent and improvident use is harming the wellbeing of humans and posing environmental risks. **BPs** are generally non-volatile, photostable in aquatic environments, moderately to highly water soluble and their bioconcentration factor apparently increases in BPs with more methoxy groups, as indicated by 2,2',4,4'-tetrahydroxybenzophenone (**BP2**) having a  $\text{Log}P_{ow}$  of 2.78 and 2,2'-dihydroxy-4,4'-dimethoxybenzophenone (**BP6**) having a  $\text{Log}P_{ow}$  of 3.9 (Mao et al. 2019). They are present in sunscreens, skin lotions, hair products and face creams, and are utilized as ultraviolet(UV)-filters, protecting from the harmful UV irradiation (Han et al. 2016). They are ketones of two phenyl groups and are used as UV-filters and UV-stabilizers in food packaging (Huang et al. 2021)(Ricardo et al. 2022) and as additives in paints, textiles etc. (Wejnerowska and Narloch 2021). BPs are released into the environment by the heavy use of aforementioned products and inadequate treatment of wastewater. BPs are present in swimming pool water and urine samples (Sun et al. 2018b), and are found in many aquatic matrices (Fent et al. 2010; Ma et al. 2016) as well as in fish(Balmer et al. 2005). 2 -droxy-4-methoxybenzophenone or Oxybenzone or benzophenone-3 (BP3) was found to cause Hirschsprung's disease in the off-springs of affected mothers (Huo et al. 2016). Furthermore, several studies have pointed towards the estrogenic and anti-androgenic activity of several BPs (Díaz-Cruz and Barceló 2009). The first BP classified as a material with estrogenic activity disruptor was BP3), stimulating proliferation of breast cancer (cell line MCF-7) by the administration of a median effective concentration value of 3.73  $\mu\text{M}$  (Schlumpf et al. 2001). Furthermore,BP2 tests on ovariectomized rats unveiled estrogenic effects on their bones, liver, uterus and vagina (Schlecht et al. 2004; Seidlová-Wuttke et al. 2004). They are reportedly found in various waters,

sediments, sludge from sewage and in the muscle tissue of birds and fish among others (Balmer et al. 2005). Information about benzophenones is compiled in **Table 1**.

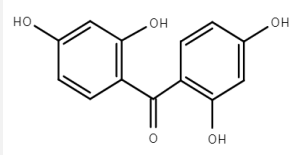
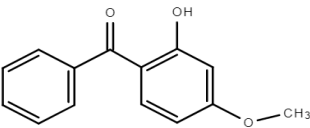
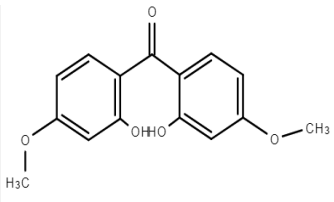
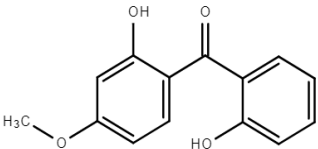
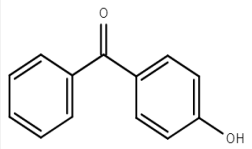
A class of preservatives called parabens (**PBs**), are widely used because of their stability and relative safety. They are p-hydroxybenzoic acid esters that are cheap, inert and exhibit low toxicity. They are commonly used in foodstuff, pharmaceuticals and personal care products as antimicrobial preservatives, extending the shelf life of the products (Han et al. 2016). They are used widely, as they do not affect the organoleptic characteristics, being odorless and tasteless, while also being stable in a wide range of pH and temperature (Vale et al. 2022). the length of alkyl chain improves their antimicrobial activity but decreases their water solubility, so shorter chain parabens (methyl- up to -butyl) are used in cosmetics (Luo et al. 2012). Recently, a link has been drawn between parabens and breast cancer (Darbre et al. 2004). Methylparaben (**Me-PB**) and propylparaben (**Pr-PB**) are mainly detected in treatment plant effluents and are most abundant in sludge. This can be explained by their moderate hydrophobicity and their ability to bind to the solid fraction of the effluents ( i.e. suspended particulate matter or sewage sludge), while they suffer from swift degradation when they are found in wastewater (Haman et al. 2015). Reduction of parabens can happen in a few minutes in the presence of residual chlorine, while biodegradation is another common degradation route in wastewater, and may lead to the underestimation of the paraben concentration. This means that time consuming sampling methods might underestimate the total paraben content. The main degradation product of parabens is p-hydroxybenzoic acid (Haman et al. 2015). Parabens persist in the environment, and the effluents exiting the wastewater treatment plants are only in part treated (Haman et al. 2015). Wastewater treatment plant effluents and leaching contribute to the high concentrations of parabens in the environment. Furthermore, recreational activities like swimming, as well as the indirect leaching from laundry waters and showering waters are some additional pathways for the release of PBs in the environment. They also act as pseudo persistent pollutants, leading to their bioaccumulation (Han et al. 2016). In a study by Okubo et al., MePB, Ethylparaben (**Eth-PB**), Pr-PB and butylparaben (**Bu-PB**) as well as other branched parabens like isopropylparaben and isobutylparaben stimulated the proliferation of MCF-7 cells, with factors such as chain length and chain branching to increase the potency of their effects (Okubo et al. 2001). Longer chain and branched-chain parabens tend to degrade less. Me-PB, Eth-PB, Pr-PB and Bu-PB are the main parabens detected in sediment, but the lack of studies renders those findings inconclusive. Parabens are detected in swimming pool water, river and marine waters as well as in the flesh of fish (Haman et al. 2015). Parabens negatively affected the reproduction of *Daphnia magna* and *Pimephales promelas* causing reproductive deterioration, growth abnormalities and in greater

concentrations proved to be fatal (Dobbins et al. 2009). Concerning in-vitro experiments, PBs have been demonstrated to have estrogenic and anti-androgenic effects. Specifically, micromolar concentrations of MePB, EthPB, PrPB and BuPB inhibited the activity of estrogen sulfotransferase, an effect that is increasing with the increase in paraben ester chain length (Davidson 2005). The anti-androgenic activity of Me-PB, Pr-PB, and Bu-PB was established by measuring the inhibition of the testosterone-induced transcriptional activity in a human embryonic kidney cell line. Parabens were able to inhibit the activity of aromatase, an enzyme that converts androgens into estrogens, but in effective concentrations far exceeding those present in products. A link between breast cancer and the estrogenic activity of PBs has been investigated in the in the last 20 years, with several studies in 2004 (Davidson 2005), as well as some newer studies establishing a link between urinary paraben concentrations and breast cancer (Parada et al. 2019), but ultimately the link is not proven. Information about Parabens is compiled in **Table 2**.

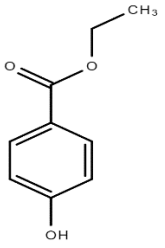
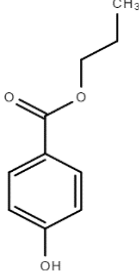
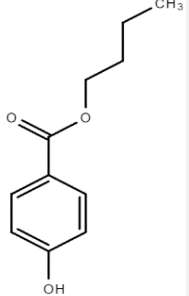
Nitrophenols are a class of nitrated phenol compounds that find use in the manufacturing of gasoline additives, drugs and lumber preservatives (Zhang et al. 2022b). Nitrophenols can be a product of the microbial hydrolysis of pesticides, such as parathion (Sethunathan 1973). They are included in the United States Environmental Protection Agency's (USEPA) priority pollutant list (Atlanta, GA: U.S. Department of Health and Human Services 2022). They can be released in the environment as a result of anthropogenic activities, as they are used in the production of fungicides, paints, dyes, and rubber chemicals (Services 2002). Other than that, they, and specifically, 2-Nitrophenol (**2NP**) and 4-nitrophenol are formed naturally as they are a degradation product of pesticides and can be formed by the nitration of phenols in the environment (Michałowicz and Duda 2007). As an example, NPs can be formed in the reaction of phenol with nitrite ions present in water under the influence of UV irradiation and in a wide pH range (Michałowicz and Duda 2007). The 2NP and 4-nitrophenol are detected in river, rain waters and in snow (Michałowicz and Duda 2007). The 2NP showed inhibitory activity, and additive toxicity when present with other nitrophenols (Zhang et al. 2022b). Another nitrophenol, the 3-methyl-4-nitrophenol (**3Me-4NP**) is a major degradation product of the common organophosphate insecticide fenitrothion, that is present in water, soil and foodstuff (Zayed and Mahdy 2008; Min et al. 2017), as well as in the exhaust particles of Diesel fuel (Li et al. 2009). It is a reproductive and immune system inhibitor, an endocrine disruptor (Li et al. 2009; Tanaka et al. 2013; Yang et al. 2016), also causing gonadal cell proliferation in female mice and gonadal cell apoptosis on rats of both sexes (Han et al. 2018). Furthermore, mutagenic activity was observed for 2,3-dinitrophenol, 2,5-dinitrophenol, 3,4-dinitrophenol, 2,4,6-trinitrophenol and 2-nitro-5-aminophenol (Michałowicz and Duda 2007). Structure information and physicochemical data about the nitrophenols is

presented in **Table 3**. Thus, it is evident that we need to monitor the concentrations of BPs, NPs and PBs in the environment and foodstuff. Detection methodologies have been developed for that purpose.

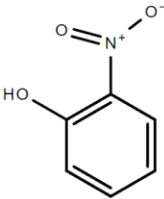
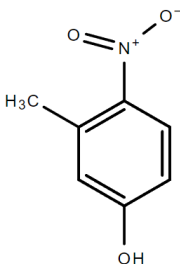
**Table 1:** Benzophenones (The  $pK_a$  and  $\text{Log}P_{ow}$  values were taken from PubChem except when differently noted).

BPs	Molecular Formula	Structure	$\text{Log}P_{ow}$	$pK_a$	CAS Number	Wavelength (nm)
2,2',4,4'-tetrahydroxybenzophenone or Benzophenone-2 (BP2)	C <sub>13</sub> H <sub>10</sub> O <sub>5</sub>		2.78	$pK_{a1} = 7.1$ and $pK_{a2} = 7.9$	131-55-5	285
2-hydroxy-4-methoxybenzophenone or Oxybenzone or benzophenone-3 (BP3)	C <sub>14</sub> H <sub>12</sub> O <sub>3</sub>		3.79	7.1 (phenol)	131-57-7	285
2,2'-dihydroxy-4,4'-dimethoxybenzophenone or Benzophenone-6 (BP6)	C <sub>15</sub> H <sub>14</sub> O <sub>4</sub>		3.90	6.81±0.35 (Predicted)	<a href="#">131-54-4</a>	285
<a href="#">2,2'-dihydroxy-4-methoxybenzophenone</a> or dioxybenzone or Benzophenone-8 (BP8)	<a href="#">C<sub>14</sub>H<sub>12</sub>O<sub>4</sub></a>		3.82	6.78	131-53-3	285
4-hydroxybenzophenone (4OH-BP)	C <sub>13</sub> H <sub>10</sub> O <sub>2</sub>		3.07	8.14 ( <a href="https://www.chemicalbook.com/ProductManual.aspx?ProductId=3130519">https://www.chemicalbook.com/ProductManual.aspx?ProductId=3130519</a> )	1137-42-4	285

**Table 2:** Parabens (The  $pK_a$  and  $\text{Log}P_{ow}$  values were taken from PubChem except when differently noted).

Paraben	Molecular Formula	Structure	Log $P_{ow}$	$pK_a$	CAS Number	Wave length (nm)
Ethylparaben (Eth-PB)	$C_9H_{10}O_3$		logK <sub>ow</sub> = 2.47	8.34	120-47-8	254
Propylparaben (Pr-PB)	$C_{10}H_{12}O_3$		3.04	8.5 (phenol)	94-13-3	254
Butylparaben (Bu-PB)	$C_{11}H_{14}O_3$		3.57	8.47	94-26-8	254

**Table 3:** Nitrophenols: (The  $pK_a$  and  $\text{Log}P_{ow}$  values were taken from PubChem except when differently noted).

Nitrophenol	Molecular Formula	Structure	Log $P_{ow}$	$pK_a$	CAS Number	Wavelength (nm)
2-Nitrophenol (2NP)	$C_6H_5NO_3$		1.79	7.23	88-75-5	285
3-Methyl-4-Nitrophenol (3Me-4NP)	$C_7H_7NO_3$		2.48	$7.39 \pm 0.10$	2581-34-2	285

## 1.2 Methods of detection

### 1.2.1 Non-chromatographic methods

The detection of benzophenones has been reportedly realized with an array of techniques. Lin et al., have reported the detection of benzophenone in recycled packaging paper materials through an enzyme-linked immunosorbent assay. It is an enzyme immunoassay that is used for the detection of benzophenone that is leaching from the food-packaging into the food (Lin et al. 2011). In another study, molecularly imprinted polymers were used for the creation of an **amperometric sensor** for benzophenone, that can migrate in foodstuff from the packaging. The polymer o-phenylenediamine was electropolymerized on the surface of an electrode made of glassy carbon, and the imprinted sensor showed great recognition capabilities for

benzophenone(Li et al. 2012). **Voltametric sensors** have also been used. Elwy et al. achieved the detection of Benzophenone-4 using a multiwalled carbon nanotube / benzethonium chloride-modified carbon paste electrode (Elwy et al. 2020), while Mutić et al., developed pyridium-based ionic liquid modified carbon paste electrodes for the voltametric detection of BP3 (Mutić et al. 2024). Methods based on **luminescence** were also developed, as they are straightforward and cheap. Zhang et al., utilized a Zinc- carboxyphenyl phosphonic acid-based coordination polymer that was post synthetically modified with terbium ( $Tb^{3+}$ ) and used as an excellent ratiometric **luminescent** probe for the detection of benzophenone (Zhang et al. 2023). In another study, a metal-organic framework (**MOF**) was synthesized by linking europium with two organic linkers was used to create a ratiometric fluorescent probe for the detection of various BPs. The device possesses the added benefit of portability, assisting in in-situ detection (Zhou et al. 2023).

An amplitude of non-chromatographic detection methods for parabens has been reported. There is a large body of work for paraben detection with **electrochemical sensors**. Bouaziz et al., developed a sensor using iodine-doped ZnO for the detection of EthPB by means of **cyclic voltammetry** (Bouaziz et al. 2022). In another work, carbon electrodes modified with a graphene-derived nanocomposite and polyvinylpyrrolidone/polyaniline produced by screen printing have been reported for electrochemical PB detection (Kajornkavinkul et al. 2016). In Soysal's work, a pencil graphite electrode was modified with a molecularly imprinted polymer and detected Me-PB through differential pulse voltammetry (Soysal 2021). Another **voltammetric** method for the detection of Me-PB has been reported using a Glassy Carbon Electrode modified Multi-Wall Carbon Nanotubes/Nafion Composite (Luo et al. 2012). Molecularly imprinted polymer technology was used to construct paraben selective working electrodes for the electrochemical determination of parabens (Yücebaş et al. 2020). Hajian et al. reported a biosensor-based carbon paste electrode functionalized with hemoglobin and multi-walled carbon nanotubes that was used for the electrochemical determination of methylparaben. This voltammetric determination was based on the catalytic effects of hemoglobin while in the presence of hydrogen peroxide, which causes the oxidation of the phenolic hydroxyl groups of methylparaben (Hajian et al. 2015). **Luminescent** detection is also possible, although it is rare. There have been reported uses of optical probes, such as the mercaptosuccinic acid-capped CdTe **quantum carbon dots** used in the work of Prapainop et al. The determination addresses the total content of parabens in the sample, with a prior step of alkaline hydrolysis in order to transform them to p-hydroxybenzoic acid, achieving the detection via the quenching of the fluorescence of the quantum dots (Prapainop et al. 2019). Furthermore, the **spectrophotometric** detection of some parabens, such as Me-PB has been reported (Elghobashy et al. 2016; Majeed Khorsheed Ahmed et al. 2016). The PB

detection can be done with some other less conventional methods, such as the non -capillary electrophoresis/ UV detection (Lincho et al. 2021) and flow injection analysis/ chemiluminescence detection or UV detection (Ocaña-González et al. 2015).

A plethora of sensors have been reported for nitrophenol determination. Many recent works have been published about the use of **fluorescent sensors** for the determination of 2NP, 3-nitrophenol, and 4-nitrophenol, (He et al. 2022; Han et al. 2023; Luo et al. 2023; Wang et al. 2023a). Furthermore, **electrochemical sensors** have been reported, 4-nitrophenol has been detected by amperometric and voltammetric sensors (Fanjul-Bolado et al. 2006) (You et al. 2023). **Colorimetric** sensors were developed for the detection of 4-nitrophenol, using inverse opal polymeric photonic crystals. The crystals immersed in deionized water possessed a Bragg diffraction of 555 nm, while the presence of 4-nitrophenol in concentrations ranging from 10 to 80 mM will shift the Bragg diffraction from 576 to 654 nm, changing color from green to red. The redshift will reach a maximum at 654nm due to maximum swelling providing a naked-eye semi-quantitative determination (Li et al. 2020). **Spectroscopic** detection methodologies, such as Surface enhanced Raman Spectroscopy have been utilized for the detection of 4-nitrophenol (Hostert et al. 2021). More specialized detection methods utilize biosensors, where an e. Coli-based sensor is incubated with 4-nitrophenol concentrations, which exhibit fluorescence based on the concentration of 4-nitrophenol (Ma et al. 2023).

### 1.2.2 Chromatographic methods and sample pretreatment

Furthermore, chromatographic methods have been reported to find use for the detection of BPs NPs and PBs in the bibliography. Chromatographic methods make use of a High-Performance Liquid Chromatography (**HPLC**) or Gas Chromatography (**GC**) system for separation, with subsequent identification and quantification with detectors like Ultraviolet (**UV**), Photodiode array detector (**PDA**) or Mass spectrometer (**MS**), Flame ionization detector, photoionization detector, electrochemical and conductivity detectors. Other more rare techniques include the micellar electrokinetic chromatography. For the determination of such analytes, HPLC systems are much more common than GC, as the analytes are generally non-volatile, and as such, an extra derivatization step is mandatory. The detection of **BPs** has been facilitated with Both HPLC and GC, albeit liquid chromatography is more common (Gavrila et al. 2023). This is because a derivatization process is required for some non-volatile hydroxylated BP derivatives, thus complicating the process. These BPs are the following: 2,4-dihydroxy-benzophenone (or benzophenone-1), BP2, BP6, 2-hydroxy-benzophenone, 3-hydroxy-benzophenone, 4-hydroxybenzophenone (**4OH-BP**) and 2,3,4-trihydroxy-benzophenone. Oubahmane et al. in their review,

report cases where GC is chosen, with the derivatization step added for the non-volatile analytes (Oubahmane et al. 2023). Another less conventional detection is the micellar electrokinetic capillary chromatography coupled with a UV/Vis detector (Narloch and Wejnerowska 2021). **Parabens** have been determined both by liquid and gas chromatography coupled with various detectors, in a plethora of works. Namely, HPLC coupled with fluorescence detectors (Lucas-Sánchez et al. 2022), HPLC coupled with UV detectors, electrochemical detectors and chemiluminescence detectors, GC with Flame ionization detector, photoionization detector and MS detector, as well as micellar electrokinetic chromatography coupled with a UV detector (Ocaña-González et al. 2015). **Nitrophenols** are determined with methods spanning from GC– Flame ionization detector and GC–flame photometric detector, GC-MS and HPLC-PDA (Aprea et al. 2002)(Maceira et al. 2020).

Chromatographic techniques are often preceded by various sample preparation techniques. Sample preparation techniques are the backbone of the analytical method, encompassing extraction, preconcentration and cleaning of target analytes from interferences found in the matrix. Liquid-liquid extraction, solid phase extraction (SPE), and **quick, easy, cheap, effective, rugged, and safe** are some widely used sample treatment techniques. Gavrila et al. summarize the recent trends in BPs extraction, showcasing the usage of solid phase extraction, **quick, easy, cheap, effective, rugged, and safe**, and liquid-liquid extraction, as sample preparation techniques (Gavrila et al. 2023). Similar pretreatment techniques have been utilized for PBs (Piao et al. 2014) and NPs (Pastor-Belda et al. 2018). Although liquid-liquid extraction, solid phase extraction, and **quick, easy, cheap, effective, rugged, and safe** are widely used techniques, the scientific advances enable the development of superior miniaturized extraction methods.

### 1.2.3 Microextraction

Conventional pretreatment methods, like solid phase extraction, tend to be replaced with cleaner, faster, and cheaper miniaturized microextraction methods. Conventional solid phase extraction and liquid phase extraction methods tend to get replaced by their miniaturized versions, while a plethora of novel methods have been developed. Microextraction methods are generally more streamlined, requiring lower volumes of extracting organic phase while simultaneously lowering the analysis time. adhering to the practices of green chemistry while also being economically viable. Such methods that **replace the conventional liquid phase extraction** are the liquid phase microextraction, the dispersive liquid-liquid microextraction (in its conventional and the in-syringe mode), the ultrasonic assisted emulsification microextraction, the hollow fiber liquid phase microextraction, the single-drop microextraction etc. (Pastor-Belda et al. 2018). Some techniques **replacing the conventional solid phase extraction** are the solid phase microextraction (the

miniaturized version of solid phase extraction) and some similar techniques, such as the Stir Bar Sorptive Extraction (Pastor-Belda et al. 2018), the fabric phase sorptive extraction (Gavrila et al. 2023), thin film microextraction and the in-tube solid phase microextraction, a method that is utilizing a coated capillary tube (Vuckovic 2013). In the case of the solid phase being dispersed in the liquid sample, the common microextraction methods are the dispersive solid phase microextraction and the magnetic dispersive solid phase microextraction. These can directly be applied to liquid samples, but in the case of a solid sample, a prior solid-liquid extraction step is mandatory. Replacing solid phase extraction with solid phase microextraction reduces the extraction solvent usage while also needing smaller sample volumes. This results in a non-exhaustive technique, where only a small percentage of the analytes is used. Other than the conventional solid phase microextraction format, the extracting phase can be immobilized on different substrates, either on fibers, on thin film (thin film microextraction), or in tube (in-tube microextraction) (Vuckovic 2013). The magnetic dispersive solid phase microextraction further simplifies the procedure, enabling the separation of the dispersed extraction phase from the sample simply via the usage of an external magnetic field. Methods such as single-drop microextraction and liquid phase microextraction use a smaller amount of extracting phase and hollow fiber liquid phase microextraction engulfs said phase in a **polypropylene hollow fiber (PPHF)**. The engulfing of the extracting phase in a PPHF ensures that the analytes move from the main sample volume to the acceptor phase through the fiber and are subsequently preconcentrated and cleaned from interferences. One goal of such techniques is to eliminate the need for chromatographic separation. The extracting phase inside the fiber selectively preconcentrate the target analyte while excluding interferences, resulting in a clean extract that can be directly sampled with the use of a syringe and injected into an MS or UV system (Carasek et al. 2023). Such techniques have been used for the extraction of parabens (Piao et al. 2014), nitrophenols (Pastor-Belda et al. 2018), and BPs (Gavrila et al. 2023).

Microextraction methods are non-exhaustive, making them the preferred methods of extraction, as the small sample volume requirement enables detection when sample volume is limited, while also requiring lower volumes of extracting solvent adhering to green chemistry practices (Lord and Pawliszyn 2000). An example of this is the molecule specific detection for **PBs** which uses molecularly imprinted polymer-modified capillary tubes before the HPLC-UV detection (Cheng et al. 2020).

#### 1.2.4 On-fiber solid phase microextraction

Solid phase microextraction has been widely used since its introduction in the 1990s as it is a simple, convenient, and low solvent-consumptive method that has been used for sample pretreatment of food, environmental, and other samples, and has been coupled with chromatographic methods. Fibers functionalized with various adsorbents have been used as an extracting medium. Some on-fiber solid phase microextraction methods have been proposed, where an adsorptive material is placed on a fiber to be used for a microextraction procedure. In this context, fused silica fibers and steel fibers have been coated with adsorptive materials and although exhibiting great results for sample pretreatment, they have some drawbacks, mainly their mechanical fragility and ease of coating stripping. In the case of fused silica, the coating can be stabilized by covalently bonding the polymer phase to the underlying fused silica substrate employing sol-gel deposition, but the fragility remains an issue. Furthermore, the high cost and tedious preparation of those fibers make their repeated use imperative, leading to carry-over effects (Azenha et al. 2006).

As a cheap alternative, PPHFs exhibit mechanical resistance avoiding the breaking problem of fused silica fibers (Yang et al. 2015). So, hollow fiber-solid phase microextraction is an attractive new alternative to the other fiber-based microextraction methods. PPHFs are a polymer of propylene that is formed as hollow tubes, with the inside of the fibers called the lumen. The lumen can be modified with other substances, or even store another material by filling them and sealing the ends, allowing the external environment to come to contact through the PPHF pores, but not allowing the material to leak out. Furthermore, their low cost makes their single use and subsequent disposal possible. The PPHFs were reportedly coated with multi-walled carbon nanotubes, graphene oxide, and polymer coatings (Yang et al. 2015). The PPHFs are used for hollow fiber liquid phase microextraction, the pores are filled with microliters of organic solvent forming a thin layer that is called a supported liquid membrane and serving as the extracting phase, the fiber is then filled with an acceptor phase and sealed. The analytes that were initially adsorbed in the supported liquid membrane are further desorbed/transferred in the acceptor phase. The system can be a two-phase system if the hollow fiber is filled with the organic solvent and is directly compatible with capillary gas chromatography, or a 3-phase system if the acceptor phase is an aqueous solution and will be compatible with HPLC coupled with capillary electrophoresis or MS. Furthermore, the PPHF pores will filter out other molecules, making them a great fit for complex matrices and resulting in a clean extract. Thus, it is a simultaneous clean-up and enrichment technique suitable for complex matrices. The fiber is submerged in a sample and the analytes travel through the pores of the PPHF via diffusion, and will

initially populate the supported liquid membrane and then populate the acceptor solvent inside the fiber (Bello-López et al. 2012). For the supported liquid membrane, 1-octanol was chosen for the fiber impregnation, as it was non-volatile, possessed low viscosity to help with molecular mobility and good fiber impregnation, and immiscible with water to avoid analyte loss during the extraction process (Kraševac and Prosen 2021). As proposed by Kraševac and Prosen, one common driving force behind the three-phase systems (systems with an aqueous donor phase and an aqueous acceptor phase, separated with an organic supported liquid membrane) is the gradient of pH between the sample (donor) and the solvent in the lumen (acceptor). The analytes in question have values of  $pK_a$  above 7, meaning that the protonated, non-ionic form will be predominantly present at acidic pH values and the ionic, deprotonated form (the conjugate base) will be predominantly present at alkaline pH values. Setting the pH of the donor phase at acidic values means that the neutral analytes will migrate to the supported liquid membrane due to better solubility, and because the pH of the acceptor phase is alkaline, the analytes are ionized and extracted from the supported liquid membrane and into the acceptor phase (Kraševac and Prosen 2021). In their review, Yang et al. present various works where hollow fibers are modified and used as adsorbents in the sample preparation. Multiwalled carbon nanotubes dispersed in 1-octanol were injected in the lumen of a PPHF and then sealed, to create a **hybrid liquid/solid phase** adsorbent, the octanol-multi-walled carbon nanotubes dispersion acted as the acceptor phase, extracting the analytes from the donor phase, followed by a desorption step with methanol/ultrasonication (Yang et al. 2015). There are cases where the multiwalled carbon nanotubes can be placed in the pores of the PPHF, while an acceptor phase is located inside the lumen, the analytes are first adsorbed on the multiwalled carbon nanotubes from the donor solution and through the PPHF, and then desorbed in the acceptor phase, helping the analyte to flow through the fiber and ensuring a higher selectivity and enrichment. In another method, a silica-based organic-inorganic polymer containing functionalized multi-walled carbon nanotubes were deposited with the sol-gel technique inside the PPHFs was used as a solid phase microextraction adsorbent (Yang et al. 2015). PPHFs loaded with a sorbing material on their exterior have also been reported, PPHFs were surface functionalized with covalent organic framework-V and filled with a magnetic material in the edges, in order to form a makeshift stir-bar-modified adsorptive fiber for the Stir Bar Sorptive Extraction microextraction of BP (Liu et al. 2022).

## 1.3 Metal-Organic Frameworks

### 1.3.1 Introduction to metal-organic frameworks

Among the promising materials that find use as adsorbents in microextraction methodologies are the metal-organic frameworks (MOFs), a class of materials that piqued the scientific interest in the last decades. As the nomenclature suggests, MOFs are organometallic materials that form frameworks consisting of a metal cluster, otherwise known as a **secondary building unit**, coordinated with organic ligands, creating an extended structure by repeating the same building block. MOFs most commonly are crystalline but can also be amorphous (Fonseca et al. 2021). Those structures attract great scientific interest because of their ability to manipulate the size of the pores and topology (Uflyand et al. 2021). That coupled with superb porosity, abnormally high surface area, reversible adsorption, and tunable functionalization makes them great for selective analyte adsorption (Tran et al. 2023a). The area of the surface of the MOFs is typically from 1000 to 10,000 m<sup>2</sup>/g, and the porosity is typically 50% or more of the crystalline volume of the MOF, surpassing other popular adsorbents like carbons and zeolites. MOFs' permanent porosity makes them particularly useful, to prove such property we would need to measure the reversible sorption isotherms of a gas at low pressure and temperature conditions. It was first proven by the carbon dioxide and nitrogen isotherm measurement on a layered zinc-terephthalate MOF (Furukawa et al. 2013). This gave rise to a class of materials that found usage in the fields of detection, separation, and ion exchange with the storage of molecular hydrogen gas being particularly of interest. The materials also find use in the fields of catalysis, owing to the tunable sites in the pores of the material, sensors, drug delivery, and electronics (Uflyand et al. 2021). The applications in the field of analytical chemistry are varying and include: food analysis, environmental analysis and wastewater treatment, biomedical applications, and are utilized for their adsorptive capabilities for selective and efficient extraction (Uflyand et al. 2021). As adsorbents, in the current bibliography MOFs find application for the extraction of an array of organic contaminants, such as dyes, pharmaceuticals, organic solvents, heavy metals, as well as other substances characterized as emerging pollutants (Dhaka et al. 2019; Chen et al. 2023; Mohan et al. 2023).

Some classifications of the MOFs include **(a)** the University of Oslo frameworks (**UiOs**) **(b)** porous coordination network frameworks (**PCNs**) **(c)** Zeolitic Imidazolate Framework (**ZIFs**) **(d)** Iso-reticular MOFs (**IRMOFs**), **(e)** coordination pillared layer frameworks, and finally **(f)** Materials Institute Lavoisier (**MILs**). The ZIF MOFs are structures consisting of zeolites of Co(II) or Zn (II) that are linked with imidazolate, the UiO MOFs are a zirconium octahedral cluster linked with 12 BDC linkers covalently, MILs are a formation of trivalent metal ions such as chromium ions (Cr<sup>3+</sup>), aluminum ions (Al<sup>3+</sup>), iron ions (Fe<sup>3+</sup>),

gallium ions ( $\text{Ga}^{3+}$ ), vanadium ions ( $\text{V}^{3+}$ ), Indium ions ( $\text{In}^{3+}$ ) and Iridium ions ( $\text{Ir}^{3+}$ ), or clusters of them and linking with a carboxyl containing linker, such as trimesic acid and terephthalic acid. In the case of PCN MOFs a cluster of  $\text{Zr}_6$  coordinates with metal-porphyrin linkers. For the coordination pillared layer framework MOF, the nitrogen-containing neutral heterocyclic ligands are coordinated with hexagonal coordinating metals, and in one case of IRMOFs, aromatic carboxyl ligands are coordinated with clusters of  $\text{Zn}_4\text{O}$  (Perera et al. 2023). Another widely used MOF is the Hong Kong University of Science and Technology - 1 (**HKUST-1**), a copper-based MOF with trimesic acid ligands.

The MOF structure is made up of organic ligands that function as bridges between metal atoms or clusters, which act as nodes, to form MOF crystals that can have an indefinitely repeating crystalline pattern, from crystal edge to crystal edge. The ligands that are used can be anionic, offsetting the positive charge of the metal cations. Some of the anionic ligands that are most common are **Benzene-1,4-dicarboxylic acid** or terephthalic acid ( $\text{H}_2\text{BDC}$ ), **benzene-1,3-dicarboxylate** (isophthalate), **trimesic acid**, and **oxalate**. The angle between the carboxyl ends can change the properties of the final product. The  $\text{H}_2\text{BDC}$  ligand has two carboxyl groups at a  $180^\circ$  angle and can act as a long bridge carboxyl end to carboxyl end. It can also form short carboxylate bridges in each carboxylate end, effectively creating a bridge inside the carboxylate end, from oxygen to oxygen and linking four metal ions in total. Isophthalate has a  $120^\circ$  rigid angle, and trimesic acid is a rigid planar ligand that has 3 carboxyl groups at a  $120^\circ$  angle and can produce multidimensional MOFs (Janiak and Vieth 2010). In the case of neutral ligands, the charge is neutralized by the anions present in the salt (i.e.  $\text{NO}_3^-$ ,  $\text{SO}_4^{2-}$ ,  $\text{Cl}^-$ ). Some examples of neutral ligands are 4,4'-bipyridine, pyrazine, 1,4-diazabicyclo[2.2.2]octane, bis(pyridin-4-yl)-1,2-ethene, and 2,4,6-tris(4-pyridyl)-1,3,5-triazine, and can also produce MOFs of various topologies and pore size. Both types of ligands can produce 1-dimensional (**1D**), 2-dimensional (**2D**) and 3-dimensional (**3D**) MOFs (Janiak and Vieth 2010). Charge in the MOF can be of value, as adsorption of anionic and cationic molecules can be done through electrostatic and ion exchange processes, as in the case of anionic and cationic dyes (Uflyand et al. 2021).

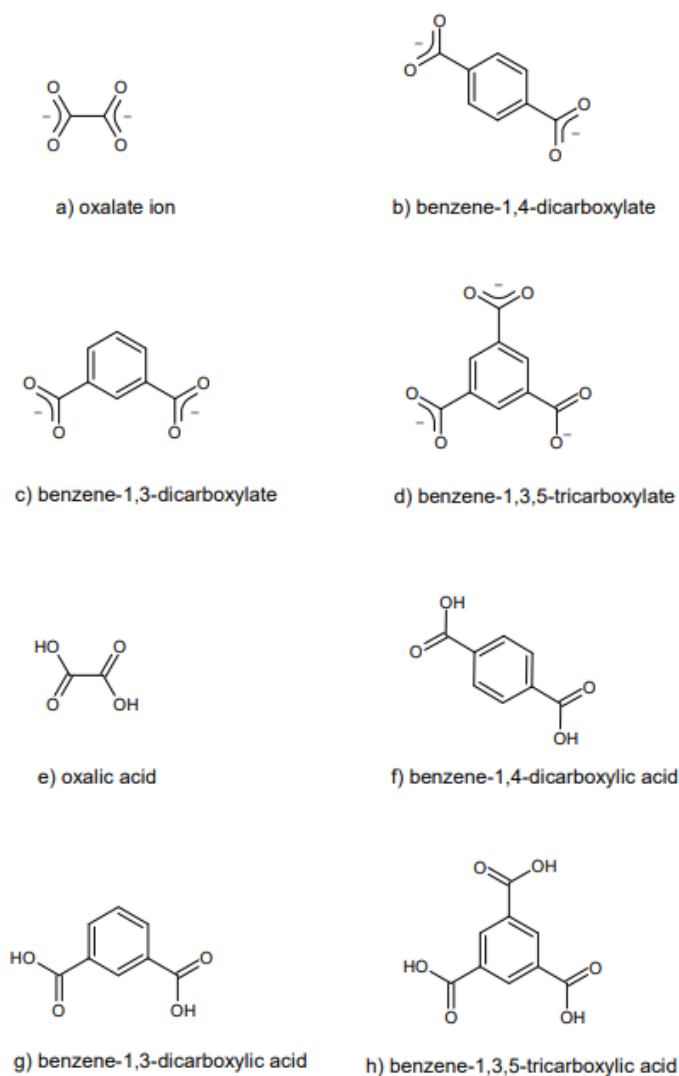


**Figure 1** : Common ligands and their anionic forms

MOFs are used as catalysts for photocatalysis and electrocatalysis, as well as hosts for metal nanoparticles (Bavykina et al. 2019), and gas storage, where they find application for the adsorption of H<sub>2</sub>, CO<sub>2</sub> and NH<sub>3</sub> to name a few (Firooz and Armstrong 2022). MOFs find use in catalysis, gas storage, and various analytic applications that will be detailed further below. One non-analytic application that is especially important is the use of **MOFs in drug delivery**. MOFs are micro and nanosized materials that are part of the wave of smart drug release systems. The ability to control their structure, size, pore size, and dimensions as well as the ease of their functionalization make them optimal for drug loading and delivery. Many MOFs are comprised of biologically safe constituents and are thus great candidates for this cause. Furthermore

conventional carriers such as quantum dots, liposomes, polymers, and inorganic nanoparticles that can have lower drug loading, instability problems, and systemic side effects/toxicity are being replaced with MOFs (He et al. 2021). The large BET surface enables them to carry a variety of chemicals with ranging physico-chemical such as peptides, drug molecules, and biomacromolecules. Properties stimuli such as pH, adenosine triphosphate, and UV light inherently affecting the MOF, can trigger the **release of the drug** from the framework (Lawson et al. 2021). MOFs' Moieties can be modified to control drug release from the pores, while, choosing the appropriate constituents for the MOF will affect its rate of degradation to a desired biological environment (Lawson et al. 2021). So, MOFs can be modified to target the desired cells. The leading of this micro-bot-MOF device through a desired track inside a complex microfluidic network is facilitated by the controlling from a weak rotational magnetic fields, in a micro-bot-MOF technology application (Wang et al. 2019b) Fe-based MOFs can in act synergistically with the cargo drug and provide intracellular infection alleviation and participations in improving radiation efficacy in the fight against cancer. Specifically in the case of ZIF-8@ artificial bacterial flagella microrobots, a spiral-like microstructure known as artificial bacterial flagella was fabricated with two-photon polymerization stereolithography and coated with titanium and nickel to give them magnetic properties while also being biocompatible. It was then treated with O<sub>2</sub> plasma to enable PDA growth on the surface, which in turn enables the growth of MOF crystals as it drives heterogeneous nucleation. The resulting nano-swimmer device is thermally and chemically stable, but pH responsive. The ZIF-8 MOF is stable in alkaline but degrades in slightly acidic pH media, making it ideal for targeting cancer cells, as the extracellular medium in cancer tissues is shown to be slightly acidic (pH around 5-6) (Wang et al. 2019b). The magnetic properties allow the controlled delivery of the micro-bot-MOF with the application of a weak rotational magnetic field, while only releasing the drug in the cancer cell vicinity because of the pH responsive MOF degradation.

### 1.3.2 MOF in analytical chemistry

Pristine MOFs have either been used without modification, or they have been modified to fit the analytical need, overcoming existing challenges and improving the existing practices in the fields of sample collection, extraction, preconcentration, and chromatographic separation as well as finding usage in the development of sensors. Improvements are also opted for the sensitivity, selectivity, and detection limit of the methods. Materials with high active surface area and functionalizable sites can be ideal for sensors. The current trend for sensor development is for the connected automation in sensing, while possessing other attractive characteristics such as low limits of detection, rapid detection, selectivity, and low cost alongside with portability. MOFs can be used for the creation of rapid real time sensors for in situ detection on various

substrates including foodstuff. MOFs find usage in the development of **electrochemical sensors**. MOFs are generally poor electron conductive materials. That, coupled with their poor stability in aqueous medium inhibited their use as electrochemical sensors. To combat that, various strategies are employed to work around those characteristics by increasing their water stability and conductivity. Redox of the cations in the MOF, provides a way for electrons to move, tuning the ligand may improve the charge transfer, and creating hybrid MOF conductive materials by combining MOFs with metal nanoparticles, carbon nanostructures, and conductive polymers will be further discussed below. Even so, there are some advantageous characteristics about MOFs that make them promising materials for electrochemical sensors, and are the three below as stated in a review by Kajal et al:

- A) MOFs have unsaturated metal coordination sites, uniform network structure, and unique structural benefits, including large surface area, tunable porosity, and crystalline form. These different features provide MOFs with an excellent catalytic capacity, making them helpful in effective coating materials for electrocatalytic electrodes that are used in sensing applications.
- B) The large surface area and high porosity help with the mass transfer of the analytes and their pre-concentration in the sensor's double layer, increasing the response of the electrical signal and subsequently the sensitivity towards said analyte.
- C) The MOF channel shape, size, and vacant sites present selectivity through molecular exclusion (Kajal et al. 2022)

Electrochemical redox reactions are pH dependent, so the ability of the MOFs to act as buffering agents because they possess Lewis sites is assisting in the redox reaction (Kajal et al. 2022).

An electrochemical sensor's sensitivity relies upon its electroactive area and the mass transfer of the analytes. The sensors' performance can be improved by improvements in the electroactive area, which can be increased by **decreasing the particle size** of the MOFs that are used for the sensor. The performance of the sensor can be improved by increasing the selectivity for target compounds by **altering the surface chemistry** of the MOF. To aid the mass diffusion towards the sensors surface, smaller scale MOFs have been used, as they have more exposed active sites, and superior mass diffusion properties, allowing the analytes to reach said sites. Furthermore, **creating MOF composites**, such as composites with graphene oxide, reduced graphene oxide, graphene carbon electrode, carbon paste electrode, carbon nanotubes, metal nanoparticles, and metal-oxide nanoparticles may improve the electrochemical properties of the resulting sensor as well as solve the problems of poor conductivity and extreme aggregation that could

hinder their usage as sensor materials (Kajal et al. 2022). The selectivity of the sensor is also a feature of merit, particularly when it comes to biological targets where interferences may occur. In view of that, **2D MOFs**, and **especially nanosheets**, are particularly of interest. They have many unsaturated active sites, and their planar structure enables the stimulation and transfer of electrons. MOF composites that are carbon-based are prioritized when compared to other MOFs because of their high conductivity, superior stability, and economic feasibility while exhibiting chemical inertness (Kajal et al. 2022). In an example that was presented in the review of Kajal et al., single-walled carbon nanotube-MOFs are used for pesticide detection while some sensors are fabricated using a porous carbon fiber/ZIF-67 composite for the electrochemical detection of L-cystine and nitrobenzene. As a result of the composite, the ZIF-67 nanocrystal growth is restrained, avoiding aggregation, leading to increased conductivity and mass transport channels, and available active sites for the sensitive, selective electrochemical detection of L-cystine and nitrobenzene in low potential (Kajal et al. 2022). The metal nanoparticle/ MOF hybrids, consisting of the nanoparticles placed in the cavities of the MOF, are synergistically working for sensing. Another hybrid MOF structure is formed by encapsulating metal oxide nanoparticles or metal nanoparticles in a MOF shell creating a **core-shell heterostructure**. In their review, Kajal et al. report the usage of Fe<sub>3</sub>O<sub>4</sub> nanoparticles that were coated with ZIF-8 (core shell structure) and situated inside a reduced carbon oxide lattice, forming a Fe<sub>3</sub>O<sub>4</sub>@ZIF-8/reduced graphene oxide composite. A graphene carbon electrode is modified with that composite, creating an electrochemical sensor to detect dopamine. Such electrochemical sensors are created for the detection of analytes varying from heavy metals, pesticides, antibiotics and even DNA (Kajal et al. 2022).

MOFs have also been used to fabricate biosensors, detecting metal ions, free radicals, macromolecules, small molecules, and cells in a plethora of real matrices. MOF-based electrochemical biosensors for the detection of H<sub>2</sub>O<sub>2</sub>, dopamine, glucose, and other small molecules such as ascorbic acid, uric acid, and urea as well as the neurotransmitters acetylcholine and norepinephrine are reported from Daniel et al. in their recent review (Daniel et al. 2022). Furthermore, an Ag-MOF was used for the electrochemical detection of Hg<sup>2+</sup> and a Cu-MOF for Cr<sup>3+</sup> as reported by Shubhangi et al. in their review (Shubhangi et al. 2024). A MOF named Fe-MIL-101 is tailored by the addition of modulators such as acetic acid, hydrochloric acid, and nitric acid during the synthetic process, in order to exhibit more active oxidation sites for the voltammetric detection of 2-nitrophenol (Chen et al. 2022b).

MOFs have also been used for the fabrication of **optical sensors, i.e., luminescence and colorimetric sensors**. Shubhangi et al. recently compiled a review on the subject, some examples presented in their work of MOF-based **luminescent sensors** include the fluorescent sensor based on Fe-MIL-88NH<sub>2</sub>@RhB Cu<sup>2+</sup> detection, JXUST-11 (a Europium-MOF) photoluminescent detection of Al<sup>3+</sup> and Ga<sup>3+</sup> (Shubhangi et al. 2024). More intricate luminescent MOF sensors have been fabricated, one of them being the MOF-plant hybrid sensor detailed in a work by Liang et al. In detail, MOFs have been synthesized inside living organisms, such as plants, by immersing their roots in an aqueous solution of the MOF constituents. The subsequent MOF-plant nano-biohybrid work as pre-concentrators through their passive fluid transport system, concentrate the analytes around the MOFs in their tissue, and detect selectively through a turn-on fluorescence mechanism (Liang et al. 2020). **MOF-based colorimetric sensors are likewise developed**. In a work by Duan et al. Cu-MOF nanoparticles have been used for the colorimetric detection of E. coli (Duan et al. 2020). Furthermore, in a recent review by Shubhangi et al., an iridium nanocluster composite with a Titanium-MOF, a M-PCN-222 (where, M = Mn, Fe, Co, and Ni), and a Cyclodextrin MOF have been reportedly used for colorimetric sensors for H<sub>2</sub>O<sub>2</sub> detection (Shubhangi et al. 2024).

Development of **MOF-based optical biosensors** for the detection of biomarker molecules is prevalent. As reviewed by Shubhangi et al. the detection of radicals, metal ions, macromolecules such as L-cysteine and glucose are reported (Shubhangi et al. 2024). Other optical biosensors that can identify bacteria, viruses, and cells include, among others:

- Sensors with copper catecholate nanosheets for the colorimetric detection of **macromolecules** such as acetylcholinesterase
- Sensors using the MOF-5/CoNi<sub>2</sub>S<sub>4</sub> composite for the fluorescent detection of **SARS-CoV-2** spike antigen
- Sensors for the detection of **cells (prokaryotic and eukaryotic)**
- A MIL-88@Pd/Pt based colorimetric sensor for the detection of **Salmonella typhimurium**
- A NH<sub>2</sub>-MIL-53(Fe) sensor for the photoluminescent detection of **E. coli**
- A colorimetric sensor based on MIL-101(CuFe) for the detection of the recent **SARS-CoV-2** virus

(Shubhangi et al. 2024).

Other analytical applications for MOFs see them being used as coatings for **quartz crystal microbalance scales**, enabling them to be used for the detection of different compounds (Liu et al. 2021). Liu et al. have

coated the quartz crystal microbalance scale with MOFs that have desirable properties for volatile organic compounds sensing, forming stable and reversible microbalance.

**Spectroscopic detection using MOFs** is also possible. Although the use of MOFs in Surface-enhanced Raman spectroscopy (SERS) has typically been as scaffolds for noble metal particles that exhibit SERS activity, as they do not exhibit said activity themselves, some MOFs are SERS active and have been utilized in SERS detection (Sun et al. 2018a). MOFs with specific metal centers, linkers, and preferred topology show greater SERS functionality and have been proposed to replace typical SERS substrates. For instance, Sun et al. found that using tetrakis(4-carboxyphenyl) porphyrin as a linker and Cobalt or Copper as the metal center, will yield MOFs that are SERS active (Sun et al. 2018a)

MOFs have been used for the synthesis of novel **stationary phases for chromatographic columns**. Demands of the chemical industry based on the ever-improving scientific methods lead to the of new more efficient and advantageous methods, or improved versions of the existing ones. In that light, MOFs are promising materials that began to be utilized as **stationary phases** in the field of separation, especially **chromatographic separation**. The MOFs' high porosity, customizable pore sizes, and functionality as well as their superb surface area make them superb choices for the development of stationary phases for chromatography. MOF particles can be arranged as core-shell MOF-based composites and subsequently packed in the chromatographic column, or directly packed in a chromatographic column. The MOF stationary phase can either be hydrophobic, hydrophilic, or mixed mode (Si et al. 2022). A stationary phase must meet some criteria to be a viable option. It needs to possess chemical and thermal stability, exhibit great selectivity to target compounds. A stationary phase must also possess excellent column efficiency, which is expressed as theoretical plate numbers, to match the benchmarks of stationary phases that are sold commercially. MOFs do enact separation both through size and interactions (Kotova et al. 2022).

Kotova et al. have recently published a review detailing the use of MOFs as **stationary phases** for HPLC (Kotova et al. 2022). The vanadium (IV) terephthalate MOF named MIL-47(V) was first used in 2007 to separate C8 alkyl-aromatic compounds. It is a hydrophobic porous material with one-dimensional diamond shape micropores, that has reportedly been used to separate a mixture of ethylbenzene, meta-xylene, and para-xylene. Here, the target molecules' shapes and locations within the pores of the MOFs played a crucial. role in the separation. The packing of the MOF in a chromatographic column has been problematic, the tiny particles (<5 mm) with an irregular, polydisperse, and anisotropic shape were causing packing issues (blocking of column frit, high pressure), despite the fact that this MOF was stable and offered

good separation. The issue could be resolved by **packing core-shell MOF composites** in the column. Many MOF core-shell composites such as ZIF-8@SiO<sub>2</sub> and UiO-66(Zr)@SiO<sub>2</sub> nanoparticles have been packed in stationary phases and used for chromatographic separation. Some examples of MOFs being used as stationary phases for liquid chromatography are the MIL-53(Al), and the MIL-101 (Cr) (Gu et al. 2011) as well as the core-shell structure of HKUST-1/ magnetic silica (Kotova et al. 2022).

**GC columns coated with MOFs** have also been reported. The dynamic coating was used to coat capillary columns with MIL-101 separating even p-xylene and m-xylene, which is a challenging task because of their identical boiling temperatures. For p-xylene, this was achieved with theoretical plates of 3800 m<sup>-1</sup>. Furthermore, capillary columns dynamically coated with MIL-100 (Fe, Cr) have been reportedly used for the separation of alkane isomers, with the Fe-based MOF achieving better results over the chromium-based. The MIL-100 MOF has mesoporous channels of 2.4 nm and 2.7 nm, accessible through microporous windows ( 0.5nm and 0.9 nm). There have also been reports of UiO-66 dynamically coated capillary columns used for the separation of benzene homologues and alkane isomers.(Kotova et al. 2022). Several different MOFs have been utilized for GC stationary phases, including IRMOF-3, MOF-5 (IRMOF-1), ZIF-7, ZIF-8, and MIL-101 (Cr). (Gu et al. 2011).

Stationary phases with **enantioselective** sites can be used in chiral separation, and MOFs exhibiting such properties have been used to fabricate enantioselective chromatographic columns. The chiral properties of the MOFs can arise from a chiral organic linker, or from the compounds trapped in the pores being enantioactive. HPLC applications make use of a planar MOF, with the condensed formula (Me<sub>2</sub>NH<sub>2</sub>)<sub>2</sub>Mn<sub>4</sub>O (d-cam)<sub>4</sub> (H<sub>2</sub>O)<sub>5</sub> (d-cam = d-camphorate), that contains coordinately unsaturated sites and was used for the separation of ibuprofen enantiomers. In a GC application, the mesoporous MIL-101-NH<sub>2</sub> was post synthetically modified by covalently adding chiral recognition sites. The resulting chiral MOF was used with a capillary column on 12 racemic mixtures. (Kotova et al. 2022). MOFs can also be used in open-tubular capillary electrochromatography to achieve the separation of isomers (Adel et al. 2023) One such example is ZIF-90, which achieves the separation of isomers, basic and neutral compounds, and nonsteroidal anti-inflammatory drugs. An additional example is the separation of enantiomers of phenylalanine, tryptophan, metoprolol, amlodipine, esmolol, and bisoprolol using (3-Aminopropyl)triethoxysilane-glutaraldehyde @ L-Histidine-NH<sub>2</sub>-MIL-53 MOF. Another MOF composite, the (3-Aminopropyl)triethoxysilane@ZIF-90, has been used as a stationary phase, coupled with lactobionic acid as chiral selector in the background solution,

to separate 5 drugs (enantiomers of metoprolol, propranolol, atenolol, bisoprolol, sotalol) in a racemic solution (Adel et al. 2023). Core-shell MOF composites are also used for chiral separation with HPLC, GC, and capillary electrochromatography (Si et al. 2022).

MOFs have also found use in the field of size exclusion chromatography. One of the earliest examples of **size exclusion chromatography** was proposed in 2009 using HKUST-1, a MOF possessing square-shaped pores with an aperture of  $9 \times 9 \text{ \AA}$ , to separate benzene, naphthalene, and anthracene. Benzene's kinetic diameter is smaller than the aperture of the pores of the MOF, resulting in fast diffusion equilibrium and being eluted in 38 min. On the other hand, naphthalene, having a stronger interaction with the pores, was eluted after 180 min while anthracene demonstrated strong partitioning with the pores, as its size matches the channel aperture, was eluted after 4 hours. Additional tests opting for the separation of benzene, naphthalene, and 1,3,5-triphenyl-benzene, demonstrate that the bulky 1,3,5-triphenyl-benzene is virtually unretained. This data suggests that molecules that are smaller or larger than the pore aperture are unretained and eluted fast, while those close to the size of the aperture are retained (Ahmad et al. 2009). Other examples of size exclusion chromatography include gas chromatography columns modified with pillar layer frameworks (Mertens et al. 2015). In another work, a MOF synthesized by  $\text{Zr}_6$  clusters and the tetratopic ligands TCPB- $\text{Br}_2$  [1,4-dibromo-2,3,5,6-tetrakis (4-carboxyphenyl) benzene] named NU-906 was packed inside a chromatographic column. The resulting column was used for the efficient fructose/glucose dynamic separation, with size exclusion playing a major role, with great selectivity (Xin et al. 2023).

### 1.3.3 Factors governing MOF stability

The MOF stability can be deduced by taking into account the thermodynamic and kinetic factors. The thermodynamic factors can be inferred by looking at the properties of the metal center, the ligand, and the strength of their bond. The Kinetic factors have to do with the hydrophobicity of the MOF as well as the steric factors that can lead to a stable material. One of the most important tools for deducing the metal-ligand bond strength is the **hard/soft acid/base** theory. **The metal-ligand hard/soft acid/base theory** dictates that hard acids form stable MOFs when linked with hard bases, and soft acids form stable MOFs when linked to soft bases. In order to understand the principle, we must look at the definitions of hard and soft acids and bases.

- **Hard acids** are categorized as electron acceptor atoms that possess high oxidation states, atomic and ionic radii of small dimensions, and poor polarizability. They have very energetic lowest-

unoccupied molecular orbitals (LUMO) that are devoid of easily excited outer electrons associated with affinity for ionic bond formation.

- **Hard bases** are considered to be electron donors that are weakly polarizable, highly electronegative, and not readily oxidizable. Ionic bonds are often formed by hard bases, owing to their high-energy empty LUMOs.
- **Soft acids** are electron acceptors with large atomic and ionic radii and oxidation states that are either zero or slightly positive. They possess readily available excited outer electrons that have a propensity to create covalent bonds. Soft base constitutes an electron donor atom with large ionic and atomic radii, that is highly polarizable and has a low electronegativity. It is easily oxidizable along with empty lower orbitals.
- **Soft bases** are electron donor atoms with large ionic and atomic radii and possess low electronegativity and high polarizability. They are easily oxidizable along with empty lower orbitals.
- **Borderline hard-soft acid-base** are species that possess characteristics that categorize them in between soft-hard acids and bases. (Hamisu et al. 2020).

In order to produce a **stable MOF**, hard Lewis acids like the high valent metal ions ( $\text{Ti}^{4+}$   $\text{Zr}^{4+}$   $\text{Al}^{3+}$   $\text{Fe}^{3+}$  and  $\text{Cr}^{3+}$ ) coordinate with hard Lewis bases like carboxylate ligands or phosphate-based ligands (containing hard electron donor atoms like oxygen), while soft Lewis acids like low valent metal cations ( $\text{Zn}^{2+}$   $\text{Co}^{2+}$   $\text{Ni}^{2+}$   $\text{Cu}^{2+}$ ) coordinate with soft Lewis bases like azolate or pyrazolate based ligands. So, the MOFs between hard acids and hard bases (**Hard-Hard MOFs**) as well as those between soft acids and soft bases (**Soft-Soft MOFs**) are stable, while those between hard-acid soft-base or soft-acid and hard-base are unstable. For instance, MIL-101(Cr) and MOF-5(Zn) are both carboxylate-based MOFs that are using the BDC ligand. According to the **hard/soft acid/base** theory, BDC is a hard base, while  $\text{Cr}^{3+}$  is a hard acid and  $\text{Zn}^{2+}$  is a soft acid, so MIL-101(Cr) is more stable than MOF-5(Zn) (Wang et al. 2022).

When discussing the complex stability, features concerning the **metal center**, such as the **ionic radius** and the **oxidation state are touched upon in the hard/soft acid/base theory**. Other factors concerning the metal center are the **Irving- Williams series of bivalent metal stability** ( $\text{Mn} < \text{Fe} < \text{Co} < \text{Ni} < \text{Cu} > \text{Zn}$ ) when they are coordinated with different ligands, the **reduction potential of the metal center**, as well as the effect of the **solubility product constant ( $K_{sp}$ )** of the metal center (an indicator of the chemical inertness of the metal center in an aqueous environment) (Burtch et al. 2014).

The ligand can also affect the stability of the MOF. Factors such as, the type of ligand, the ligand  $pK_a$  value, the **chelate effect** and other factors, such as the **resonance** of the bonds of the MOF can influence the resulting stability. Ligands can also affect the resulting MOF stability through the **Ligand field strength/crystal field strength**, as is the case in the aqua complexes of divalent ions of first-row transition metals, which generate more hydration thermal energy than would be predicted based on the ion sizes and charges. Complexes with ligands other than water are also predicted to be stable because of crystal field stabilization energy, many ligands that form  $\pi$ -bonds through back-donation are considered to be strong field ligands, indicating the role of crystal field stabilization energy to the MOF stability (House 2013).

Regarding the **chelate effect**, chelating ligands such as oxalates, ethylenediamine, and diethylenetriamine can form multiple bonds with the metal center and they are called multidentate ligands for that reason. They exhibit greater stability compared to non-chelating ligands that bind to simply one site, such as cyanide, chloride, and water (Muthaiah et al. 2020). **Resonance** can further increase the stability of a MOF. A  $\pi$ -bonding between metal and ligand can increase the delocalization of the charge and thus the stability of the MOF (Muthaiah et al. 2020). Other factors, such as **steric factors** also affect the MOF stability, and can also be manipulated by the choice of ligand. Furthermore, **ligand rigidity** can be important to stabilize the MOF, as rigid ligands help MOFs maintain their structure. In detail, when the ligand terminals are displaced from the metal nodes in the transition state of decomposition, shorter ligands are bent to greater angles for the same displacement, when compared to longer ligands, and thus demand higher decomposition activation energy, making the MOF more stable (Wang et al. 2022). Introducing **functional groups to the MOF structure may impact the MOF in many ways:**

- 1) They can change the hydrophobic or hydrophilic character of the MOF.
- 2) The ligand's structure may twist as a result of the steric-hindrance effects introduced by large functional groups. A large degree of ligand deformation will cause MOF instability.
- 3) Different functional groups possess different electron-withdrawing or electron-donating properties, affecting the electron density of the framework and thus its oxidation resistance.

Hence, **reactive oxygen species** will easily oxidize MOFs that have electron-donating groups in their structure such as amines, hydroxyl, alkoxy, and alkyl, thus making the framework electron-rich and easily susceptible to electrophilic attack from the reactive oxygen species. On the contrary, the presence of electron-withdrawing groups such as carboxylic ( $-\text{COOH}$ ), halogen ( $-\text{X}$ ), and nitro ( $-\text{NO}_2$ ) in the framework will protect from such destructive reactions. Among the common MOFs such as MIL-101(Cr),

UiO-66, NH<sub>2</sub>-UiO-66, NH<sub>2</sub>-MIL-125(Ti), MIL-100(Fe), and ZIF-8 that are used in water treatments exhibit thermodynamic or high kinetic stability, but among them UiO-66, UiO-67 and MIL-101(Cr) have no change in their patterns of XRD or the BET surface after two months in immersion. On the other hand, it only takes three days for ZIF-8, NH<sub>2</sub>-MIL-101(Al), NH<sub>2</sub>-MIL-53(Al), NH<sub>2</sub>-UiO-66, Cu-trimesic acid and MIL-53(Al) to show changes in the same measurements (Wang et al. 2022).

The **hard/soft acid/base** theory has been challenged in cases such as the SCN<sup>-</sup> ion. The sulfur atom is a soft electron donor meaning that the SCN<sup>-</sup> ion bonds to soft acids through the sulfur, while the nitrogen is a harder donor enabling interaction with hard acids through the nitrogen-side of SCN<sup>-</sup>. The stability exhibited by the complexes [Co(NH<sub>3</sub>)<sub>5</sub>NCS]<sup>2+</sup> and [Co(CN)<sub>5</sub>SCN]<sup>3-</sup> is a deviation from the **hard/soft acid/base** principle. As might be predicted, in the first complex, the nitrogen atom of the thiocyanate forms a bond with Co<sup>3+</sup>. However, in the latter complex, the SCN<sup>-</sup> is linked to Co<sup>3+</sup> via the sulfur atom, in contradiction with the **hard/soft acid/base** theory. The effect the remaining five ligands have on the metal ion explains the different behavior of those complexes. In [Co(NH<sub>3</sub>)<sub>5</sub>NCS]<sup>2+</sup>, the Co<sup>3+</sup> ion is acting as a hard Lewis acid and complexing five NH<sub>3</sub> molecules are acting as hard bases. As a result, the Co<sup>3+</sup> ion retains its hard acid nature as an electron pair acceptor. In the case of the [Co(CN)<sub>5</sub>SCN]<sup>3-</sup> ions, the five CN<sup>-</sup> ligands have a soft base character, and they alter the Co<sup>3+</sup> character to the point where it behaves as an soft acid (electron acceptor) toward SCN<sup>-</sup>. This effect is commonly known as the symbiotic effect and suggests that the character of the Co<sup>3+</sup>, when other ligands are already complexed with it, is dependent on the softness or hardness of said Ligands.

We should highlight the **influence of the pH** on the stability of the MOF. The Hard-Hard MOFs are generally stable in acidic environments, while the Soft-Soft MOFs are stable in alkali environments. **In alkaline environments**, the main method of MOF degradation is by means of ligand exchange of the MOF ligands by the competitive hydroxide ions. The OH<sup>-</sup> is a hard Lewis base and thus very destructive to a Hard-Hard MOF when compared to the Soft-Soft MOFs, explaining the low stability of **hard-hard** MOFs in alkaline environments (Wang et al. 2022). The ligands of **soft-soft MOFs** have high pK<sub>a</sub> values, so they are stable in alkaline conditions and are highly basic. They exhibit a high affinity for H<sup>+</sup> ions, so they tend to degrade in acidic environments. Furthermore, we can infer the stability of a MOF in alkaline environments by looking at the pK<sub>sp</sub> (solubility product) values of the metal ions of their metal core. In alkaline environments, frameworks decompose by the formation of metal hydroxides. Metal ions with higher pK<sub>sp</sub> will have a greater affinity for OH<sup>-</sup>, low-valent transition metal ions have lower pK<sub>sp</sub> values

than the high-valent ones, so their affinity for OH<sup>-</sup> is lower, and thus the stability of the MOF is greater (Pramanik et al. 2023).

**In acidic environments**, MOF degradation happens mainly through the competition of H<sup>+</sup> for the protonation of the ligands, so stability in the acidic conditions is connected somewhat to the  $pK_a$  of the Ligands. A higher  $pK_a$  value means greater affinity between the ligand and the protons. Then, at pH values lower than  $pK_a$  of the ligand, protons will compete with the metal ions for the coordination of the ligands and lead to the decomposition of the MOF. The ligands of the hard-hard MOFs are acidic and have low  $pK_a$  values, and thus are stable in low pH values as they have lesser affinity for the competing H<sup>+</sup> (Wang et al. 2022). Furthermore, MOFs can alter the pH of the solution and act as buffers (for instance, the pH of aqueous solutions of MIL-100(Fe) (1.0 g/L), MIL-53(Fe) (1.0 g/L), UiO-66 (0.5 g/L) and NH<sub>2</sub>-UiO-66 (0.5 g/L) are 2.9, 4.5, 3.5 and 3.8, respectively). The MIL-100 (Fe) only released 2.7% of the ligands when the initial pH was between 4 and 10. When the initial pH was set to 10, the final pH dropped to 5 after the pH alteration by the MOF, but when monitoring the pH at a constant value of 7 with the addition of sodium hydroxide solution during the extraction, there was damage at the MOF indicated by its XRD pattern loss (Wang et al. 2022). Although most MOFs are stable in a range of initial pH, they are stable in very narrow ranges when the initial pH is maintained/equilibrated. For example, MIL-101 (Fe) is stable at pH 3.0 and NH<sub>2</sub>-MIL-101(Fe) at pH 4.0, and both UiO-66 and NH<sub>2</sub>-UiO-66 don't exhibit substantial ligand loss in the range of pH 2-6, UiO-66 is generally stable at pH 3.8–5.0 and only loses 5.1% of its ligands at equilibrated pH 7.

The stability of MOFs in certain environments, such as in the **presence of inorganic anions, organic pollutants, and metal ions is also examined**. For instance, Lewis bases such as heavy metal oxo-anions and anions like Cl<sup>-</sup>, F<sup>-</sup>, NO<sub>3</sub><sup>-</sup>, CO<sub>3</sub><sup>2-</sup>, SO<sub>4</sub><sup>2-</sup>, and PO<sub>4</sub><sup>3-</sup> can enact ligand exchange, and thus degrade the MOF. MOFs like Uio-66 are great at phosphate anion adsorption but will also degrade in their presence. A way around that is to introduce defects to the Uio-66 MOF, the phosphate anions then prefer to be adsorbed to those defects and only exchange with ligands when the defects are saturated (Wang et al. 2022). The affinity of such Lewis bases for ligand exchange with the Uio-66 MOF follows this order:



Certain anions such as F<sup>-</sup>, PO<sub>4</sub><sup>3-</sup>, and AsO<sub>4</sub><sup>3-</sup> will strongly adsorb on the MOF and will not get desorbed even after multiple elution cycles. On the other hand, Cl<sup>-</sup> and SO<sub>4</sub><sup>2-</sup> will result in ligand release only in high concentrations, indicating that we can use certain MOFs for certain environments. Similar procedures can

evaluate the stability of a MOF in other environments. Organic pollutants such as phosphonates, with  $pK_a$  values lower than that of the ligand of MOF-808 (trimesic acid), can exchange its ligand. In the same review, it is also reported that in the cases where a MOF is used for heavy metal adsorption, those same metals can exchange the metal ions of the MOF (Wang et al. 2022).

One of the most acid-resistant MOFs, BUT-8(Cr)A retains its crystalline structure even in concentrated  $H_2SO_4$ . Similarly, PCN-601(Ni) which is one of the most alkaline stable MOFs, has been demonstrated to withstand boiling in a saturated sodium hydroxide solution. ZIF-based MOFs were stable in alkaline environments and UiO MOFs were stable in acidic conditions (Pramanik et al. 2023). It is thus deemed important to choose the right MOF for the correct matrix, as the pH value and presence of ions and organic pollutants in a sample such as wastewater may lead to the degradation of the MOF.

**Table 4:** Some examples of stable MOFs, their metal node and ligand, and softness-hardness.

MOF	Metal node	Ligand
ZIF-8	Zn cluster (soft acid)	Imidazolate (soft base)
UiO-66 (and isorecticular UiO-67 and UiO-68)	Zr cluster: $Zr_6O_4(OH)_4$ octahedra (hard acid)	$H_2BDC$ (hard base)
MOF-808	$Zr_6$ nodes (hard acid)	trimesic acid (hard base)
MIL-53	M-OH nodes (M: $Cr^{3+}, Fe^{3+}, V^{3+}, V^{4+}$ ) (hard acids)	$H_2BDC$ derivatives (hard bases)
MIL-101 (Cr)	$Cr^{3+}$ (hard acid)	$H_2BDC$ (hard base)
$Cr_3 O(OH)(H_2 O)_2 (BDC)_3$		

### 1.3.4 MOF Stability in water

One of the prevailing issues with MOFs is their water instability. Burtch et al. in their comprehensive review focus on the MOF water stability, providing a tangible method to assess it (Burtch et al. 2014). They give four classifications for the water stability of MOFs: **1) thermodynamically stable** when they are stable in an aqueous solution for a week or an acidic/basic/boiling solution for a day, **2) high kinetic stability** when they are stable in high humidity conditions but brief exposure to an aqueous solution will result to decomposition, **3) low kinetic stability** when they are stable in low humidity environments, and finally **4)**

**unstable** when they will break down in any exposure to moisture (Burtch et al. 2014). A practical way to infer the water stability is by comparing the structural properties such as PXRD and BET before and after exposure to aquatic conditions.

In a way to determine the factors that are most notable for the stability of the MOFs, they examined the simplest and most meaningful chemical properties, that are then presented in a flowchart. The flowchart organizes structural characteristics that are of relevance to the MOFs' thermodynamic or kinetic water stability and the subpoints of the chart are factors specifically related to this structural characteristic and the direct quantification can be done through the structure's crystallographic information file or by doing a molecular simulation of the crystallographic information file. The most important parameters are at the top, so the top of the chart is **thermodynamic stability**, where the mechanism is the unfavourability of irreversible structural degradation by hydrolysis under any water loading. The factors that affect the **metal-ligand bond strength**, such as  $pK_a$  of the ligand as a bond strength indicator between metal and ligand, properties of the metal such as **oxidation state** and **ionic radius** can be used to rationalize the stability of most stable MOFs. **Water liability** is the other factor and was proven to be linked to the inertness of the metal center. For instance, the greater stability of MIL-53(Cr) over MIL-47(V) can be attributed to the **big energy gap between frontier orbitals** of chromium and water. Another water liability metric is **the Irving-Williams series of bivalent metal stability (Mn < Fe < Co < Ni < Cu > Zn)** when they are coordinated with an array of different ligands. The **reduction potential** of the metal and finally the **coordinating geometry** by Pauling's rules for favorable crystalline structure of ionic crystals based on the radiuses of the cation and the anion. Those rules help us assume if ionic contributions of an ion favor the irreversible degradation of a MOF, based on the coordination geometry of the hydrolysis product state (Burtch et al. 2014).

Even if the structure is not thermodynamically inert, kinetic factors such as ligand steric effects and hydrophobicity can make the MOF somewhat stable in humid conditions by increasing the activation energy needed for the hydrolysis. For **Kinetic water stability**, the water may be unable to be adsorbed in the pores due to pore hydrophobicity, and if it does, it may be unable to cluster near the metal and react, a phenomenon that is called internal hydrophobicity. For the reaction to happen the activation energy must also be surpassed. Moving downwards the flowchart, we examine the case in which the water molecule can approach the metal site, but the activation energy barrier of the transitional state is not surpassed. Further down the flowchart are the **steric factors**. A high coordination number can crowd the metal center and protect it from water cluster formation. Even if the bond gets hydrolyzed, the high number of bonds to support the structure means there will be deformation tolerance. Another steric factor is the structural

transitions such as ligand rotational effects, where if a ligand exhibits greater torsional strain, the resulting MOF will be less stable. Interpenetrating MOFs can have greater stability and functionalized ligands can sterically lock other easily labile ligands in place, as they are bulky (Burtch et al. 2014). All the above can be seen in the flowchart in **Figure 2**. Aqueous degradation of the MOF happens by 2 mechanisms **a) ligand displacement** and **b) hydrolysis of the metal center**. The ligand displacement mechanism involves the insertion of a water molecule into the metal–ligand bond of the framework ( $M^{n+} - L^{n-} + H_2O \rightarrow M^{n+} - (OH_2) \cdots L^{n-}$ ), leading to the formation of a hydrated cation and the release of free ligand. On the other hand, the hydrolysis reaction involves the dissociation of the metal–ligand bond and the water molecule, which results in the formation of a hydroxylated cation and a free protonated ligand ( $M^{n+} - L^{n-} + H_2O \rightarrow M^{n+} - (OH)^- + HL^{(n-1)-}$ ). It should be noted, as it was stated in the section [1.3.3](#), that proton ( $H^+$ ) and hydroxide ions ( $OH^-$ ) are much more destructive to MOFs than the neutral water molecules (Wang et al. 2022).

Stability mechanism	Governing structural properties		
<p>Unfavorable for irreversible hydrolysis reaction to occur</p>	<div style="text-align: right; padding-right: 20px;"><b>Thermodynamic stability</b></div> <div style="border: 1px solid black; border-radius: 15px; padding: 10px; margin: 10px auto; width: 80%;"> <p style="text-align: center;"><b><u>Innertness of metal cluster</u></b></p> <table style="width: 100%; border-collapse: collapse;"> <tr> <td style="width: 50%; vertical-align: top;"> <p><b><u>Metal-Ligand bond strength</u></b></p> <p>Ligand effects :</p> <ul style="list-style-type: none"> <li>-pKa of coordinating atom</li> </ul> <p>Metal effects :</p> <ul style="list-style-type: none"> <li>-oxidation state</li> <li>-ionic radius</li> </ul> </td> <td style="width: 50%; vertical-align: top;"> <p><b><u>Liability with water</u></b></p> <p>Metal species :</p> <ul style="list-style-type: none"> <li>-Reduction potential</li> <li>-Irving-Williams sequence</li> <li>-Energy difference of the frontier orbitals</li> </ul> <p>Coordinating geometry :</p> <ul style="list-style-type: none"> <li>-Pauling rules</li> </ul> </td> </tr> </table> </div>	<p><b><u>Metal-Ligand bond strength</u></b></p> <p>Ligand effects :</p> <ul style="list-style-type: none"> <li>-pKa of coordinating atom</li> </ul> <p>Metal effects :</p> <ul style="list-style-type: none"> <li>-oxidation state</li> <li>-ionic radius</li> </ul>	<p><b><u>Liability with water</u></b></p> <p>Metal species :</p> <ul style="list-style-type: none"> <li>-Reduction potential</li> <li>-Irving-Williams sequence</li> <li>-Energy difference of the frontier orbitals</li> </ul> <p>Coordinating geometry :</p> <ul style="list-style-type: none"> <li>-Pauling rules</li> </ul>
<p><b><u>Metal-Ligand bond strength</u></b></p> <p>Ligand effects :</p> <ul style="list-style-type: none"> <li>-pKa of coordinating atom</li> </ul> <p>Metal effects :</p> <ul style="list-style-type: none"> <li>-oxidation state</li> <li>-ionic radius</li> </ul>	<p><b><u>Liability with water</u></b></p> <p>Metal species :</p> <ul style="list-style-type: none"> <li>-Reduction potential</li> <li>-Irving-Williams sequence</li> <li>-Energy difference of the frontier orbitals</li> </ul> <p>Coordinating geometry :</p> <ul style="list-style-type: none"> <li>-Pauling rules</li> </ul>		
<p>Not favorable because water molecules cannot cluster near metal site</p>	<div style="text-align: right; padding-right: 20px;"><b>Kinetic stability</b></div> <div style="border: 1px solid black; border-radius: 15px; padding: 10px; margin: 10px auto; width: 80%;"> <p style="text-align: center;"><b><u>Hydrophobicity</u></b></p> <ul style="list-style-type: none"> <li>-water unable to adsorb in the pores (pore hydrophobicity)</li> <li>-water unable to cluster near the metal (internal hydrophobicity)</li> </ul> </div>		
<p>Water can approach metal site, but the hydrolysis is not favorable because of the transition site energies</p>	<div style="text-align: center; margin-bottom: 10px;"> <div style="border: 1px solid black; border-radius: 10px; padding: 5px; display: inline-block;"><b><u>Steric factors</u></b></div> </div> <div style="display: flex; justify-content: space-around;"> <div style="border: 1px solid black; border-radius: 15px; padding: 10px; width: 45%;"> <p style="text-align: center;"><b><u>Around the metal site</u></b></p> <p>Ease of water approach :</p> <ul style="list-style-type: none"> <li>-Metal coordination</li> <li>-Structural transitions</li> </ul> </div> <div style="border: 1px solid black; border-radius: 15px; padding: 10px; width: 45%;"> <p style="text-align: center;"><b><u>Around labile ligands</u></b></p> <p>Ease of displacing ligand :</p> <ul style="list-style-type: none"> <li>-Interpenetration</li> <li>-Ligands rigidity and sterics</li> </ul> </div> </div>		

Figure 2: MOF water stability.

### 1.3.5 MOF iso-reticular design

The design of MOFs further expanded with new principles stemming from the iso-reticular chemistry. Early MOF development saw single metal atoms used, utilized as nodes, connected by ditopic linkers (ligands capable of coordination at two separate sites) such as dicarboxylates, utilized as spacers (Furukawa et al. 2013). In contrast, the construction of MOFs following a geometric principle uses inorganic metal-containing secondary building units as the nodes and connects them with organic ligands that possess more rigid structures, to form structures such as squares, octahedra, and others (Furukawa et al. 2013). This

secondary building unit approach to the MOF design led to the identification and selection of some select few preferred topologies. Topology is set to describe MOFs and other crystalline systems, stretching, bending, and squeezing of the bonds leaves the topology of the MOF unaltered, but breaking the bonds will alter it. Network topology as a concept is similar to the concept of stereoisomers, such as E,Z, cis, trans, fac, and mer, and is used in the same manner for codenaming. The topologies are given specific three letter codenames from the Reticular Chemistry Structure Resource, such as diamond, quartz, and others (Öhrström 2015). Also, the post-modification of these frameworks led to the creation of catalytic sites inside the pores. Post-synthetic functionalization of the MOFs, as well as the extended MOFs that are created from their iso-reticular expansion, do not change their underlying structure, and crystalline order in divergence with other extended solids (Furukawa et al. 2013). This method brought the identification of a select few preferred topologies that achieved permanent porosity and, because of the large subsequent bibliography, led to the iso-reticular principle of MOF design, which accomplished a variety of structure sizes and nature while maintaining the topology intact. Iso reticular chemistry within MOFs essentially refers to keeping the same structure but changing the chemical building blocks. Some frequent topologies are the pyrite nets, the rutile nets, and the primitive cubic nets (Zhang et al. 2015). The usage of symmetric building blocks is expected to yield symmetric nets, and 80% of the MOF structures that can be found in the Cambridge Structural Database belong to a few default nets. For instance, tetrahedra building units with most likely result in diamond nets and triangles will yield SrSi<sub>2</sub> type silicon nets. (Zhang et al. 2015)

A particularly important MOF for iso-reticular design was MOF-5, alternatively known as IRMOF-1, as it gave birth to the iso-reticular series of MOFs that were named IRMOF 1-16, a family of 16 cubic MOFs created from IRMOF-1. They were created by means of iso-reticular expansion of IRMOF-1, meaning that ligands were exchanged for expanded (larger) ones and variously functionalized ones, but keeping the underlying topology of IRMOF-1. (Furukawa et al. 2013). The iso-reticular topology of these MOFs is typically referred to as primitive cubic net. Another example of iso-reticular topology expansion would be the case of MOF-177, a MOF synthesized by Zn<sub>4</sub>O nodes and 4,4',4''-benzene-1,3,5-triyl-tribenzoate ligands, that exhibits a qom topology. Exchanging the existing triangular organic ligands with larger-chain ones results in MOF-180 [ligand = 4,4',4''-(benzene-1,3,5-triyltris(ethyne-2,1-diyl))tribenzoate] and MOF-200 [ligand = 4,4',4''-(benzene-1,3,5-triyl-tris(benzene-4,1-diyl))tribenzoate]. The MOF-177 is comprised of Zn<sub>4</sub>O(CO<sub>2</sub>)<sub>6</sub> cores conjugated with tritopic 1,3,5-benzenetribenzoate linkers, in a structure that leaves a central cavity where desired molecules can be adsorbed. Substituting the existing linkers for larger linkers, like in the cases of MOF-180 and MOF-200, results in greater spacing in the cavity, and resulting in

materials that can store different molecules. The MOF-177 expanded structures are non-interpenetrative in contrast to MOF 5 extended topologies, highlighting the great value of selecting optimal topologies (Ullah et al. 2019).

### 1.3.6 Post synthetic modification

The versatility of MOF design from different building blocks, and their unprecedented tunability encourage the engineering of the MOFs to achieve very specific functions. Powder-form MOFs, MOFs stabilized on other materials, and Membranes based on MOFs find application in analysis (Fu et al. 2021). Some properties can be bestowed on the MOFs from the synthetic design as we saw previously, but in some cases, post synthetic modifications can introduce such functionalities that are not otherwise possible from the synthetic procedure (Chen and Zhao 2023). Their further use is sometimes limited by some factors like their instability in aqueous environments, non-eclectic behavior towards the desired molecule, or difficulty grafting on a substrate. The surface of the MOFs can be post-synthetically modified to achieve hydrophobic properties. In that manner, Zhu et al. proposed a surface functionalization of various MOFs with 1,2-dipalmitoyl-sn-glycero-3-galloyl, a lipid molecule with a long hydrophobic chain (Zhu et al. 2018).

Manipulating the architecture of the cavities of the MOFs can lead to a material with the desired interaction with target molecules. An example of post-synthetic modification is removing solvent molecules from the HKUST-1 structure, exposing Lewis acid-catalyzing metal sites. In a similar manner, MIL-101 can also act as a Lewis acid catalyst after the removal of some ligands (Alaerts et al. 2006). A plethora of MOFs have been used for heavy metal adsorption, the unmodified and their modified counterparts have been successfully utilized for the adsorption of Pb, Hg Cr, Cd and As ions. MOFs can be **functionalized** with groups such as amino, thiol, azine, and quinine among others, in order to improve their metal interactions. The functionalization of MIL-68 and NH<sub>2</sub>-MIL-53 with sulfur has been reported to lead to greater adsorption capabilities towards Hg<sup>2+</sup>. (Wen et al. 2018). In a case where the **charge** can inhibit the adsorption by means of electrostatic repulsion, post synthetic modifications can alter the MOF charge to the benefit of the adsorption. Reportedly, in the case of a Zn-MOF that contains the (4S,5S)-5-(pyridin-4-ylcarbonyl)-2,2-dimethyl-1,3-dioxolane-4-carboxylic acid ligand, pyridyl groups that are not used for cross-linking can be subjected to N-alkylation by using iodomethane or iodohexane, changing the charge from negative to positive. Likewise, 2-aminoterephthalate MOFs can be altered by reacting the amino group with acetic acid anhydride, to form amides (Janiak and Vieth 2010).

**Post-synthetic metathesis and oxidation** is another way to improve the performance of a MOF. The labile PCN-426-Mg, which was unstable even in water, was utilized as a template and through single crystal to single crystal transformation and subsequent air oxidation, PCN-426-Cr(III) and PCN-426-Fe(III) were received. PCN-426-Cr(III) was stable at pH = 1–12 and PCN-426-Fe(III) was stable at pH 4–10. The formation of chemically inert Cr(III)–O and Fe(III)–O bonds significantly improve the MOF stability when compared to the labile Mg–O bond (Pramanik et al. 2023).

When a MOF cannot be directly synthesized, **post-synthetic ligand exchange** can achieve the introduction of the desired ligands in an already synthesized MOF. Furthermore, this procedure can solve other issues with some MOFs. In the case of Zr- phosphonate MOFs, the direct affinity of the Zr and phosphonates leads to 2D densely packed layered structures with low porosity. This outcome that can be averted with spacers that introduce 3D steric hinderance, a method that is difficult and costly. On that front, Zr carboxylate MOFs have been used as templates, and in a post-synthetic ligand exchange they introduced a phenylphosphonate ligand but in a limited stoichiometric ratio, in order to preserve the MOF structure. It was found that using ligands with high steric hinderance like diphenylphosphinic acid can achieve stable MOFs after the ligand exchange without the strict stoichiometry (W. Zhang, A. Bu , Q. Ji , L. Min, S. Zhao, Y. Wang 2019).

### 1.3.7 MOFS in extraction of analytes and mechanisms of interaction

Solid phase extraction cartridges and other extraction devices are developed in conjunction with MOFs. In a recent review by Kotova et. al., the detection of carvacrol and thymol in food and plant samples was facilitated with a MOF composite where polyaniline was polymerized inside the pores of MIL-101(Cr) and distributed on the surface of the composite using silica microparticles, and the resulting material was packed into cartridges. The resulting solid phase extraction cartridges were comparable to the commercially available polydimethyl siloxane/polyaniline/SiO<sub>2</sub> cartridges, and were 11.5 to 22.5 times more effective for the extraction of carvacrol and thymol (Kotova et al. 2022). Furthermore, UiO-67 crystals have been used for the trace enrichment of phenoxyacetic acid herbicides, and a Zn-histidine MOF was used for the extraction of organophosphorus pesticides in groceries, as reported in the same review (Kotova et al. 2022). A more advanced MOF-based sorbent reported by Kotova et al. in their review, is a mixed matrix membrane where NH<sub>2</sub>-MIL-53(Al) is grafted on polyestersulfone and cross-reacted with L-Histidine to give chiral separation properties. The resulting material was used as an solid phase extraction cartridge

for chiral separation but was only limited to small molecules because of the pore size of the MOF (Kotova et al. 2022).

MOFs interact with the target adsorbents and their interactions are driven by adsorptive and size-dependent mechanisms. The adsorption can be divided into physical adsorption (adsorptive adsorption), and chemical adsorption (reactive adsorption) (Wen et al. 2018). Physical adsorption is primarily driven by electrostatic interactions, Van der Waals forces, diffusion (Wen et al. 2018), and other interactions such as Hydrogen bonds,  $\pi$ - $\pi$  stacking, and hydrophobic interactions (Wang et al. 2019a). Chemical adsorption includes coordination interaction, chemical bonding, and Lewis acid-base interactions (Wen et al. 2018). The Lewis acid-base interaction with the metal of the MOF can happen when a defect occurs by removing a ligand or a coordinating solvent molecule, and the resulting cavity enables the interaction (Perera et al. 2023). Finally, as mentioned previously, pristine MOFs have been modified to exhibit enantiomeric properties, and used for the development of **enantiomeric separation** membranes, such as the mixed matrix membrane polyestersulfone / NH<sub>2</sub>-MIL-53(Al)-L-histidine (Kotova et al. 2022).

### 1.3.8 MOFs in Microextraction

MOFs have been used as extracting phases for solid phase extraction and microextraction methods, coupled with chromatographic analysis. Multiple dispersive solid phase microextraction procedures have been developed using MOFs such as MIL-101(Cr) for hormone detection, MIL-101 for the detection of herbicides, UiO-66-NH<sub>2</sub> for the detection of Chlorophenoxy-acids and herbicides, HKUST-1 for the detection of parabens, NH<sub>2</sub>-MIL-53(Al) for the detection of phenol among multiple others (Ghorbani et al. 2019). The non-spherical structure and small average particle size of MOFs discourage their use as typical packed-sorbent solid phase extraction materials. Dispersive extraction methods can be valid alternatives, but they are also limited by the difficulties of the quantitative recovery of the nanomaterial afterwards by means of centrifugation or filtration. Thus, a common methodology is combining the MOFs with a magnetic nanoparticle and the usage of the resulting composite as a magnetic adsorbent. **Magnetic dispersive solid phase microextraction** has been developed as an alternative to the already established solid phase extraction as the magnetic nanoparticles that were dispersed in large volumes of sample, could be retrieved easily with the usage of an external magnetic field applied by a magnet. At the same time, magnetic dispersive solid phase microextraction has helped avoid some common solid phase extraction problems arising from the sorbent packing in the cartridges, like clogging of the packed bed and the usage of high

back pressures. This magnetic hybrid can be created either by the direct mixing of the MOFs and the magnetic nanoparticles, either in situ growth of the MOF in a mixture containing the magnetic nanoparticles and the MOF precursors (either single step, or layer-by-layer coating of the nanoparticles), magnetic nanoparticle, or by in situ growth of the magnetic nanoparticles in a mixture containing the reagents and an already synthesized MOF. Carbonization of MOF under an inert atmosphere can produce magnetic porous carbons that have also been utilized (Maya et al. 2017).

Examples of magnetic dispersive solid phase microextraction by using directly mixed MOFs and magnetic nanoparticles include the MIL-101(Cr) directly mixed with Fe<sub>3</sub>O<sub>4</sub>@SiO<sub>2</sub> magnetic nanoparticles as a way to detect polyaromatic hydrocarbons from lake water and wastewater, 4 pyrazole/pyrrole and pesticides, and UiO-66 directly mixed with carboxylic acid functionalized Fe<sub>3</sub>O<sub>4</sub>@SiO<sub>2</sub> for the detection of domoic acid (Maya et al. 2017). Various examples of MOFs grown in-situ on magnetic nanoparticles have also been reported and are compiled in the review of Maya et al. Some demonstrative examples include MIL-101(Cr)/Fe<sub>3</sub>O<sub>4</sub>@SiO<sub>2</sub> for estrogen extraction, the MIL-101(Fe)/Fe<sub>3</sub>O<sub>4</sub>@SiO<sub>2</sub>(functionalized with NH<sub>2</sub> group) for the extraction of organophosphorus pesticides from urine and hair samples, the MIL-101(Fe)/Fe<sub>3</sub>O<sub>4</sub>@ethylenediamine for the extraction of Cd<sup>2+</sup>, Pb<sup>2+</sup>, Zn<sup>2+</sup>, and Cr<sup>2+</sup> from agricultural samples, and the ZIF-8 grown in-situ on various magnetic nanoparticles used for the extraction of fungicides, phthalate esters, arsenic and polycyclic aromatic hydrocarbons (Maya et al. 2017). In a work by Saikia et al., Fe<sub>3</sub>O<sub>4</sub> nanoparticles were in situ grown on MIL-101(Cr) as an example of the magnetic nanoparticles grown in-situ on the MOF (Saikia et al. 2015). Magnetic porous carbons received from the direct carbonization of ZIF-67, Co(ZIF-8), and MIL-53(Fe) have also been reported in the same review (Maya et al. 2017). An example of their usage is the magnetic porous carbon derived from ZIF-67 that was used for neonicotinoid insecticides and phenylurea herbicides.

**MOF-based membranes** are used as another alternative to the solid phase extraction and provide miniaturized extraction conditions. In a typical procedure, the membranes are submerged in the sample where they extract the target molecules, and then they are mechanically separated from the sample without further complications or material loss in the process. This acts as a substitute for the magnetic dispersive solid phase microextraction and avoids the use of magnetic composites. The simplest membranes are the pure **MOF crystalline membranes** that exhibit permanent porosity without the need for modifications or support, but some of them are lacking in mechanical strength and flexibility, the second type of membranes are the **MOF/polymer composite mixed matrix membranes**, and finally the membranes created by **MOF-coated substrates**, with some substrates being flexible organic membranes or inorganic oxide solids (Fu et

al. 2021)(Perera et al. 2023). In that manner, MOFs can be stabilized in the pores of a porous polymer material such as the PPHFs, via physical adsorption, and used as adsorbents for microextraction. Fu et al., also report the filling of the nanochannels of Bullet-shaped single polyethylene terephthalate membranes with a post-sulfonated UiO-66-derivative (Fu et al. 2021). The sub-nanometer MOF channels have been used for the molecular sieving of  $H^+$  ions, with selectivity over other monovalent ions such as  $Na^+$ ,  $Li^+$ , and  $K^+$ . MOF membranes that can separate ions of the same valence, as well as similar sizes, are lacking. Such a membrane was reportedly fabricated by Wang's group and reviewed by Fu et. al., it is an ultrathin ZIF-8 membrane fabricated by a nano-porous Graphene oxide-assisted interfacial growth method on an anodic aluminum oxide substrate. It was used for the ultrafast selective transport of alkali metal ions and could selectively transport  $Li^+$  ions through as opposed to  $Rb^+$ , achieving a  $LiCl/RbCl$  selectivity of 4.6, as opposed to the 0.6 of conventional membranes (Fu et al. 2021). Chiral separation MOF membranes were also proposed for the selective separation of S-methyl phenyl sulfoxide over the R-enantiomer, giving way to a chiral selectivity never before possible (Fu et al. 2021). MOF-coated substrates such as stainless-steel fibers are being utilized as mediums for microextraction, the MIL-88B has been stabilized on stainless steel fibers and used for the microextraction of polychlorinated biphenyls (Wu et al. 2014), Zhang et al have also modified a stainless steel fiber with MIL-88B-graphene oxide and utilized it for the microextraction of phthalic acid esters from vegetable oils (Zhang et al. 2018). The desired MOF may exhibit difficulty in grafting on the desired substrate. To help with that, the substrate surface can be modified before the MOF grafting, as it is reported in the review by Zhang et al. for the MIL-88(Fe)/GO-coated stainless steel fibers (Zhang et al. 2018).

### 1.3.9 Materials institute Lavoisier (MIL)

MILs are MOFs synthesized by the institute of Lavoisier. They find use in the detection and removal of phenols, organic dyes, herbicides, insecticides, and medical products, among many others (Keshta et al. 2023). They are a class of MOFs that excel over common MOFs such as HKUST-1 and MOF-5 as they are more stable in water, so they have been developed for detection in water samples. Their usage extends to the field of catalysis, as the aforementioned hydrothermal stability allows the use in environments where other MOFs would suffer severe structural degradation (Wang et al. 2016). Common MILs are listed in Error! Reference source not found. and make use of various central metal ions and organic ligands. They can be synthesized by employing various synthetic methods such as solvothermal synthesis, hydrothermal synthesis, microwave-assisted synthesis, electrochemical synthesis, ultrasonic assisted synthesis, and mechanochemical synthesis. An example of such material is the MIL-101(Cr) a chromium-based cage-like

framework with mesoporous structural characteristics proposed by Férey et al. in 2005 (Férey et al. 2005). The metal center consists of chromium oxide clusters that are linked by amino-terephthalic acid (**NH<sub>2</sub>-H<sub>2</sub>BDC**) linkers. Those linkers contain an aromatic ring, enabling the post-synthetic functionalization of the resulting MOF. Coupling that with the stability it exhibits in acidic mediums, makes MIL-101(Cr) an excellent material (De Decker et al. 2015). A MIL codenamed MIL-88B is a MOF solvothermally reacted from FeCl<sub>3</sub> and H<sub>2</sub>BDC in an autoclave and is a safer option as it is replacing the toxic chromium metal clusters. Replacing H<sub>2</sub>BDC with NH<sub>2</sub>-H<sub>2</sub>BDC results in the amino MIL-88B (NH<sub>2</sub>-MIL-88B) (Li et al. 2021). The NH<sub>2</sub>-MIL-88B needle-shaped crystals are reported to have a length of 1,5 μm and 300nm width (Ma et al. 2013). The structure of NH<sub>2</sub>-H<sub>2</sub>BDC as reported in the work of (Bauer et al. 2008) can be seen in **Figure 3**.

Microextraction methods have been developed by using MIL-88B as is in dispersive solid phase microextraction methods (Pezhhanfar et al. 2022) and by loading it on fibers (Zhang et al. 2018) (Wu et al. 2014). Zhang et al. etched MIL-88B with citric acid to create multi-shelled ringnet hollow MIL-88B and then they loaded it on stainless steel fibers (Zang et al. 2023). In the same vein, the NH<sub>2</sub>-MIL-88B is utilized for microextraction methods (Wang et al. 2023b).

**Table 5:** *Common MIL MOFs, as reviewed by (Zhang et al. 2022a)*

<b>MIL</b>	<b>Central metal</b>	<b>Organic ligand</b>
<b>MIL-53</b>	Cr, Fe, Al	H <sub>2</sub> BDC
<b>MIL-68</b>	In, Ga, Fe, V	H <sub>2</sub> BDC
<b>MIL-88A</b>	Fe	Fumaric acid
<b>MIL-88B</b>	Fe	H <sub>2</sub> BDC
<b>MIL-100</b>	Cr, Fe, Al	Trimesic acid
<b>MIL-101</b>	Cr, Fe, Al	H <sub>2</sub> BDC
<b>MIL-125</b>	Ti	H <sub>2</sub> BDC

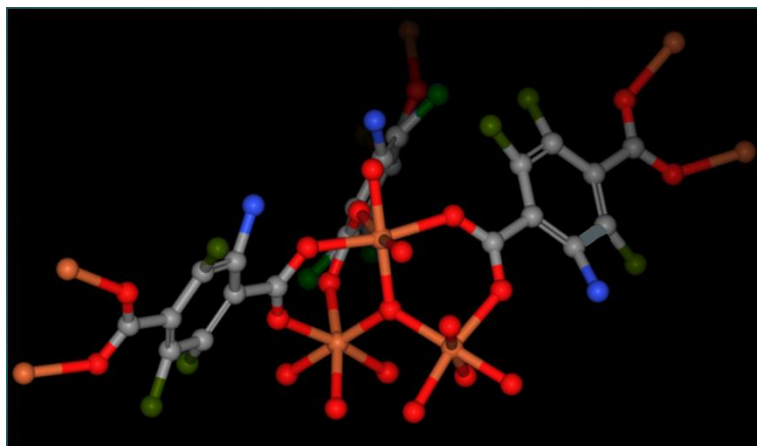


**Figure 3:** 3D depiction of the NH<sub>2</sub>-MIL-88B structure. The elements are depicted as colored bars and balls: carbon (grey), nitrogen (blue), oxygen (red), iron (orange), hydrogen (green).

NH<sub>2</sub>-MIL-88B is often used for the photocatalytic degradation of various compounds and can also find application in electrochemical sensors. An example is the electrochemical sensor for Cd<sup>2+</sup>, Pb<sup>2+</sup>, and Cu<sup>2+</sup> ions, where the detection is facilitated as the lone pair electrons of the amino group act as a Lewis base and coordinate with the heavy metal ions (Tran et al. 2023a). It is reportedly used as an adsorbent for remediation of water from 2,4,6- trinitrophenol, by interaction of the -OH groups and unsaturated Fe<sup>3+</sup> on the MOFs' surface (Guo et al. 2019). Furthermore, NH<sub>2</sub>-MIL-88B is reported as an adsorbent for dyes and medicinal products (Keshta et al. 2023). Although there is a large body of bibliography for the adsorption of various analytes on NH<sub>2</sub>-MIL-88B, it is coupled with photocatalysis and rarely, if ever, used for detection.

MIL-88B and NH<sub>2</sub>-MIL-88B are used as delivery agents and carbon monoxide carriers, because of the low toxicity of terephthalate ions and the bio-metal iron (Ma et al. 2013) Furthermore, in a post-modification procedure, heating at 373 K under a stream or a vacuum can remove non-bridging ligands, in an activation process that creates Lewis acidic sites that can attract and store carbon monoxide. (Ma et al. 2013). A NH<sub>2</sub>-MIL-88B-carbon dot/ graphene oxide composite was loaded on Polyvinylidene fluoride fibers to create composite membranes for the separation of dyes from samples (Li et al. 2021).

## 1.4 Aim of the work

The development of pretreatment methods for target analytes, featured by ease of use, low cost and greener practices are always a primary objective. In this context, we aimed to develop a PPHF supported NH<sub>2</sub>-MIL-88B MOF, thus providing a facile and easy way to extract and separate the material from the solution. The NH<sub>2</sub>-MIL-88B was stabilized on the exterior porous structure of the hollow fiber, via physical adsorption, and using it as an adsorbent. The great porosity of the PPHFs aids in the stabilization of the material, and as opposed to the older methodologies, the analytes do not have to penetrate the PPHF membrane to get adsorbed in the material in the center. We then used the as-prepared modified fibers as an easy cheap and fast way to adsorb a cocktail of hazardous pollutants from the classes of benzophenones, nitrophenols and parabens and determine them by HPLC-photodiode array (PDA) detection.

## Chapter 2 Experimental

### 2.1 Chemicals and reagents

For the conducted experiments the reagents used were all at least of analytical grade. Anhydrous Iron (III) chloride (FeCl<sub>3</sub>) was purchased from Fisher chemicals, H<sub>2</sub>BDC and H<sub>2</sub>NH<sub>2</sub>BDC were purchased from Alfa Aesar, and sodium chloride (NaCl) was purchased from Merck. The analytes used were ethyl-paraben (Eth-PB), butyl-paraben (Bu-PB), propyl-paraben (Pr-PB), 2-nitrophenol (2NP), 3-methyl-4-nitrophenol (3Me-4NP), benzophenone-2 (BP2), benzophenone-3 (BP3), 4-hydroxybenzophenone (4OH-BP), benzophenone-6 (BP6) and benzophenone-8 (BP8) and were purchased from TCI chemicals and Merck. Information such as  $pK_a$ , the retention time on the chromatographic column,  $\text{Log}P_{ow}$ , the wavelength used for compound quantification, the chemical structures and the CAS number of the substances are compiled in **Table 1-3**. Stock standard solutions of 1000  $\mu\text{g}/\text{mL}$  were prepared in the laboratory, by weighing precisely 10mg of each analyte on an analytic scale and subsequently dissolving that in 10 mL of acetonitrile. The working mixtures of our analytes were prepared in ultrapure water and stored in the refrigerator for one week. All the solvents used were at least of analytical grade and the water used was ultrapure produced in the lab by a simplicity UV water purifier. In detail, N, N Dimethylformamide (DMF), and methanol (MeOH) were purchased from Fisher Chemicals and the Formic acid (FA) and ammonia (NH<sub>3</sub>) were purchased from Sigma Aldrich. The PPHFs were supplied from MEMBRANA GmbH and the helium used for the degassing of the mobile phase in the HPLC was of purity 99,999 %. The Q 3/2 Accurel PPHF membrane (600 mm i.d.,

200 mm wall thickness, 0.2 mm pore size) was purchased from Membrana GmbH (Wuppertal, Germany). The porous PPHF was cut into pieces of 4 cm long.

## 2.2 Instrumentation

The following is a full list of the equipment used during the conducted the experiments:

- Parr autoclave lined with teflon
- LAC furnace (LE laboratory chamber furnace)
- Magnetic stirrer AGE (Velp Scientifica)
- PHM83 Autocal pH-meter (Radiometer, Copenhagen, Denmark)
- Miniplus 3 peristaltic pump (Gilson, Middleton, Wisconsin)
- Vacuum pump (Buchi B-169, Switzerland)
- Analytical balance (Shimadzu, Tokyo, Japan)
- Double water distillation apparatus (Aquatron, A4D, BIBBY Scientific Ltd., UK)
- Filtration apparatus (Millipore Corporation Billerica, USA)
- Emmi-D30 ultrasonic bath with drain tap (EMAG, Germany)
- Test tube vortex shaker TK3S (Technokartell, Italy)
- Pro-research centrifuge (centurion science Ltd)
- Nitrogen generator (N<sub>2</sub>) micro nitrogen generator (Claind S.r.l., Lenno, Italy)
- X-ray diffractometer (XRD) D8 advance from bruker AXS (Madison, USA) with CuK $\alpha$  radiation ( $\lambda = 1,5406 \text{ \AA}$ )
- Scanning electron microscope (SEM) JSM 5600, operating at 20 kV (Jeol, Nieuw-Vennep, Netherlands),
- Spectrum Two FTIR using an attenuated total reflectance (ATR) accessory (PerkinElmer, MA, USA)
- Nano zetasizer (Nano ZS, Malvern, Herrenberg) with dynamic technology scattering ( Dynamic Light Scattering, DLS) for the determination of the hydrodynamic diameter and measurement of the  $\zeta$ -dynamic.
- High Performance Liquid Chromatography System (HPLC) for the separation and quantification of compounds, manufactured by Shimadzu (Shimadzu, Kyoto, Japan), consisting of:
  - i. Degassing system with helium supply (99,999% purity)
  - ii. LC20AD pump with integrated solvent mixer
  - iii. Manual sample injection loop with a volume of 20  $\mu\text{L}$

- iv. Hypersil BDS C18 chromatographic column (200 mm × 4,0 mm, MZ-Analysentechnik, GmbH, Germany) with particle size of the material filler material at 5 µm
- v. CTO 10AS thermostatic system, maintaining a constant temperature of the column at 30°C
- vi. Diode array detector (SPD-M20A DAD), tuned to a wavelength range of 200 to 360 nm
- vii. A personal computer for the collection and processing of the data using the LC-solution software version 1.21

The software used for data acquisition and post-run processing was Shimadzu's Lab Solutions, LC-solution version 1.21.

## 2.3 NH<sub>2</sub>-MIL-88B synthesis

The NH<sub>2</sub>-MIL-88B was synthesized using the same method presented in the work of Li et al, with minor modifications (Li et al. 2021). Specifically, 0.225 g of NH<sub>2</sub>-H<sub>2</sub>BDC and 0.4055 g of anhydrous FeCl<sub>3</sub> were weighed in an analytical balance and subsequently each of them was dissolved in 7.5 mL of DMF. The prepared solutions were then homogenized in an ultrasound bath for 10 min and subsequently they were mixed in a Teflon autoclave before being placed in a furnace at 110°C, for 24 hours. The prepared material was received by centrifugation and washed 3 times with DMF and 3 times with methanol before being left to dry overnight at 60°C. The synthesis of NH<sub>2</sub>-MIL88B is depicted in **Figure 4**.

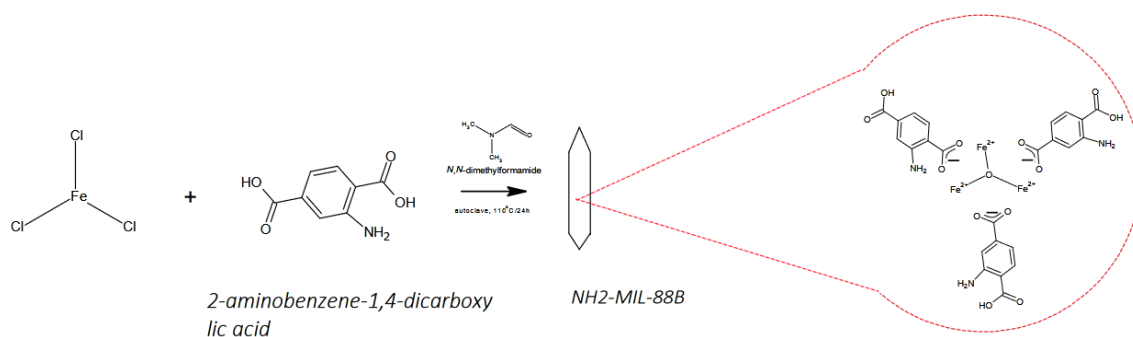


**Figure 4** : NH<sub>2</sub>-MIL88B synthesis as proposed by (Li et al. 2021).

## 2.4 Characterization of the material

The synthesized material NH<sub>2</sub>-MIL88B was characterized using **X-ray diffraction analysis**. The average hydrodynamic size of the MOF and its  $\zeta$ -potential were measured using the dynamic light scattering (**DLS**) technique. The instrument we used was the Nano Zetasizer, using suitable Malvern cells, at 25°C. Images that more accurately measure the particle size were taken using the scanning electron microscope (**SEM**). Elemental mapping of the material, the unmodified and the modified fibers was conducted by **energy-dispersive X-ray spectroscopy**, and the IR spectrum of the material was received using an **FTIR-ATR spectroscopy**.

## 2.5 Loading of NH<sub>2</sub>-MIL88B on fibers

The NH<sub>2</sub>-MIL88B MOF was used to modify the PPHFs. The sorbent was deposited to the external surface of the fiber by submerging it in a suspension. During aspiration, the methanolic suspension of NH<sub>2</sub>-MIL88B MOF was stirred to ensure homogenous and reproducible deposition of the layer on the membrane. Only the solvent of the suspension passed through the pores of the PPHF, uniformly depositing the material on the porous structure of the PPHF, creating a thin film. The PPHF on the end of the peristaltic tube modified tip was then submerged completely in the NH<sub>2</sub>-MIL88B suspension that was propelled to the fiber via a peristaltic pump. The pump flow rate and pumping time of the peristaltic pump were kept constant to ensure that the coated fibers were comparable to each other. The resulting coated fibers were dried up and weighed in an analytical balance with a precision of 0.1 mg, and the outliers were discarded. The PPHF modification is graphically presented in **Figure 5**.

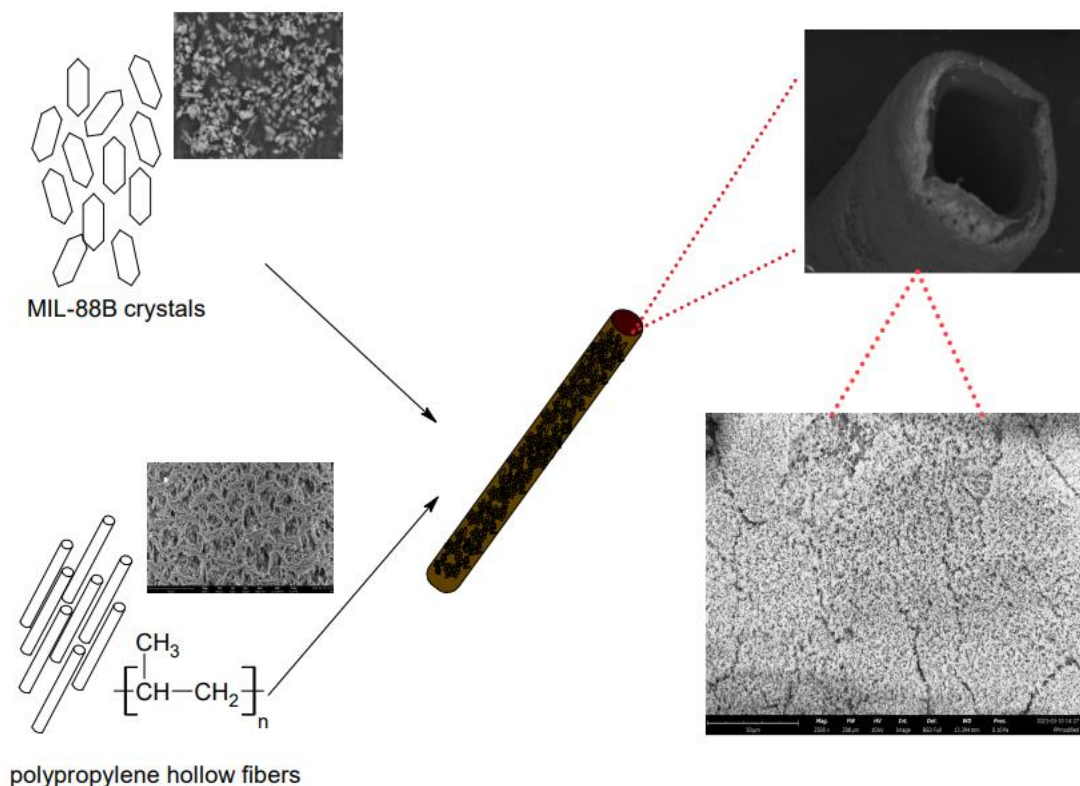


**Figure 5** : The PPHF modification procedure.

## 2.6 Extraction procedure

A home-made setup made of pharmaceutical needles attached to an arm was set up in the laboratory. The extraction procedure is depicted in **Figure 6**. Three fibers were assembled and submerged in a 70-mL sample containing NaCl 5 M, at pH=7.5. The extraction was performed with stirring at 500 rpm, for 35 min, using a magnetic stir bar, at ambient temperature (25°C). The experimental conditions were previously optimized.

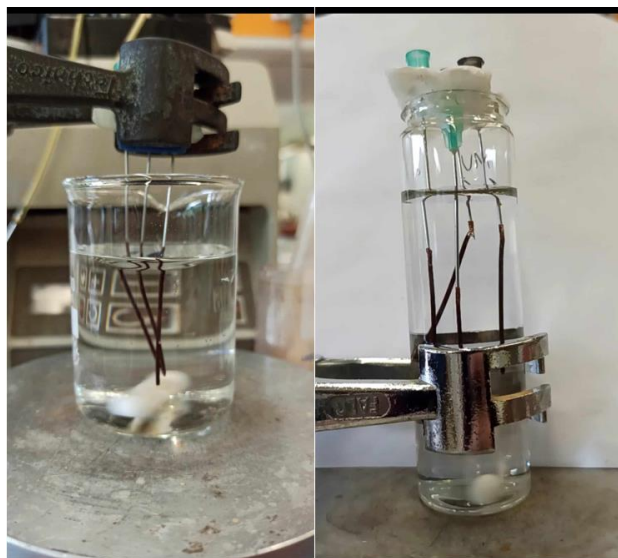


*Figure 6: Extraction procedure using 70 mL sample (left) and 25 mL sample (right).*

## 2.7 Elution process

The PPHFs used for the extraction were withdrawn from the solution and left to dry at ambient temperature to remove excess water and subsequently cut and placed inside an Eppendorf vial. The elution of the analytes was facilitated by the addition of 1 mL of MeOH and ultrasonication for 3 min in an ultrasound bath. The ultrasonicated sample was concentrated with the help of a nitrogen stream until it reached 160  $\mu$ L of final volume. Then, the sample was filtered and 20  $\mu$ L was injected into the HPLC system.

## 2.8 Chromatographic analysis

The chromatographic analysis was completed in 60 minutes and the results were evaluated in the post-run program of the software.

- The mobile phase consisted of water (A) and acetonitrile (B), whose pH was adjusted to 2,5 by the addition of 0,1 % formic acid. The flow rate of the mobile phase was set at 1,0 mL min<sup>-1</sup>. For the separation of the analytes, a gradient elution program was used. The chromatographic program, with a total time of 60 min, was the following:

- Initially 10% B, increasing to 90% B over 50 min and back to 10% B until the 60 min

As it was about a gradient elution program, 30 min were needed to re-equilibrate at the starting conditions.

## 2.9 Real samples

In order to validate the applicability of the present analytical methodology, real samples of lake water taken from Lake Pamvotis, Ioannina, Greece, seawater taken from Lefkada, Greece, and treated wastewater outflow of the biological treatment in Ioannina, Greece. The samples were filtered through a membrane filter (Whatman ME 25/21 ST) to remove suspended particles and stored in a flask with a screw cap, at 4°C. Before use, they were left to reach ambient temperature and were analyzed according to the procedure described in the sections [2.6](#) - [2.7](#) - [2.8](#). For the recovery experiments, the samples were spiked with the analytes of interest (2NP, 3Me-4NP, Eth-PB, Pr-PB, Bu-PB, BP2, 4OH-BP, BP8, BP6, and BP3) by using standard solutions of BPs, NPs, and PBs in acetonitrile. The seawater had an innate salinity of 35 mg/mL, so in a typical 70 mL sample 2450 mg are already present, so less NaCl had to be added in the case of the seawater.

## 2.10 Multivariate experiments

The experiments were done following a central composite design. The software we used to analyze the data was Statistica 13 (StatSoft, Tulsa, OK, USA). This will be further discussed in the section [3.3.6](#).



## Chapter 3 Results and discussion

### 3.1 Preliminary experiments

MIL-88B was chosen as it is easy to synthesize while both the reactants as well as the products were safe and could be easily and safely disposed of. Also, belonging to the class of MILs they exhibit great water stability. We chose NH<sub>2</sub>-MIL-88B over MIL-88B as it was more stable when loaded on the PPHFs.

For the optimization of the synthetic procedure, we chose that method which yielded higher of the product and exhibited ease of operation. A reflux synthetic methodology for the NH<sub>2</sub>-MIL-88B was tried out but it was rejected because it was difficult to monitor the exact temperature, it was more time-consuming as it needed 48h to complete, and the final yield was not sufficient. The method we chose was that proposed by Li et al. as it had an adequate yield (Li et al. 2021).

#### 3.1.1 Loading of NH<sub>2</sub>-MIL-88B on the fibers

For the modification of the fibers, 100 mg of the NH<sub>2</sub>-MIL88B were suspended in 10 mL of MeOH. The suspension was prepared by means of weak ultrasonication for 10 sec and passed through the PPHF with the help of a peristaltic pump. To the one end of the tube of the peristaltic pump was adapted a needle which was fit in the open end of the PPHF, while the other end was firmly closed. The pumping time and rate were adjusted to achieve the desired weight of coating. The choice of MeOH as a solvent instead of H<sub>2</sub>O and ethanol was made because it was less viscous and thus could easily pass through the pores of the PPHFs.

### 3.2 Characterization of the material

The material was characterized by means of infrared spectroscopy (IR) and X-ray diffraction spectroscopy, while images of the structure were taken with the help of a scanning electron microscope. An elemental mapping of the NH<sub>2</sub>-MIL-88B material and the NH<sub>2</sub>-MIL-88B-modified fibers was accomplished using the energy-dispersive X-ray spectroscopy. The point of zero charge as well as the average size of the nanomaterial were examined via the dynamic light scattering technique.

### 3.2.1 Infrared spectroscopy (IR)

The infrared spectrum of NH<sub>2</sub>-MIL-88B was inspected and the peak identification was facilitated by comparing the peaks with the peaks of the material referenced in the bibliography. A weak and broad peak at 3327 cm<sup>-1</sup> is caused by the oscillatory stretching of the N-H bond present in the NH<sub>2</sub>-H<sub>2</sub>BDC ligands. Further inspection reveals that the characteristic symmetrical and asymmetrical vibrations of the carbonyl group bonds at 1380 cm<sup>-1</sup> and 1577 cm<sup>-1</sup> are present, as well as a peak attributed to the -NH<sub>2</sub> bending and stretching at 1600 cm<sup>-1</sup> that is hidden behind the strong carbonyl peak at 1577 cm<sup>-1</sup>. The C-N bending at 1255 cm<sup>-1</sup>, and the C-H vibrations at 1161 cm<sup>-1</sup>, both correspond to the peaks reported in the literature (Yuan et al. 2019) (Tran et al. 2023b). The absence of a characteristic peak for the protonated carboxylic acids at around 1710 cm<sup>-1</sup> indicates that the carboxylic ligands present in the NH<sub>2</sub>-H<sub>2</sub>BDC are deprotonated and fully coordinated with the Fe<sup>3+</sup> ions provided from the FeCl<sub>3</sub>. The band at 767 cm<sup>-1</sup> is most likely caused by out-of-plane and in-plane bending of the -COO groups (Guo et al. 2019). The peak at 554 cm<sup>-1</sup> is most likely indicative of the Fe-O vibrations, and the infrared spectrum we received is presented in **Figure 7**.

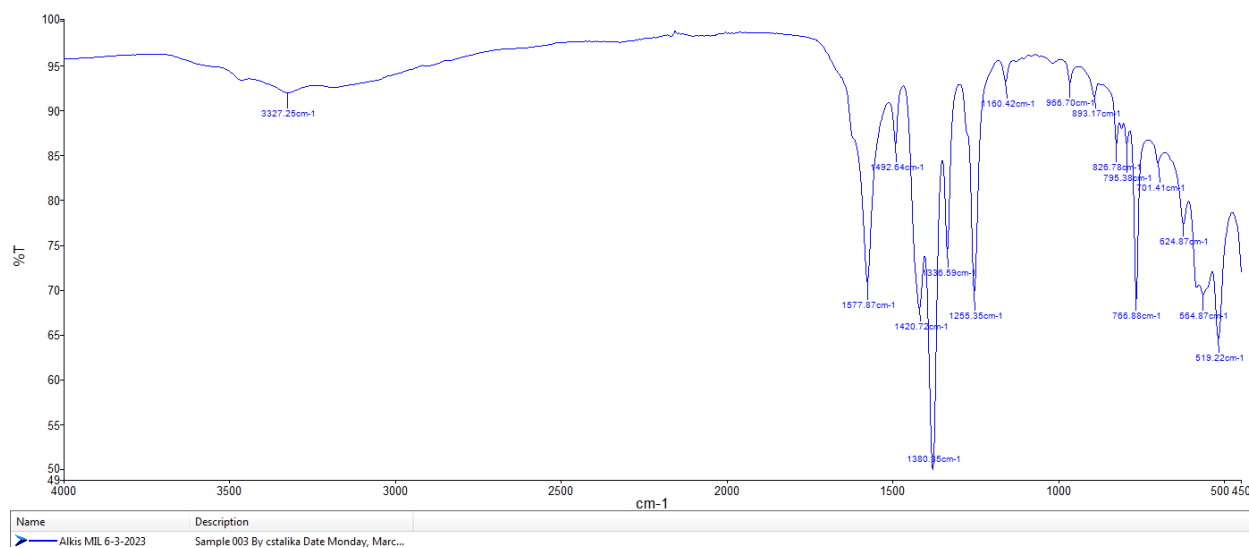


**Figure 7:** Infrared spectrum of NH<sub>2</sub>-MIL-88B.

### 3.2.2 X-ray diffraction spectroscopy (XRD)

The x-ray diffraction (XRD) of the NH<sub>2</sub>-MIL-88B was obtained and is presented in **Figure 8**. The characteristics of its crystalline lattice were compared with the ones reported in the bibliography. The characteristic 2 $\theta$  peaks are all present, namely 9.008°, 10.19°, 12.92°, 16.5°, 18.46°, 19.11°, 20.68°, 26.27°, 29.50° similar to the peaks reported in the bibliography (Li et al. 2021, Tran et al. 2023). The two characteristic peaks for NH<sub>2</sub>-MIL-88B appear at 9.3° and 10.6°, angles that correspond to the lattice faces of (002) and (101) respectively (Tran et al. 2023b). We can see in **Figure 8** that similarly to the reported XRD peaks for the angles of 9.3°, and 10.6°, the XRD spectrum of synthesized material exhibits similar peaks at 9.008, and 10.19°. The remaining peaks are most likely caused from unreacted FeCl<sub>3</sub> (Tran et al. 2023b).

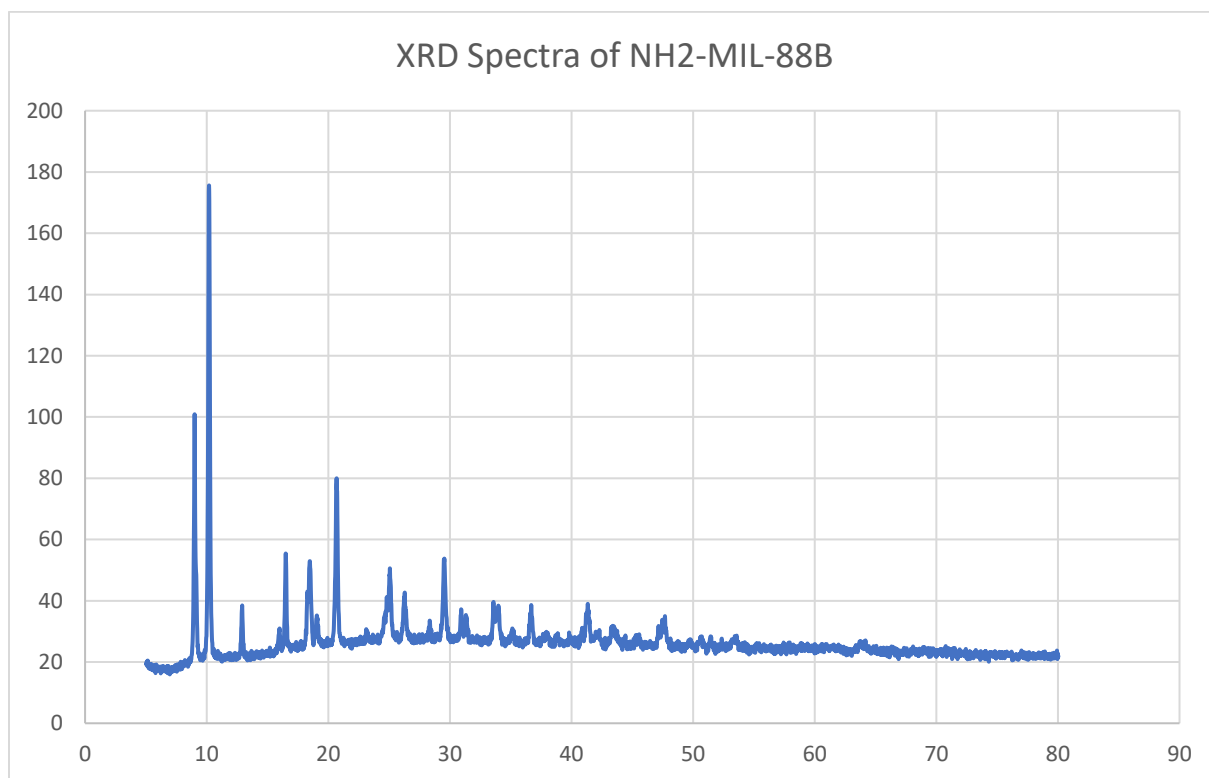


**Figure 8:** XRD Spectra of NH<sub>2</sub>-MIL-88B

### 3.2.3 Scanning electron microscope (SEM)

Images of the NH<sub>2</sub>-MIL-88B, the PPHFs, and the NH<sub>2</sub>-MIL-88B-modified PPHFs were taken with Scanning Electron Microscopy (SEM). For the SEM images, well-washed and dried material, a piece of unmodified PPHF, and a piece of the modified NH<sub>2</sub>-MIL88B-PPHF were sampled. The images can be seen below, and they confirm the expected rhomboid-like, spindle-shaped grains of the material as it is seen in the bibliography. Also, images give us an estimate of the dimensions of the crystals (Tran et al. 2023b). As can be seen from **Figure 10**, the crystals possess two dimensions of roughly 400-500 nm length and a dimension of 150-170 nm length. **Figure 11**, **Figure 12** and **Figure 13** present the SEM images of the unmodified PPHF at different magnification scales. **Figure 14** and **Figure 15** depict the modified PPHFs at magnification scales of 300  $\mu\text{m}$  and 500  $\mu\text{m}$  respectively. while **Figure 16** and **Figure 17** depict the NH<sub>2</sub>-MIL-88B crystals that are adsorbed on the surface of the PPHF, in magnifications of 10  $\mu\text{m}$  and 5  $\mu\text{m}$  respectively.

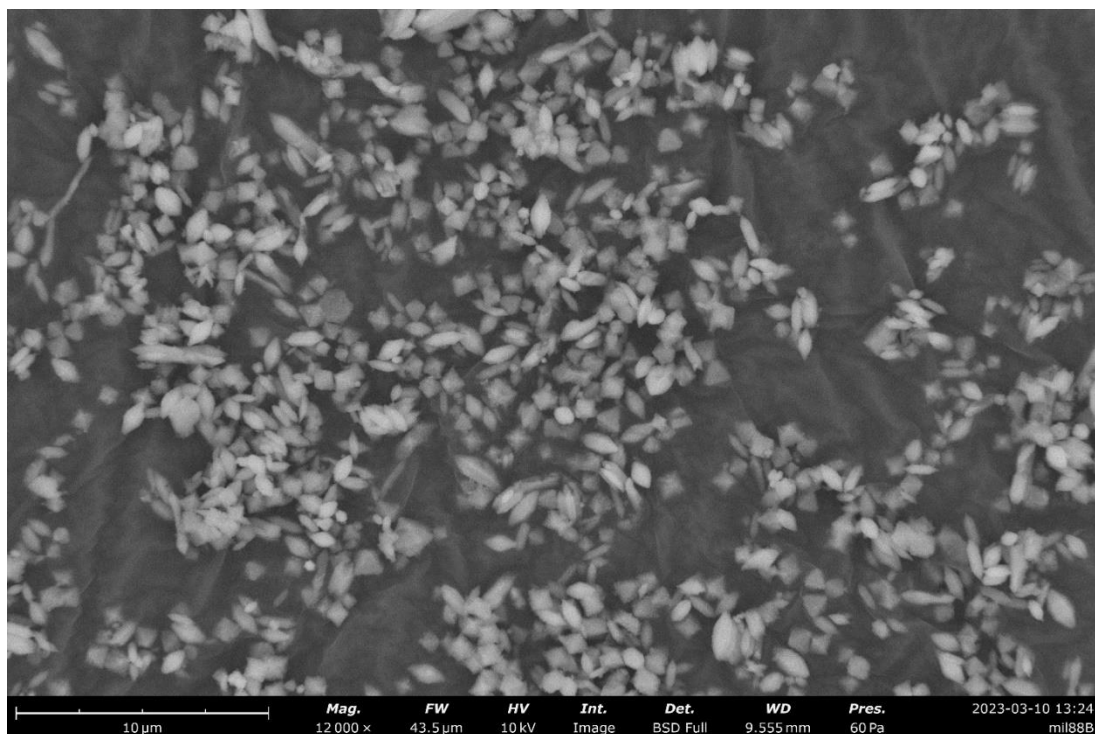


**Figure 9:** SEM image of NH<sub>2</sub>-MIL-88B.

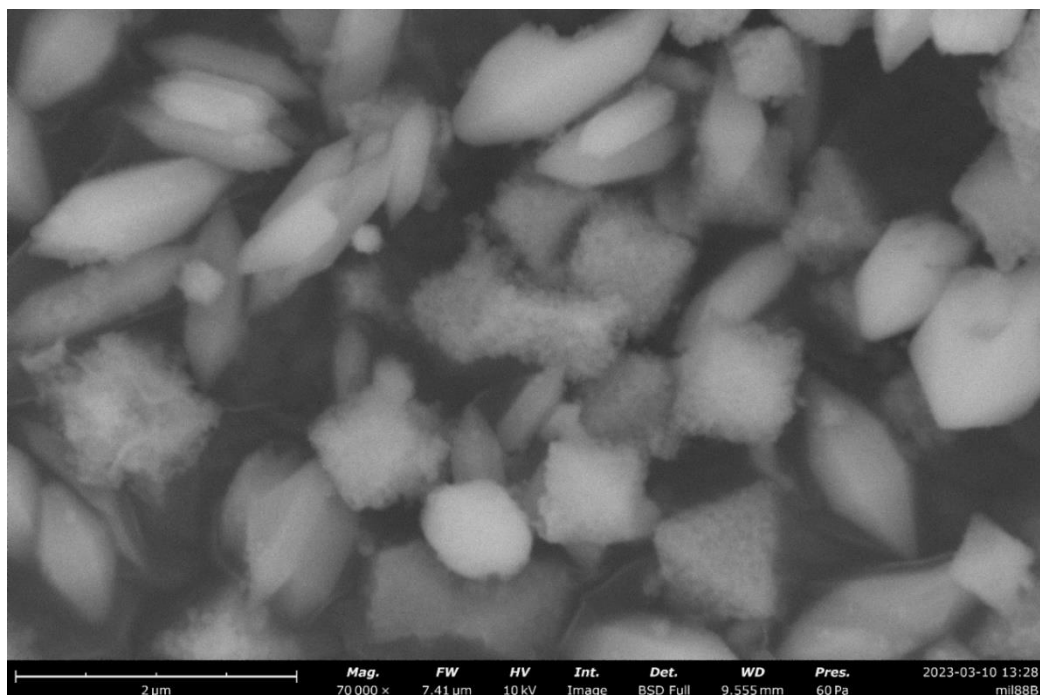


**Figure 10:** SEM image of NH<sub>2</sub>-MIL-88B.

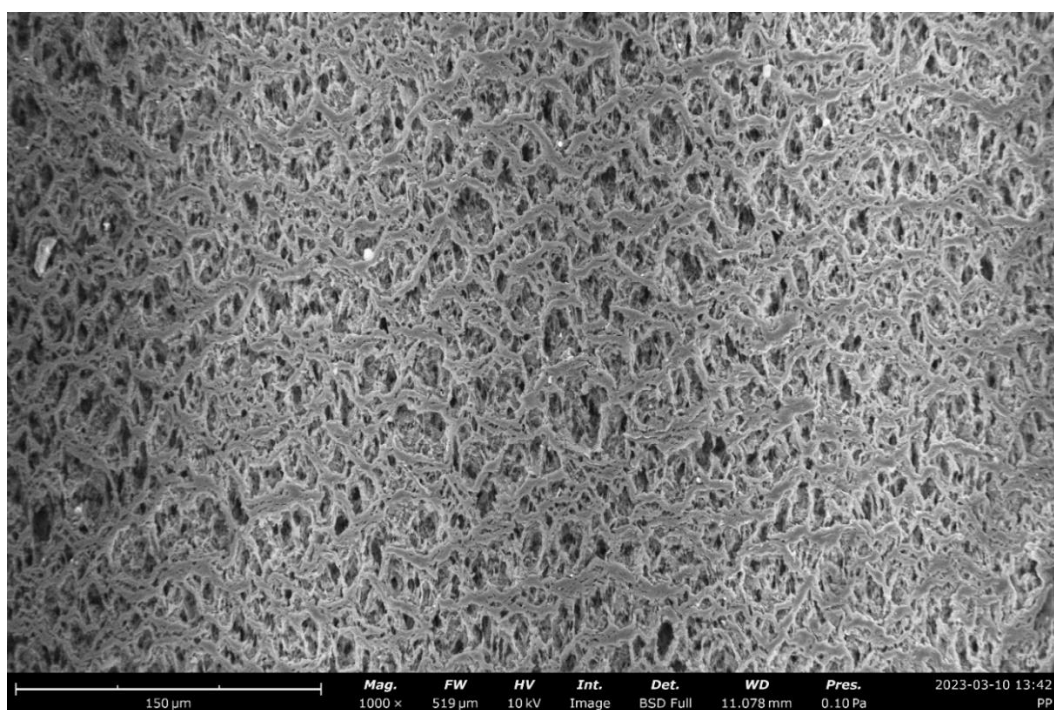


**Figure 11:** SEM image of the unmodified PPHF.

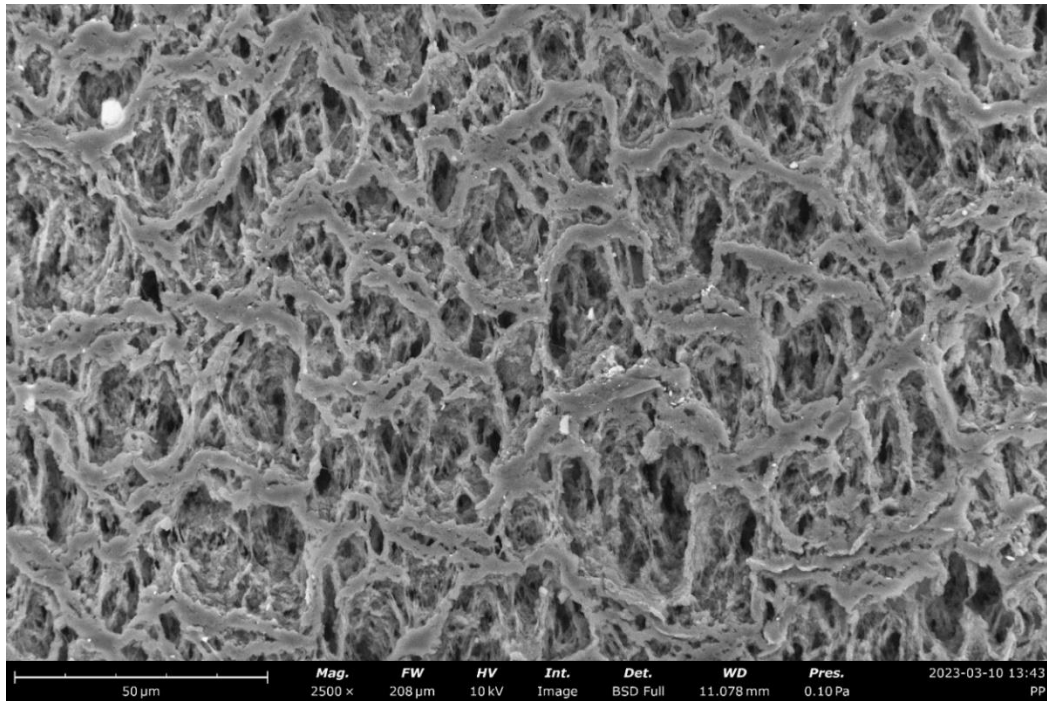


**Figure 12:** SEM image of the unmodified PPHE.

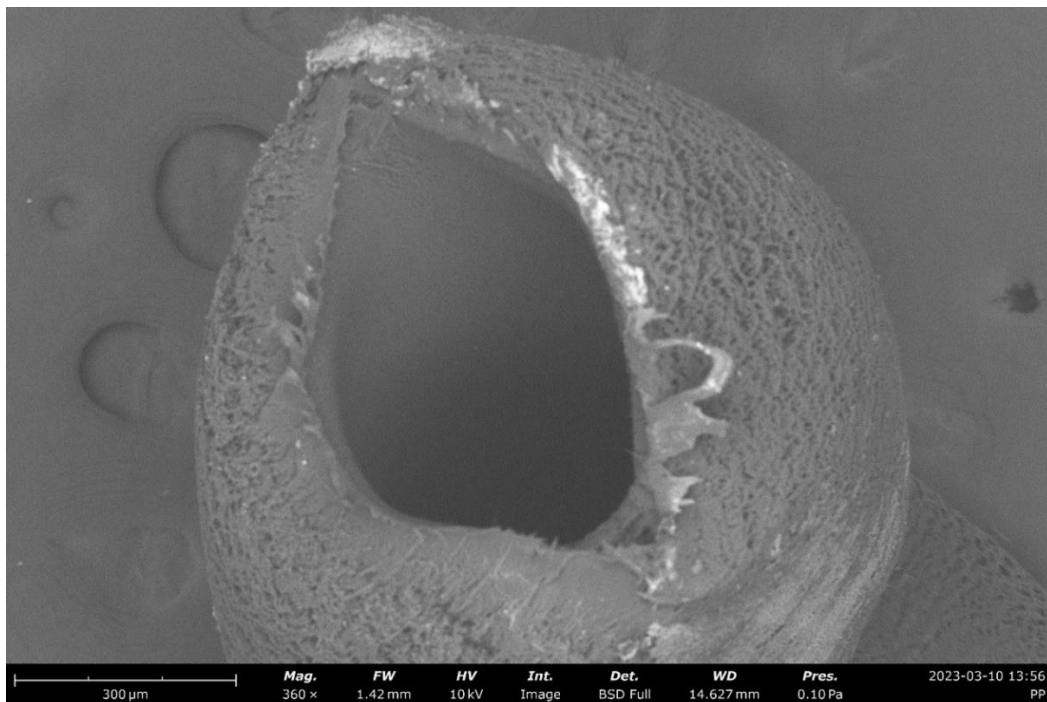


**Figure 13:** SEM image of the unmodified PPHE.

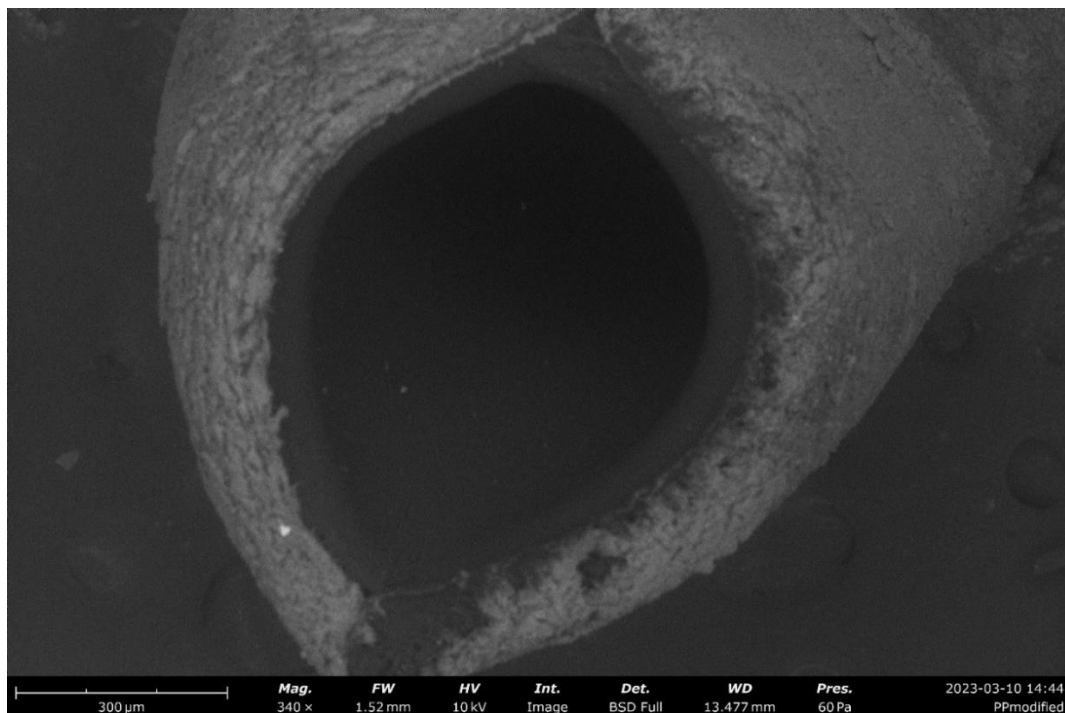


**Figure 14:** SEM image of the NH<sub>2</sub>-MIL-88B-modified PPHF.

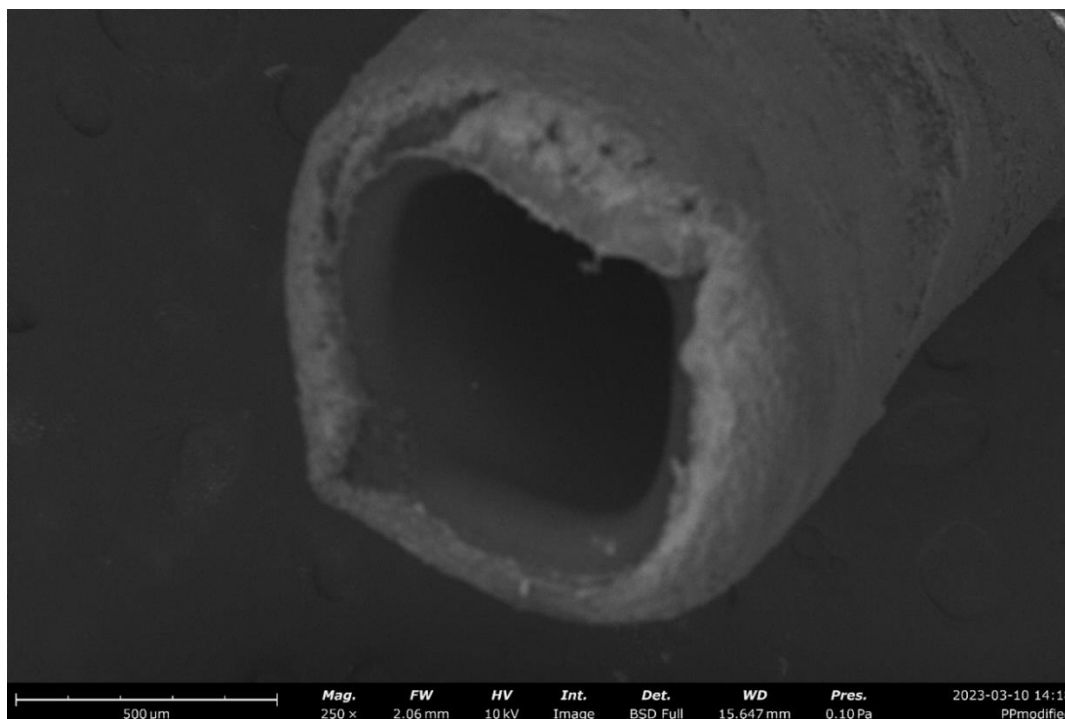


**Figure 15:** SEM image of the NH<sub>2</sub>-MIL-88B-modified PPHF.

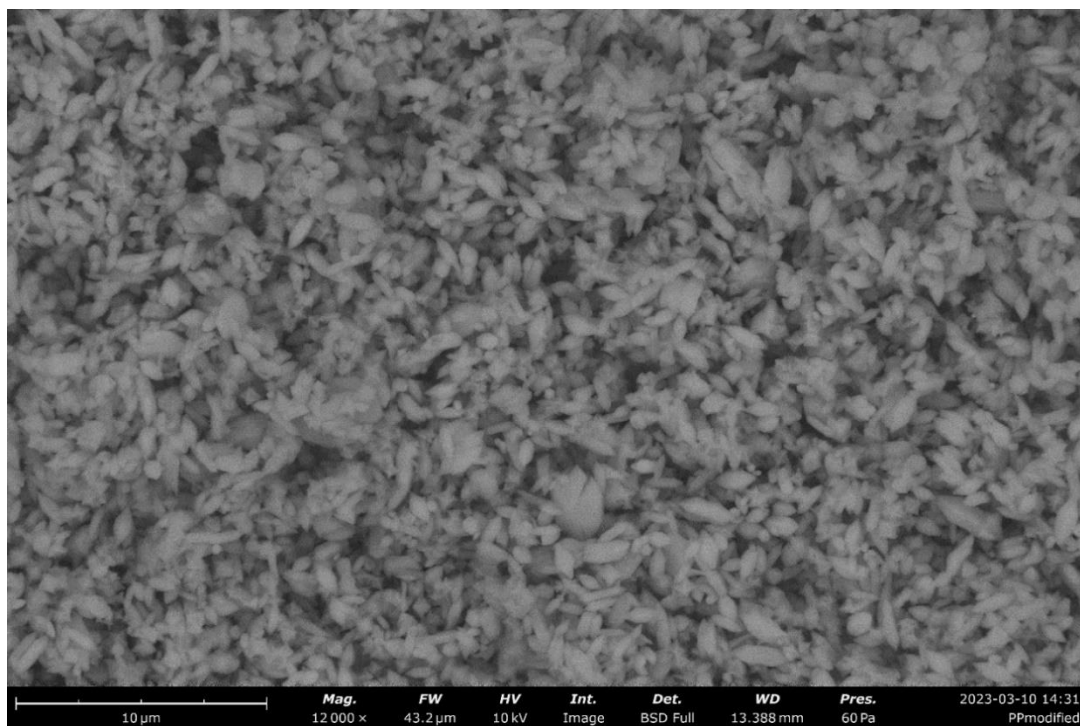


**Figure 16:** SEM image of the adsorbed NH<sub>2</sub>-MIL-88B of the surface of the PPHF.

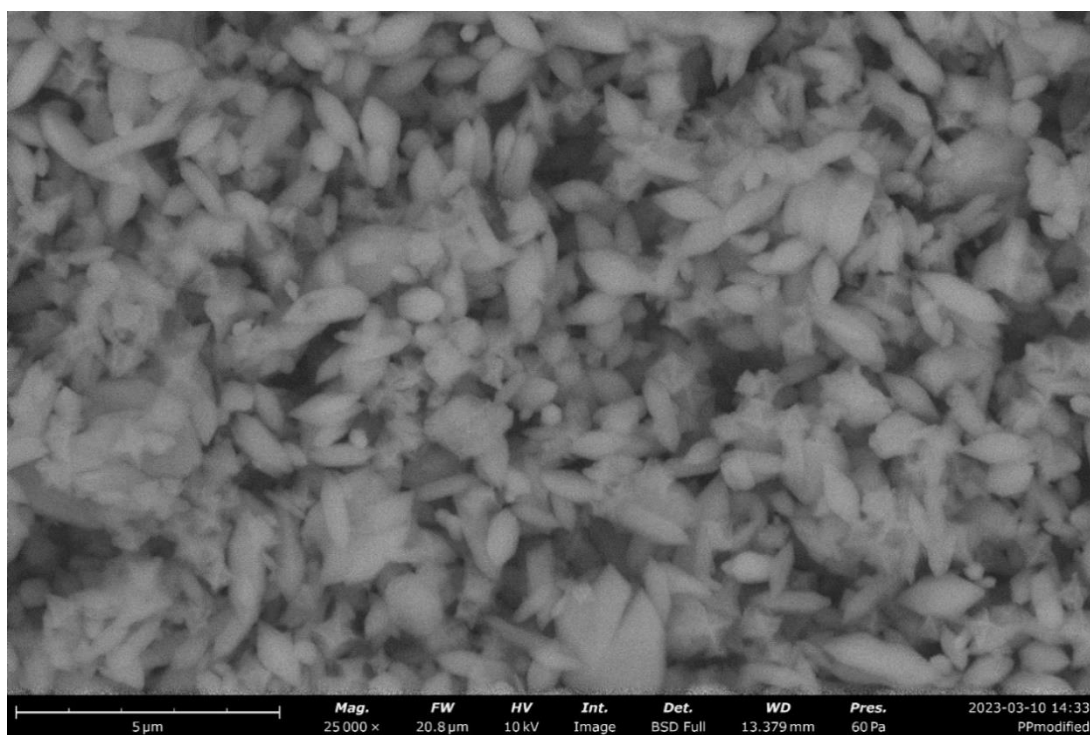


**Figure 17:** SEM image of the adsorbed NH<sub>2</sub>-MIL-88B of the surface of the PPHF.

### 3.2.4 Energy-dispersive X-ray spectrum

Energy-dispersive X-ray spectroscopy is a technique relying on the interaction between an X-ray excitation source and a sample. Its characterization capabilities are based in large on the fundamental principle that each element has a unique atomic structure that allows for a unique set of peaks in its electromagnetic emission spectrum. In the received elemental map of the NH<sub>2</sub>-MIL-88B material, the presence of carbon, nitrogen, oxygen and iron were confirmed, and their distribution in the material is uniform **Figure 18**. Information about the elemental mapping, and the corresponding color of each element are presented in **Table 6**.

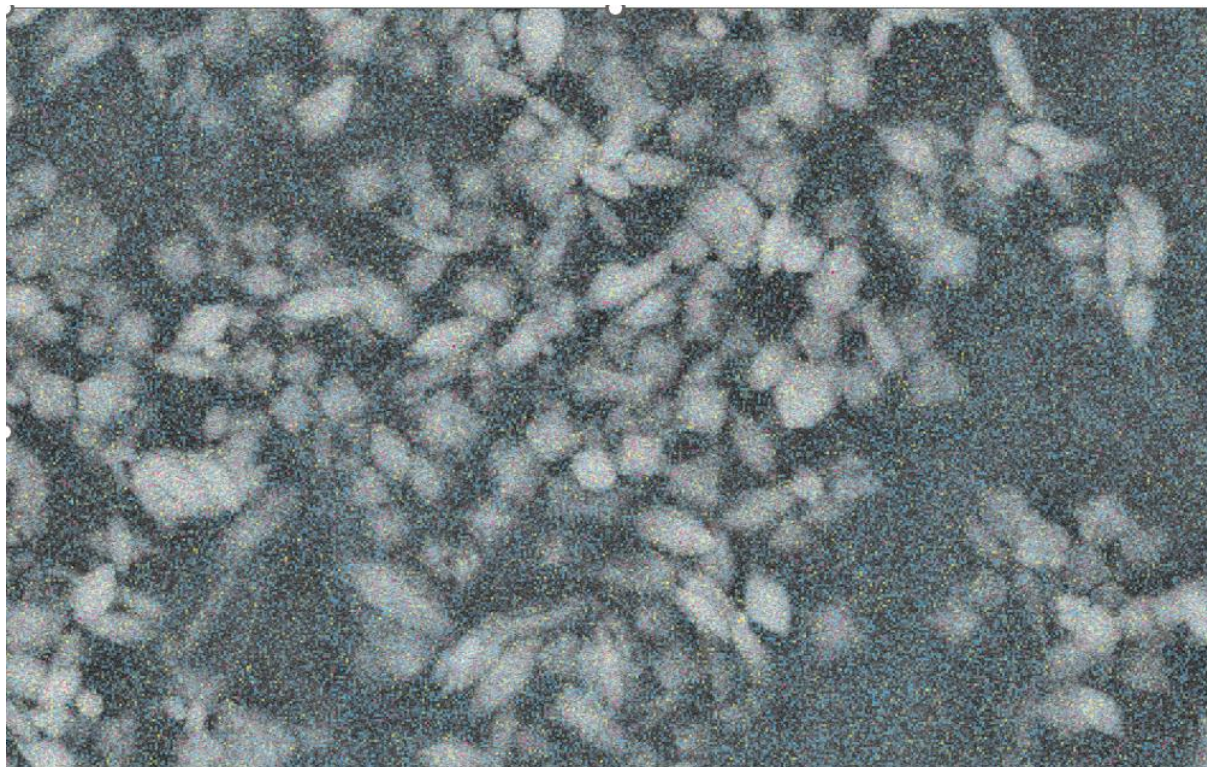


**Figure 18:** Combined elemental map of the NH<sub>2</sub>-MIL-88B depicting the distribution of carbon (blue), Nitrogen (yellow), oxygen (green), iron (red), 5 $\mu$ m.

**Table 6:** Information about the elemental mapping, and the corresponding color of each element

	Element Number	Element Symbol	Element Name	Atomic Conc.	Weight Conc. (%)
	6	C	Carbon	59.970	46
	7	N	Nitrogen	15.068	14
	8	O	Oxygen	19.403	20
	26	Fe	Iron	5.559	20

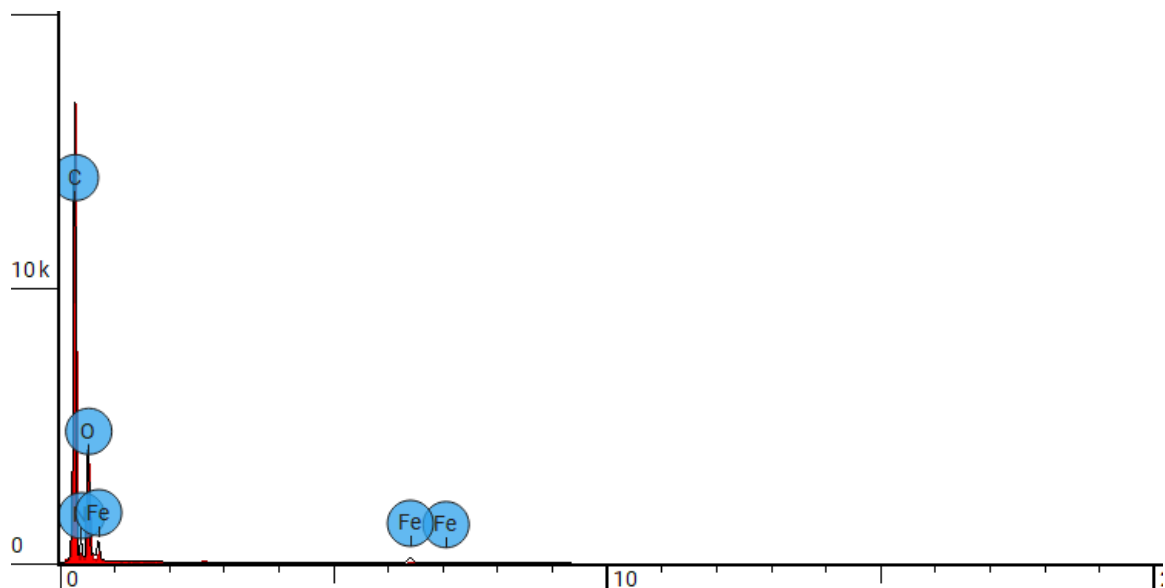


**Figure 19:** EDX results for NH<sub>2</sub>-MIL-88B (150 233 counts in 0:02:09 (1 164 c/s)).

These results are in accordance with the expected structure depicted in **Figure 20**.

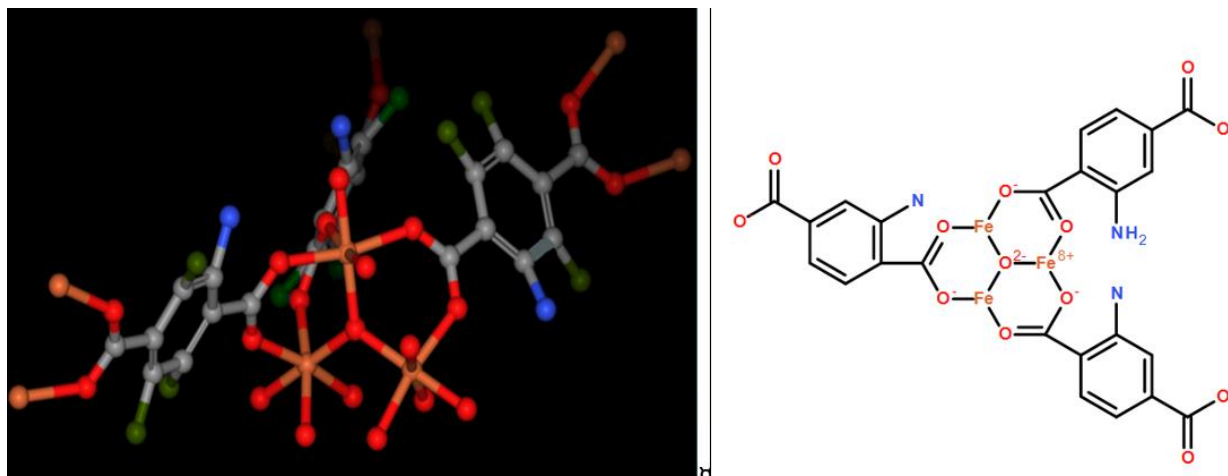


**Figure 20:** The coordination of the  $\text{NH}_2\text{-H}_2\text{BDC}$  ligands with the iron cluster, to form the  $\text{NH}_2\text{-MIL-88B}$  structure. 3D representation (left), 2D structure (right). The colored balls in the left figure represent carbon (grey), nitrogen (blue), iron (orange), oxygen (red), and hydrogen (green).

### 3.2.5 Dynamic light scattering (DLS)

Dynamic Light Scattering (DLS) is an analytical technique widely employed in the field of colloidal and nanoparticle characterization. It is an easy and fast way to measure the hydrodynamic size of dispersed nanomaterials and other small-scale materials based on their random constant movements in the dispersive medium through **Brown movement**. **Gouy-Chapman-Stern model** dictates that the dispersed particles will form an electric double layer at the interface of the nanomaterial. The thickness of the layer depends on several factors, such as the electrical conductivity of the liquid, the surface charge of the material, etc. (Fatehah et al. 2015). Thus, the average particle size and  $\zeta$ -potential of the material are measured. For the  $\zeta$ -potential, double measurements were carried out, with 12 cycles of potential measurement per measurement, at  $25^\circ\text{C}$  and  $\text{pH} = 5,3$ . The results taken from the dynamic light scattering suggest that the  $\zeta$ -potential of the  $\text{NH}_2\text{-MIL-88B}$  was  $+15,8$  mV at a pH value of  $\text{pH}=5,3$  and can be seen in **Figure 21**. That is in accord with the bibliography, where the zero point of charge of  $\text{NH}_2\text{-MIL-88B(Fe)}$  is reported to be 6.7, meaning that the material will be positively charged in more acidic mediums (Chen et al. 2022a). Furthermore, the average particle size was 410 nm as seen in the measurement presented in **Figure 22**.

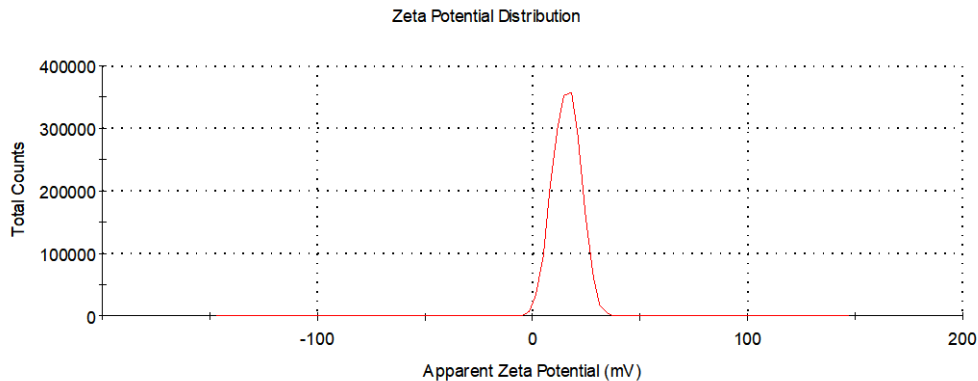


**Figure 21 :** *Zeta potential of NH<sub>2</sub>-MIL-88B.*

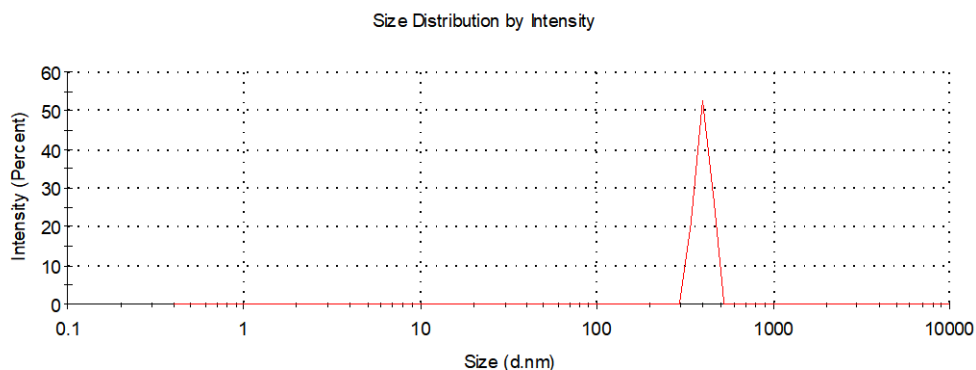


**Figure 22:** *Average particle size of the NH<sub>2</sub>-MIL-88B crystals.*

### 3.3 Chromatographic conditions

The mobile phase is acidized with formic acid, ensuring that both the analytes and the silica of the stationary phase are neutral, and thus helping with the separation and resulting in better, more symmetrical peaks. The stationary phase is reverse phase, meaning the static phase we are using is non-polar. In the beginning, the more polar moving phase will elute the more polar compounds, while the less polar ones will be distributed more in the non-polar static due to greater affinity. The gradual decrease in the polarity index of the mobile phase mixture will gradually elute the more lipophilic compounds. The elution sequence is as follows: 2NP, 3-Me-4NP, BP2 Eth-PB, 4OH-BP, Pr-Pb, BP8, Bu-PB, BP6, BP3 and can be seen in **Figure 23** and **Table 7**. The quantification was done with chromatographic peak areas at different wavelengths depending on the maxima of adsorption of the analytes. The 2NP shows a maximum absorption around 285 nm, 3-Me-4-NP at 315 nm, the BPs around 285 nm, and the PBs at 254 nm. The PDA

detector scanned the wavelengths in the range of 190-370 nm, and the temperature was set and monitored at 30°C. The retention times of all the compounds were validated by running a chromatographic run of each pure compound separately, and the resulting retention times can be seen in **Table 7**.

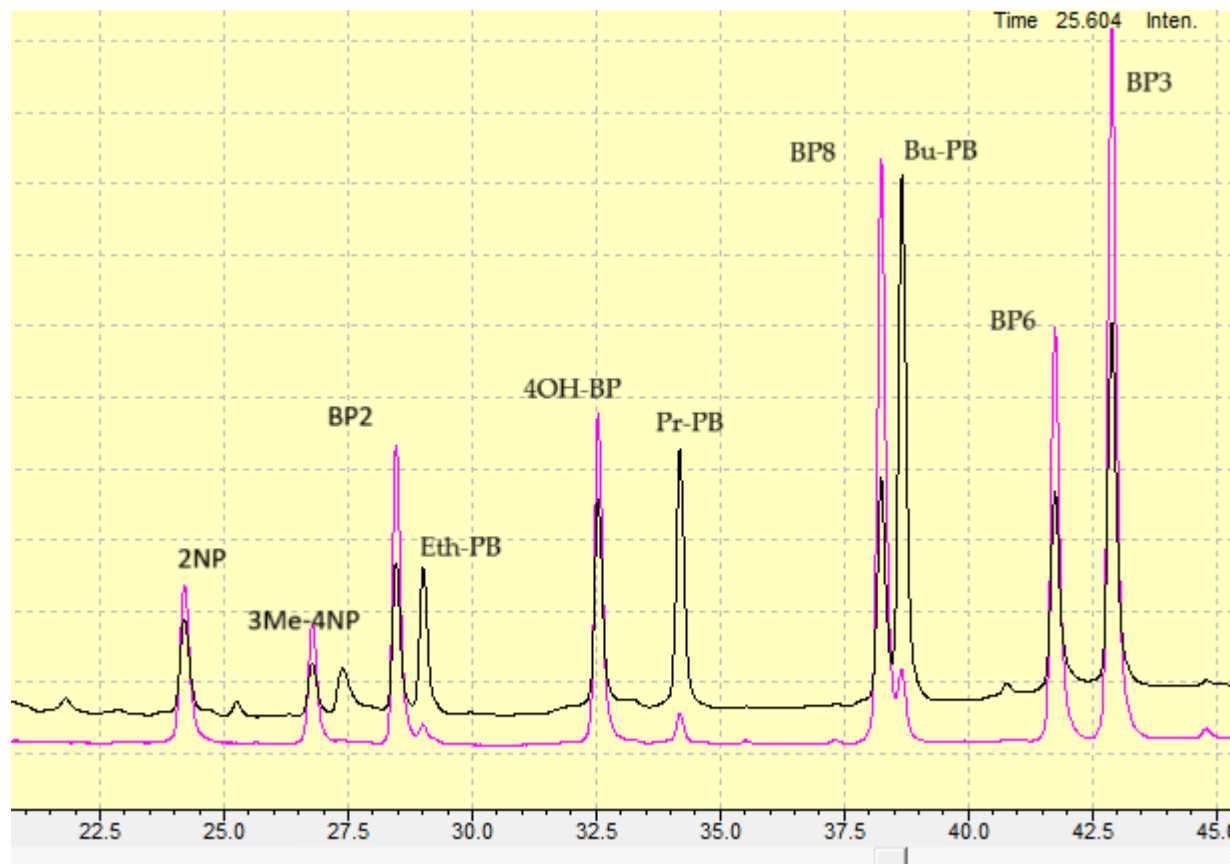


**Figure 23:** A typical chromatogram depicting the response in 254 nm (black) and 285 nm (pink). Ethyl-paraben (*Eth-PB*), butyl-paraben (*Bu-PB*), propyl-paraben (*Pr-PB*), 2-nitrophenol (*2NP*), 3-methyl-4-nitrophenol (*3Me-4NP*), benzophenone-2 (*BP2*), benzophenone-3 (*BP3*), 4-hydroxybenzophenone (*4OH-BP*), benzophenone-6 (*BP6*) and benzophenone-8 (*BP8*).

**Table 7:** Retention times of the chosen compounds under the applied chromatographic conditions.

Analyte	2NP	3Me-4NP	BP2	Eth-PB	4OH-BP	Pr-PB	BP8	Bu-PB	BP6	BP3
Rt (min)	24.18	26.69	28.33	29	32.53	34.15	38.15	38.57	41.6	42.8

## 3.4 Optimization of extraction

### 3.3.1 Effect of Salinity / Ionic strength

The investigation of the effect of ionic strength on the adsorption of the compounds is critical, as an increase in ionic strength leads to a decrease in organic compound solubility and subsequently in the increase of its distribution on the surface of the NH<sub>2</sub>-MIL-88B-modified PPHF, a process known as the salting-out effect. We examined the impact of salinity on the extraction in the range of 0–6.1 M, with 6.1 M being the maximum solubility of NaCl in water in ambient temperature and pressure. The optimal value of 5 M was determined as at higher concentrations we experienced a slight decline in the responses of some of the analytes. This decrease at greater concentrations of salt can be attributed to the increase in the viscosity that can hinder the diffusion rate of the analytes (Chatzimitakos et al. 2022). The greatest increase in adsorption was observed in the case of parabens. Interestingly, they are not significantly adsorbed in the absence of salt. These results suggest the developed method works favorably with samples with high salinity, as can be seen in the **Figure 24**

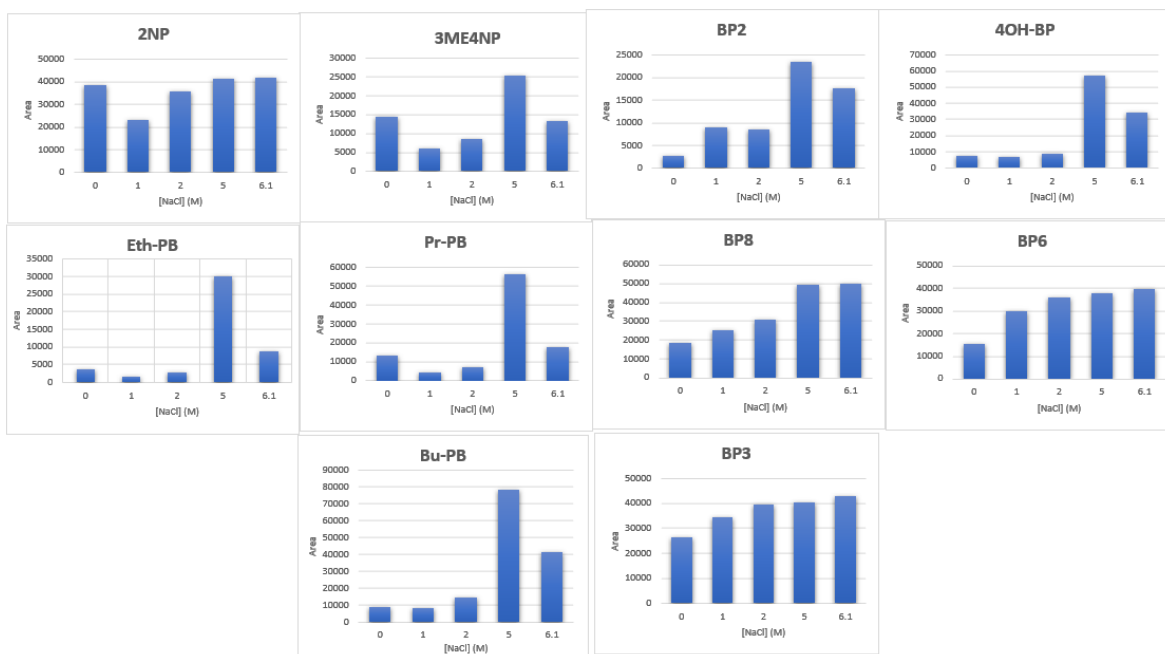


**Figure 24:** Effect of the salinity in the extraction process, the concentration of all the analytes was 0.25 µg/mL.

### 3.3.2 Effect of Humic Acids

Humic acids are ubiquitous in natural organic matter derived from decomposed plant and animal tissues. They can pose significant challenges in analytical chemistry, particularly in extraction processes. These complex compounds have a tendency to interfere with extraction procedures. In environmental sample analysis, for instance, humic acids can hinder the accurate extraction of pollutants, affecting the reliability of results. Analyte mixtures (0.025  $\mu\text{g/mL}$  of each analyte) were prepared with added concentrations of humic acids ranging from 1  $\mu\text{g/mL}$  to 15  $\mu\text{g/mL}$ . The analytical procedure was conducted as described above, encompassing the extraction with  $\text{NH}_2\text{-MIL88B-PPHF}$ , elution and chromatographic separation and quantification. The effect of the humic acids was found to be negligible.

### 3.3.3 Effect of pH

As discussed in the section [1.3.3](#) of the introduction, the pH can affect the stability and structure of the MOF, influencing its ability to act as an extracting medium. Moreover, the pH of a solution plays a pivotal role in the extraction processes utilizing metal-organic frameworks. The pH of the solution significantly influences the charge and structure of both the MOF and the target analyte. Optimal extraction efficiency is often achieved by tailoring the pH to enhance the interaction between the MOF and the analyte, thus improving the adsorption. Deviations from the optimal pH range can lead to reduced extraction efficiency or even structural instability of the MOF. The effect of pH on the extraction efficiency was investigated in the range of 3.0 to 9.0, with the optimal responses being at (initial) pH 7.5. When the pH was adjusted above 8.5 it resulted in poor responses, possibly because of a structural degradation of the MOF as it can be seen in the IR spectrum received from a  $\text{NH}_2\text{-MIL-88B}$  sample treated with NaOH depicted in **Figure 26**. Alkaline conditions (above pH 8.5) would cause structural degradation of the MOF, a change that is signaled with a simultaneous change of its color from dark brown to white. The results suggest that acidic and alkaline values of pH should be avoided, with the total responses showing a dramatic decrease at pH 3.0 and pH 8.5. The initial pH of the solutions was carefully set to 3.0, 5.0, and 7.5 with the addition of HCl and NaOH solutions. In the solutions with initial pH values of 3 and 5, the pH after the completion of extraction, was almost unchanged, and in the solution with pH 7.5, the final pH value was shifted to 6.8 because the point of zero charge of the material was close to this value. The pH graphs can be seen in **Figure 25**. Lastly, in **Figure 26** we see a superposition of the infrared spectra of  $\text{NH}_2\text{-MIL-88B}$  before and after the treatment with NaOH. The yellow line represents the untreated material, while the green, pink, and blue

lines represent the three trials of the alkali-treated material. Structural degradation can be seen, as the characteristic peaks seem to degenerate, and in one case, completely disappear.

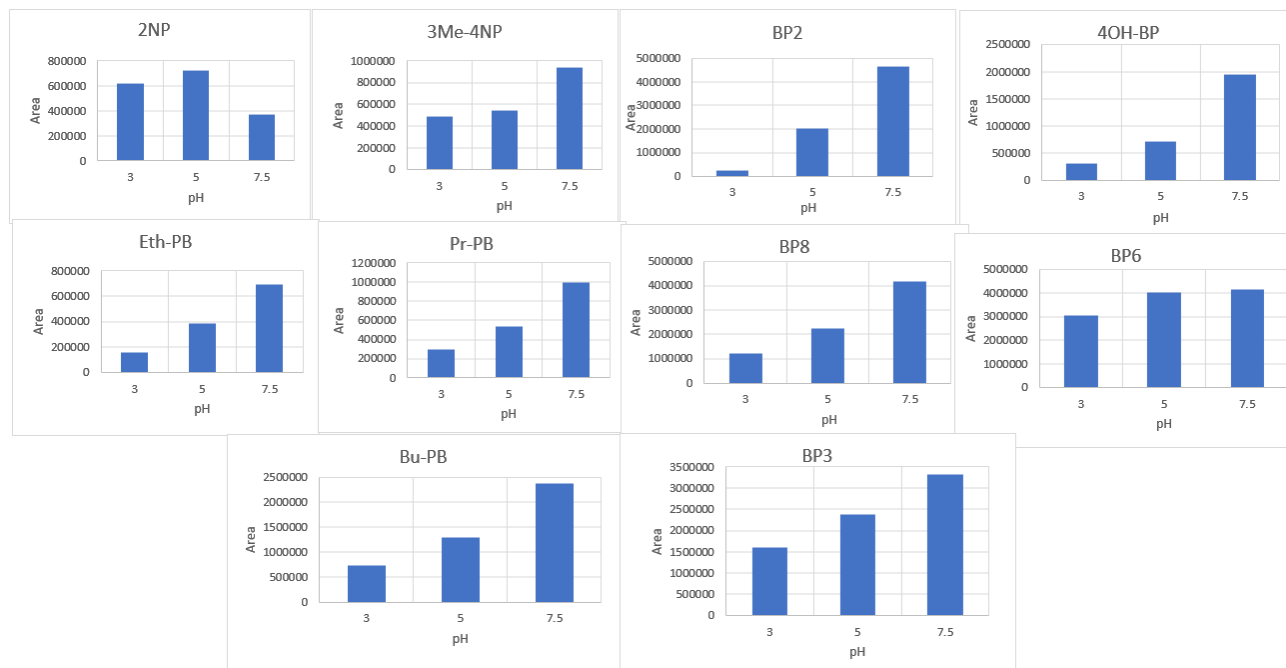


**Figure 25:** Effect of the initial pH on the extraction of analytes, the concentration of all the analytes was 0.25 µg/mL.

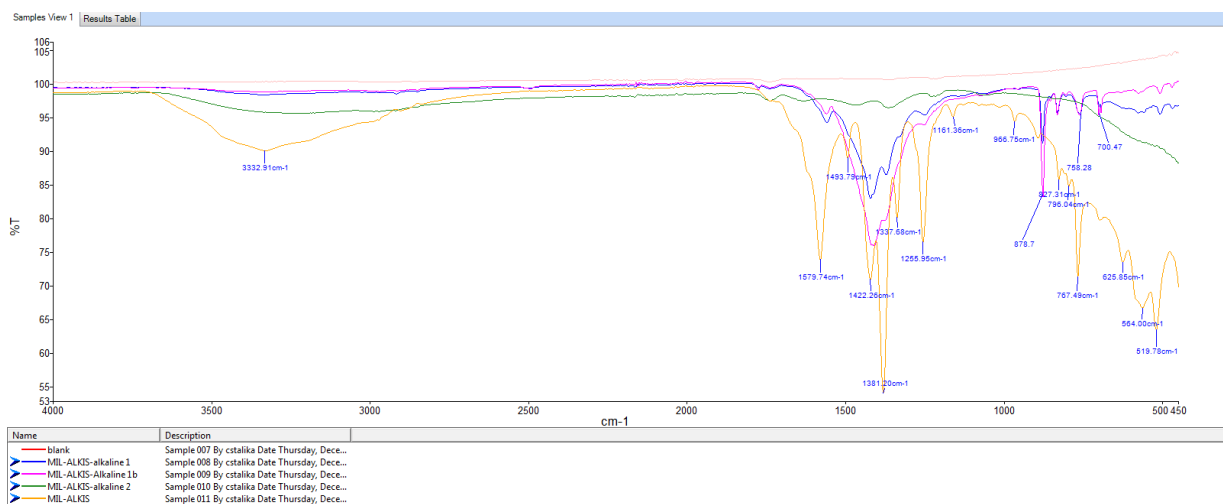


**Figure 26:** Comparison of the IR spectra of NH<sub>2</sub>-MIL-88B in acidic and alkaline solution. The yellow line represents the untreated material, while the pink, blue and green lines represent measurements for the alkali-treated material, in gradually more alkaline environments.

### 3.3.4 Effect of temperature

The temperature was set by means of submerging the system in a water bath and monitoring the temperature with a thermometer. The effect of temperature on the extraction efficiency was tested in the temperature range of 15-35°C with increments of 10. The optimal extraction efficiency was achieved at room temperature for the majority of analytes as can be seen in the graphs presented in *Figure 27*.

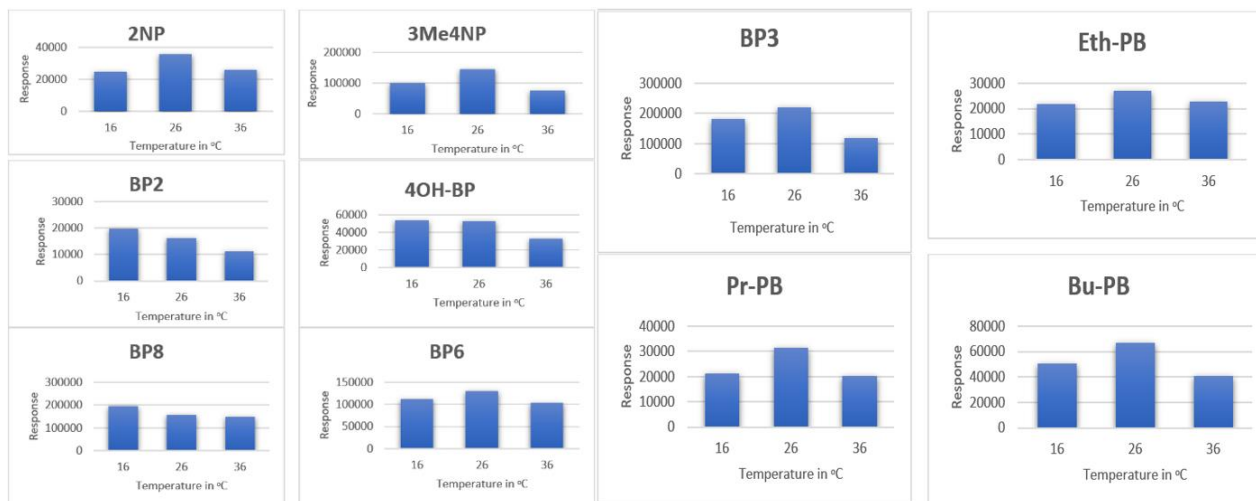


*Figure 27: The effect of temperature in the extraction of analytes, the concentration of all the analytes was 0.25 µg/mL.*

### 3.3.5 Effect of the eluting solvent

The eluting solvent's polarity, composition, and strength directly impact the desorption efficiency and selectivity. The solvent's compatibility with the detection method and its ability to elute target analytes without co-eluting interfering substances are some critical considerations. Modifying the pH of the eluting solvent can impact the ionization state of analytes and the sorbent surface, thereby influencing interactions and separation. Methanol is chosen as it can penetrate the pores of the PPHF and elute the analytes sufficiently and could suspend the MOF particles while being relatively cheap. The eluting solvent methanol without any addition was tested, while methanol with the addition of 5% formic acid, and methanol with the addition of 5% NH<sub>3</sub> was also tested and repeated the aforementioned experimental procedure. We concluded that the addition of 5% formic acid improved the elution process, as shown by the areas of the chromatographic peaks. A second elution step and subsequent addition of the two eluents was not preferred as it would extend the analysis time greatly.

### 3.3.6 Multivariate experiment

Although the preceding experiments were done with the classical methodology, changing one parameter at a time, some parameters are interdependent, meaning that one condition can be affected by the change in another. Multivariate experiments can help us work in such conditions, achieving better results, and so a multivariate experimental process was designed, in batch conditions, for the parameters of volume, stirring rate, stirring time (or extraction time), and number of fibers used.

#### **Response surface designs.**

To study the effect of experimental parameters on the response - total area response of the analytes (% extraction efficiency), a Central Composite Design was applied to four variables: sample volume (10 - 95 ml), number of fibers (0.5 - 3.5), stirring speed (170 - 870 rpm) and stirring time (6.7 - 53 min). The applied Central Composite Design consisted of 27 experiments according to the following equation:  $N = 2^k + 2k + C_0 = 2^4 + 2*4 + 3 = 27$ , where  $N$  is the total number of experiments required,  $k$  is the number of variables,  $2k$  are the axial and  $C_0$  the central points. The three central points included in the Central Composite Design were used to calculate the experimental error. Data were analyzed using Statistica 13 (StatSoft, Tulsa, OK, USA). The chemometric study for multivariate optimization was performed using the trial version of Design-Expert® Version 10 software. **Statistical analysis of the results was performed using a  $t$ -Student test to evaluate the removal rates for statistical significance.** Experiments were performed in triplicate ( $n=3$ ) and

differences in results were considered statistically significant for  $p < 0.05$ . For the multivariate experiment we will adjust values to our parameters. The volume of sample will be A, stirring time will be B, stirring rate will be C, and the number of fibers will be D.

**Table 8:** *Multivariate experiments, their conditions and responses. The separate responses were the chromatographic peak areas, and the total response was received from the separate responses after normalization.*

<b>Experiment</b>	<b>A: Volume, mL</b>	<b>B: Stirring time, min</b>	<b>C: Stirring rate, rpm</b>	<b>D: Number of fibers</b>	<b>Nitrophenol response</b>	<b>Paraben response</b>	<b>Benzophenone response</b>	<b>Total normalized response*</b>
1	52.5	30	525	2	4600	1675	7870	0.128123
2	80	45	300	1	3160	1255	5565	0.09121
3	52.5	30	873	2	4935	1715	7275	0.129169
4	52	30	525	3.5	6985	2773	10365	0.190876
5	95	30	525	2	4650	1610	9620	0.136877
6	52.5	30	525	0.5	1840	1680	4370	0.080439
7	25	15	750	1	1160	2065	5325	0.087268
8	52.5	53	525	2	5670	1582	8260	0.139237
9	52.5	30	525	2	5200	2010	8560	0.14556
10	80	15	750	3	2225	1550	6580	0.093746
11	80	45	750	1	2790	1220	5810	0.087977
12	52.5	6	525	2	1700	1280	4785	0.072411
13	25	15	300	1	1120	1005	4070	0.056374
14	25	15	300	3	2790	1645	5880	0.097802
15	52.5	30	176	2	4160	1255	4660	0.096502
16	52.5	30	525	2	4540	1500	6610	0.116647
17	25	45	750	3	5190	2020	9400	0.150327
18	80	15	300	1	1300	990	4765	0.06174
19	80	45	300	3	6530	2305	8915	0.167774
20	80	15	750	1	1225	1735	4895	0.078231
21	25	15	750	3	3840	2590	6415	0.132563
22	25	45	300	3	4070	1880	8540	0.130923
23	80	15	300	3	4320	2260	6390	0.13004

24	9.0	30	525	2	1895	1140	4960	0.072279
25	80	45	750	3	5890	2280	8680	0.159327
26	25	45	750	1	2750	1030	5825	0.083429
27	25	45	300	1	2550	982	6340	0.083152

\* Total normalized response: (total area of experiment – MIN area of the set of experiments) / (maximum area of the set – minimum area of the set)

### Nitrophenols

The nitrophenol responses presented in **Table 8** were inserted into Statistica 13 and the results are presented in **Table 9**.

**Table 9:** ANOVA for response surface for the Quadratic model Analysis of variance (partial sum of squares – type III) – Nitrophenols.

Source	Sum of Squares	df	Mean Square	F Value	p-value	Prob > F
<b>Model</b>	7.279E+007	14	5.199E+006	11.11	< 0.0001	<i>significant</i>
<i>A-Volume</i>	3.260E+006	1	3.260E+006	6.96	0.0216	
<i>B-Stirring time</i>	2.140E+007	1	2.140E+007	45.72	< 0.0001	<i>significant</i>
<i>C-Stirring rate</i>	8842.24	1	8842.24	0.019	0.8930	
<i>D-number of fibers</i>	3.445E+007	1	3.445E+007	73.60	< 0.0001	<i>significant</i>
<i>AB</i>	8.327E+005	1	8.327E+005	1.78	0.2070	
<i>AC</i>	1.953E+006	1	1.953E+006	4.17	0.0637	<i>borderline</i>
<i>AD</i>	2.970E+005	1	2.970E+005	0.63	0.4411	
<i>BC</i>	1.208E+005	1	1.208E+005	0.26	0.6207	
<i>BD</i>	2.652E+005	1	2.652E+005	0.57	0.4661	
<i>CD</i>	8100.00	1	8100.00	0.017	0.8975	
<i>A<sup>2</sup></i>	5.829E+006	1	5.829E+006	12.45	0.0042	<i>significant</i>
<i>B<sup>2</sup></i>	3.353E+006	1	3.353E+006	7.16	0.0202	
<i>C<sup>2</sup></i>	3.736E+005	1	3.736E+005	0.80	0.3892	
<i>D<sup>2</sup></i>	6.435E+005	1	6.435E+005	1.37	0.2637	
<b>Residual</b>	5.616E+006	12	4.680E+005			
<i>Lack of Fit</i>	5.350E+006	10	5.350E+005	4.02	0.2157	<i>Not significant</i>

Pure Error	2.664E+005	2	1.332E+005
Cor Total	7.841E+007	26	

The "Lack of Fit  $p$ -value" has a value of 0.215, pointing out that the lack of fit is non-significant in relation to pure error, with a 21.57% chance of a value that big occurring due to noise. Our results fit great with the proposed model. Both the stirring time and the number of fibers are statistically significant in the total responses.

The results can be separately evaluated, or as a total response. In the case of separate examination, we assessed the response for nitrophenols, parabens and benzophenones. In the case of nitrophenols, our model, A, B, D, A<sup>2</sup> and B<sup>2</sup> are statistically significant ( $p < 0.05$ ), the interaction between A and B (AB) is almost statistically significant. Furthermore, the lack of fit is not statistically significant relative to pure error, indicating a great fit if our model and the results. In **Figure 28** we can see that the paraben extraction efficiency is greater for volumes around 60 mL, 45 min of stirring time, stirring rates around 550 rpm, and 3 fibers.

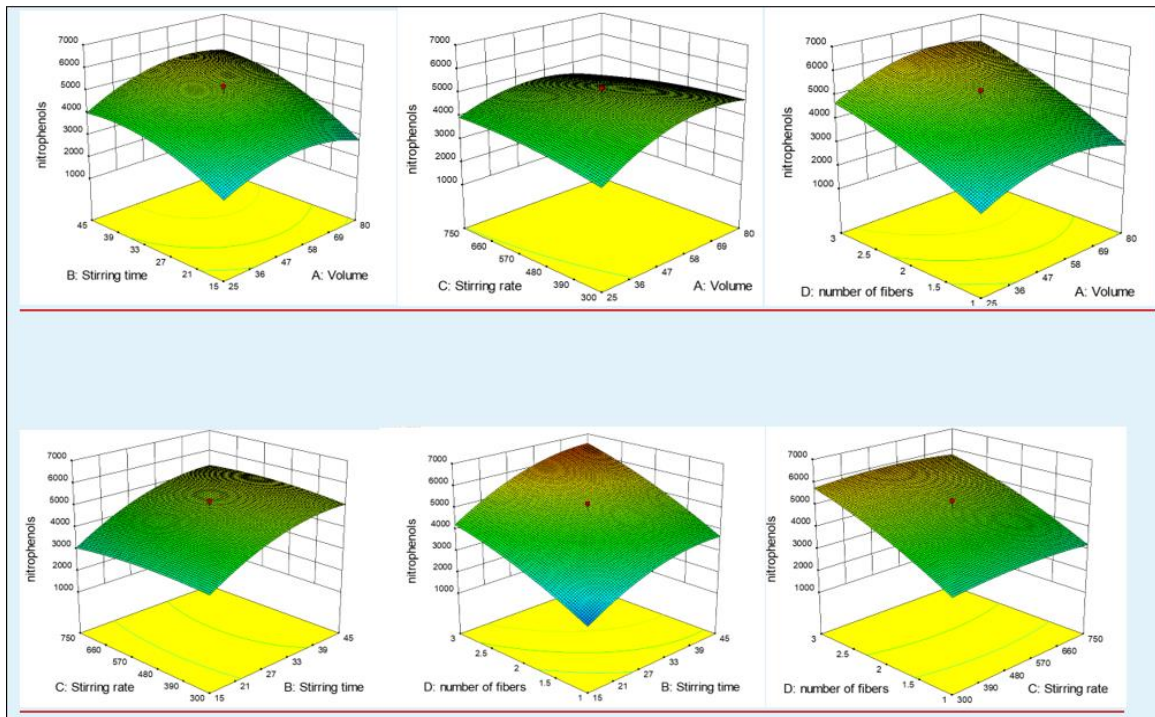


**Figure 28:** Effect of the interdependent four variables on the extraction efficiency of nitrophenols.

## Parabens

The paraben responses presented in **Table 8** were inserted into Statistica 13 and the results are presented in **Table 10**.

**Table 10:** ANOVA for response surface for the Quadratic model Analysis of variance (partial sum of squares – type III) - Parabens

Source	Sum of Squares	df	Mean Square	F Value	p-value Prob > F	
<b>Model</b>	5.554E+006	14	3.967E+005	5.29	0.0032	<b>significant</b>
<i>A-Volume</i>	58741.56	1	58741.56	0.78	0.3934	
<i>B-Stirring time</i>	7732.46	1	7732.46	0.10	0.7536	
<i>C-Stirring rate</i>	3.989E+005	1	3.989E+005	5.32	0.0397	<b>significant</b>
<i>D-number of fibers</i>	3.032E+006	1	3.032E+006	40.46	< 0.0001	<b>significant</b>
<i>AB</i>	2.299E+005	1	2.299E+005	3.07	0.1053	
<i>AC</i>	3.075E+005	1	3.075E+005	4.10	0.0656	<b>borderline</b>
<i>AD</i>	1260.25	1	1260.25	0.017	0.8990	
<i>BC</i>	2.285E+005	1	2.285E+005	3.05	0.1063	
<i>BD</i>	1.910E+005	1	1.910E+005	2.55	0.1364	
<i>CD</i>	1.347E+005	1	1.347E+005	1.80	0.2049	
<i>A<sup>2</sup></i>	1.420E+005	1	1.420E+005	1.89	0.1938	
<i>B<sup>2</sup></i>	88569.99	1	88569.99	1.18	0.2983	
<i>C<sup>2</sup></i>	48946.95	1	48946.95	0.65	0.4347	
<i>D<sup>2</sup></i>	6.846E+005	1	6.846E+005	9.13	0.0106	<b>significant</b>
<b>Residual</b>	8.993E+005	12	74945.06			
<i>Lack of Fit</i>	7.650E+005	10	76502.41	1.14	0.5546	<b>not significant</b>
<i>Pure Error</i>	1.343E+005	2	67158.33			
<b>Cor Total</b>	6.454E+006	26				

The  $p$ - value of the model is 0.0032, meaning the model is statistically significant when it comes to parabens (with a 0.32% chance of it being due to noise). The terms C, D, D<sup>2</sup> are significant for the model, AC is borderline statistically significant. Once more, when related to the pure error, the Lack of Fit is non-significant, achieving a good fit of the model with the experimental results.

In **Figure 29** we can see that the paraben extraction efficiency is greater for volumes around 70 mL, 30 min of stirring time, stirring rates around 750 rpm, and 3 fibers.

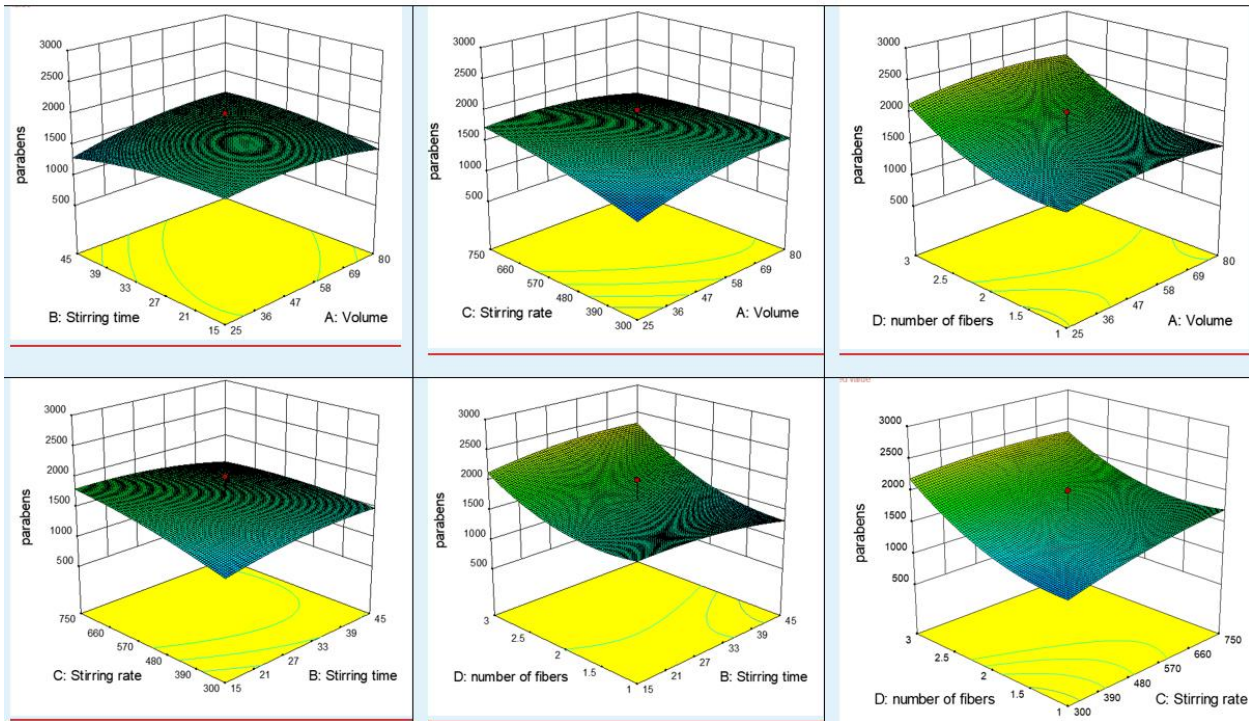


**Figure 29:** Effect of the interdependent four variables on the extraction efficiency of parabens

## Benzophenones

The benzophenone responses presented in **Table 8** were inserted into Statistica 13 and the results are presented in **Table 11**.

**Table 11:** ANOVA for response surface for the Quadratic model Analysis of variance (partial sum of squares – type III) - Benzophenones

Source	Sum of Squares	df	Mean Square	F Value	p-value Prob > F	
<b>Model</b>	6.941E+007	14	4.958E+006	3.82	0.0128	<i>significant</i>
<i>A-Volume</i>	2.366E+006	1	2.366E+006	1.82	0.2021	
<i>B-Stirring time</i>	1.950E+007	1	1.950E+007	15.01	0.0022	<i>significant</i>
<i>C-Stirring rate</i>	2.039E+006	1	2.039E+006	1.57	0.2342	
<i>D-number of fibers</i>	3.633E+007	1	3.633E+007	27.96	0.0002	<i>significant</i>
<i>AB</i>	2.691E+005	1	2.691E+005	0.21	0.6571	
<i>AC</i>	2.036E+005	1	2.036E+005	0.16	0.6991	
<i>AD</i>	45689.06	1	45689.06	0.035	0.8544	
<i>BC</i>	1.925E+005	1	1.925E+005	0.15	0.7070	
<i>BD</i>	2.092E+006	1	2.092E+006	1.61	0.2286	
<i>CD</i>	3451.56	1	3451.56	2.657E-003	0.9597	
<i>A<sup>2</sup></i>	63301.60	1	63301.60	0.049	0.8290	
<i>B<sup>2</sup></i>	1.788E+006	1	1.788E+006	1.38	0.2635	
<i>C<sup>2</sup></i>	4.502E+006	1	4.502E+006	3.47	0.0873	
<i>D<sup>2</sup></i>	20163.02	1	20163.02	0.016	0.9029	
<b>Residual</b>	1.559E+007	12	1.299E+006			
<i>Lack of Fit</i>	1.363E+007	10	1.363E+006	1.39	0.4883	<i>not significant</i>
<i>Pure Error</i>	1.955E+006	2	9.777E+005			
<b>Cor Total</b>	8.500E+007	26				

The results suggest that the model is statistically significant as shown by the  $p$  value (1.28% chance of it occurring due to noise). In the same vein, the  $p$  values show that B, D are statistically significant. The lack of fit is not significant indicating a good fit of the model with the experimental results for the BPs. In **Figure 30** we can see that the benzophenone extraction efficiency is greater for volumes around 70 mL, 35 min of stirring time, stirring rates around 550 rpm, and 3 fibers.

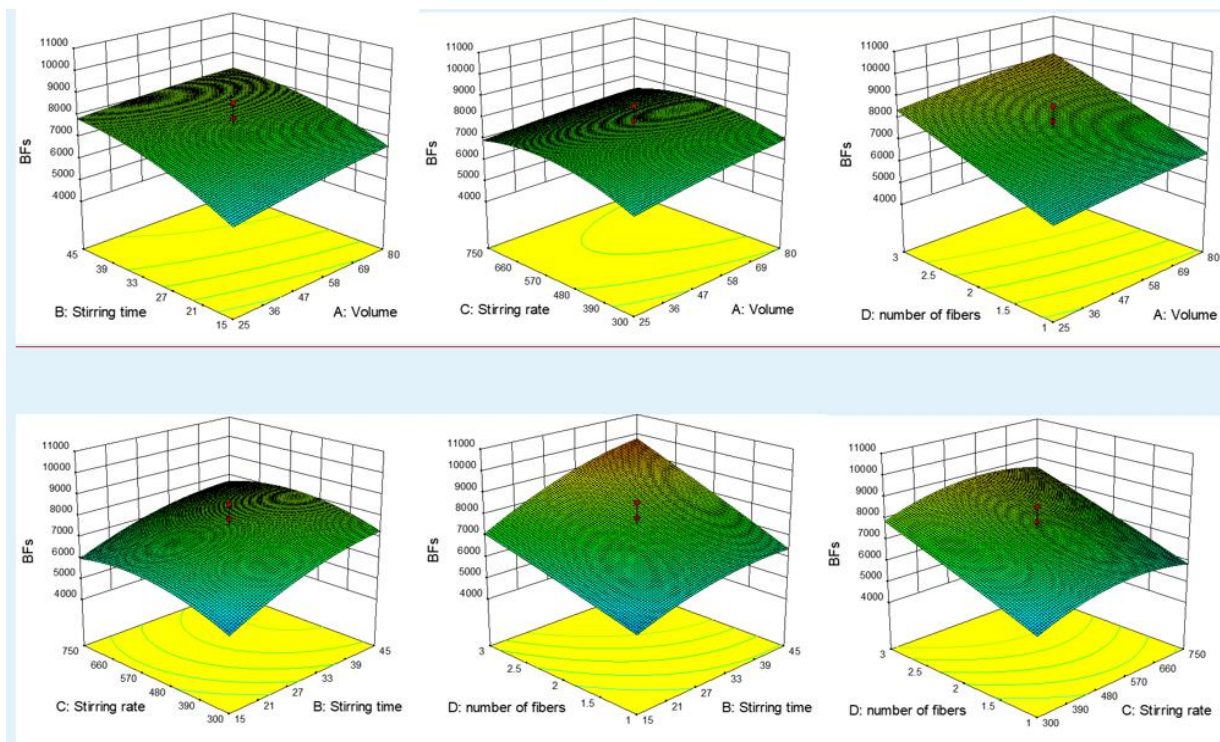


**Figure 30:** Effect of the interdependent four variables on the extraction efficiency of benzophenones

### Total response

In order to find the best model, and the optimal conditions for all three groups of analytes, the same procedure must be followed, but accounting for a total response for all three analytes. The normalized total responses presented in **Table 8** were inserted into Statistica 13 and the results are presented in **Table 12**. A normalization process is needed beforehand. The sum of the normalized values was inserted into the software for the Central Composite Design and thus, the optimum values for the multivariate experiment were calculated.

**Table 12:** ANOVA for response surface for the Quadratic model Analysis of variance (partial sum of squares – type III) – Total response

Source	Sum of squares	df	Mean square	F Value	p-value (Prob > F)	
<b>Model</b>	0.022	14	1.552E-003	3.87	0.0121	<i>significant</i>
<i>A-Volume</i>	1.094E-003	1	1.094E-003	2.73	0.1245	
<i>B-Stirring time</i>	2.386E-003	1	2.386E-003	5.95	0.0312	<i>significant</i>
<i>C-Stirring rate</i>	2.615E-006	1	2.615E-006	6.518E-003	0.9370	
<i>D-number of fibers</i>	0.012	1	0.012	30.82	0.0001	<i>significant</i>
<i>AB</i>	3.187E-004	1	3.187E-004	0.79	0.3903	
<i>AC</i>	8.140E-004	1	8.140E-004	2.03	0.1798	
<i>AD</i>	6.822E-005	1	6.822E-005	0.17	0.6874	
<i>BC</i>	1.137E-003	1	1.137E-003	2.83	0.1182	
<i>BD</i>	1.538E-006	1	1.538E-006	3.833E-003	0.9517	
<i>CD</i>	1.089E-003	1	1.089E-003	2.71	0.1253	
<i>A<sup>2</sup></i>	1.005E-003	1	1.005E-003	2.50	0.1396	
<i>B<sup>2</sup></i>	8.959E-004	1	8.959E-004	2.23	0.1609	
<i>C<sup>2</sup></i>	4.006E-004	1	4.006E-004	1.00	0.3374	
<i>D<sup>2</sup></i>	1.503E-004	1	1.503E-004	0.37	0.5519	
<b>Residual</b>	4.815E-003	12	4.012E-004			
<i>Lack of Fit</i>	4.515E-003	10	4.515E-004	3.01	0.2748	<i>not significant</i>
<i>Pure Error</i>	2.997E-004	2	1.498E-004			
<b>Cor Total</b>	0.027	26				

The  $p$  value (0.0121) of the model indicates that the model is statistically significant with a 1.21% chance of this result occurring due to noise. The B and D are the only statistically significant factors for the total response. The lack of fit is statistically insignificant with a 27.48% chance of this result occurring due to noise. The Standard deviation( $R^2$ ) of the results was 0.8186. The figures below depict the total normalized response for all the benzophenones, nitrophenols and parabens plotted against the variables of stirring time, stirring rate, sample volume, and the number of fibers. The response is the normalized total chromatographic areas which represents the extraction efficiency. The **Figure 31** depicts the extraction efficiency plotted against the stirring time and the sample volume. As we can see, for a sample volume of 25 mL the extraction efficiency increases with the increase in stirring time and reaches a peak at 35 min. For stirring time of 15 min, the response increases with the increase in sample volume.

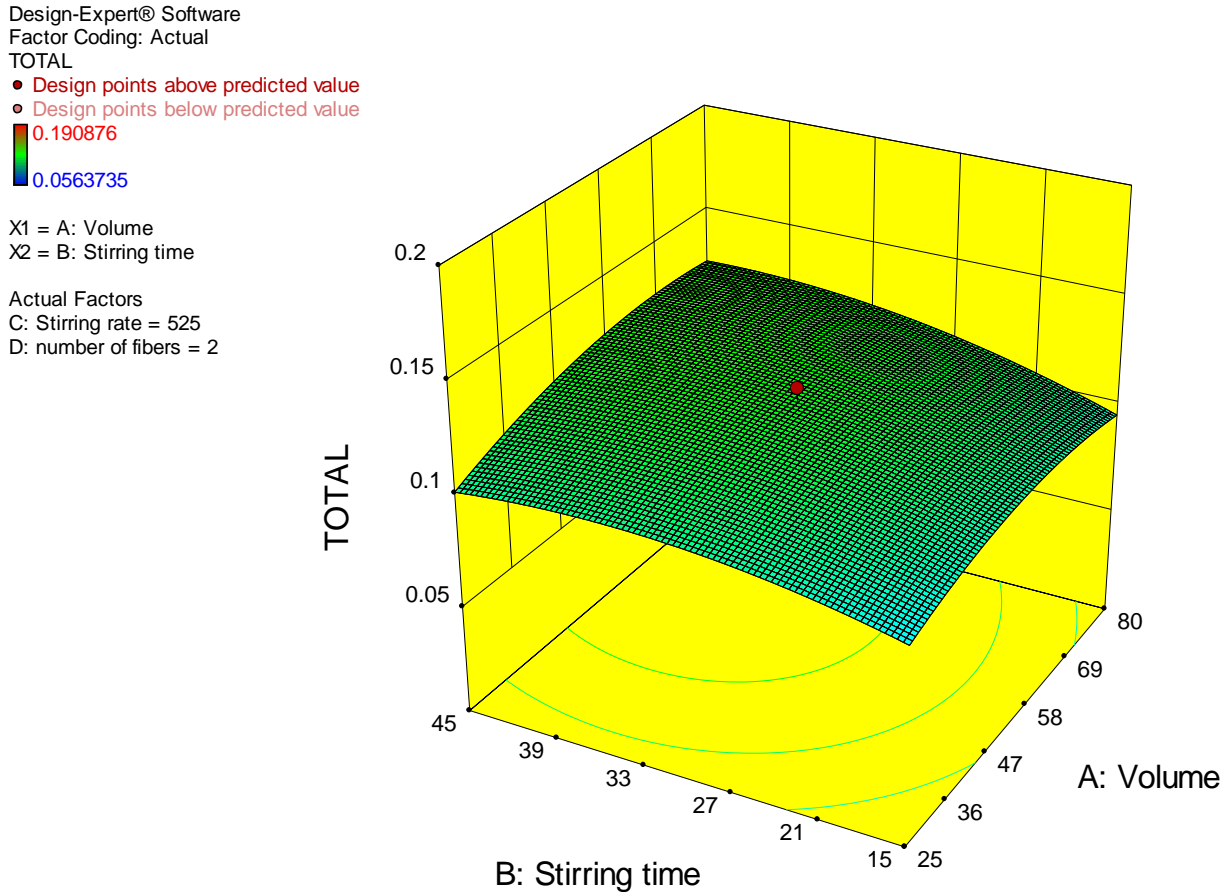


**Figure 31:** Plot of stirring time- volume.

Figure 32 illustrates how the extraction efficiency increases as the stirring rate increases for a 25 mL volume. Likewise, increasing the sample volume raises the overall response at a 300 rpm stirring rate.

Design-Expert® Software  
Factor Coding: Actual  
TOTAL

- Design points above predicted value
- Design points below predicted value



X1 = A: Volume  
X2 = C: Stirring rate

Actual Factors  
B: Stirring time = 30  
D: number of fibers = 2

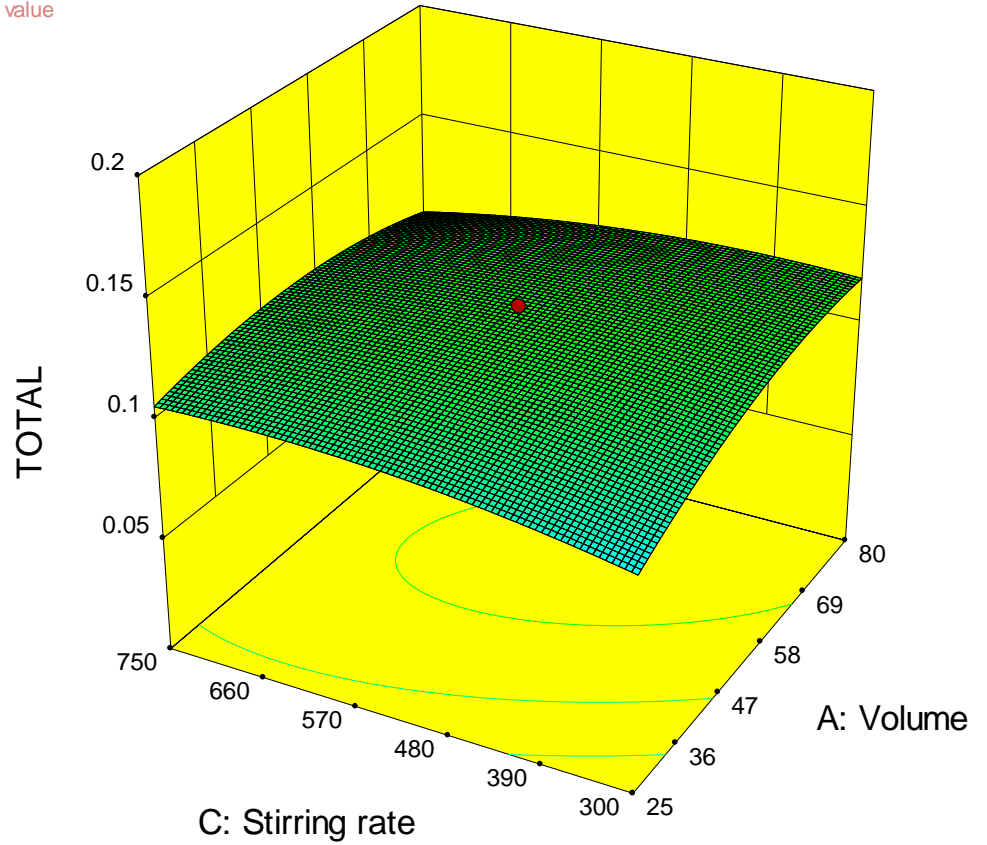


Figure 32: Plot of stirring rate- volume.

Figure 33 illustrates how the overall extraction efficiency increases as when more fobers are used for a 25 mL volume. Conversely, increasing the sample volume for 1 fiber causes the extraction efficiency to increase until 70 mL, at which point it starts to decline.

Design-Expert® Software  
Factor Coding: Actual  
TOTAL

- Design points above predicted value
- Design points below predicted value



X1 = A: Volume  
X2 = D: number of fibers

Actual Factors  
B: Stirring time = 30  
C: Stirring rate = 525

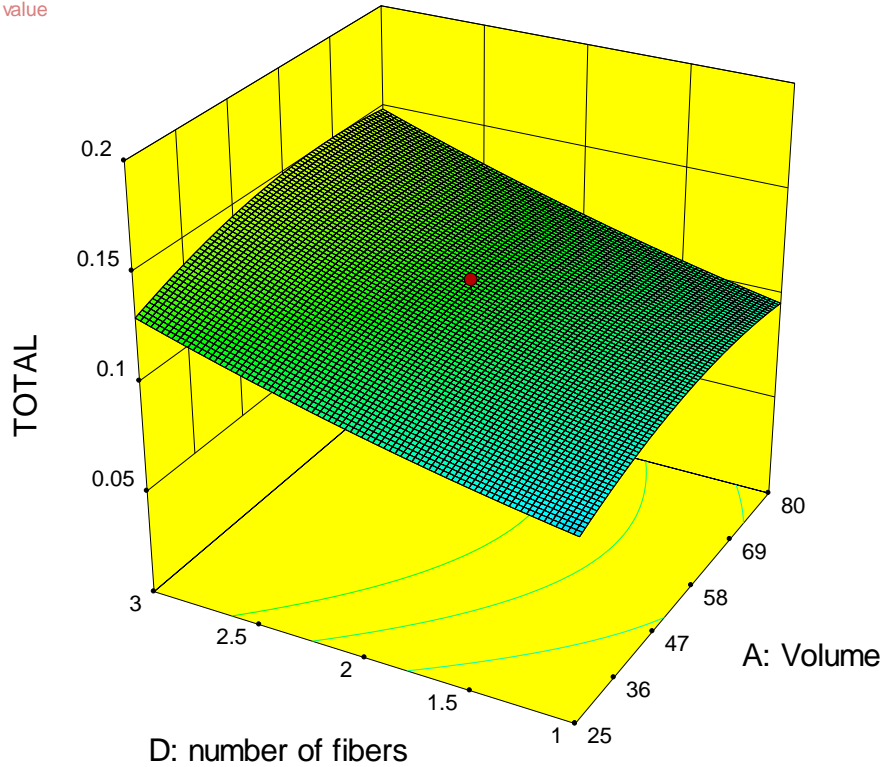


Figure 33: Plot of the number of fibers – volume.

As can be seen in **Figure 34**, the extraction efficiency increases for greater stirring rates at 15 min of stirring time. Similarly, at 300 rpm of stirring rate the extraction efficiency increases with the increase in stirring time.

Design-Expert® Software

Factor Coding: Actual

TOTAL

● Design points above predicted value

○ Design points below predicted value

0.190876

0.0563735

X1 = B: Stirring time

X2 = C: Stirring rate

Actual Factors

A: Volume = 52.5

D: number of fibers = 2

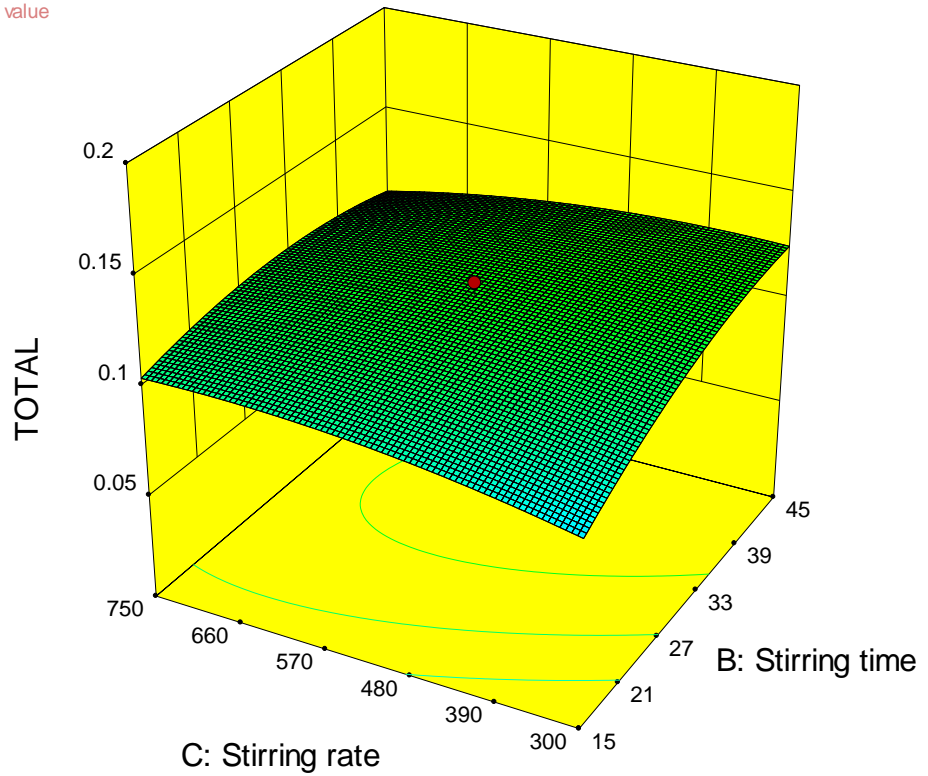


**Figure 34:** Plot of stirring rate- stirring time.

Figure 35 depicts the effect of number of fibers and stirring time on the extraction efficiency. For 15 min stirring time, increasing the number of fibers increased the extraction efficiency. For one fiber, the total response increased with the increase in stirring time.

Design-Expert® Software  
Factor Coding: Actual  
TOTAL

● Design points above predicted value

● Design points below predicted value

0.190876

0.0563735

X1 = B: Stirring time  
X2 = D: number of fibers

Actual Factors  
A: Volume = 52.5  
C: Stirring rate = 525

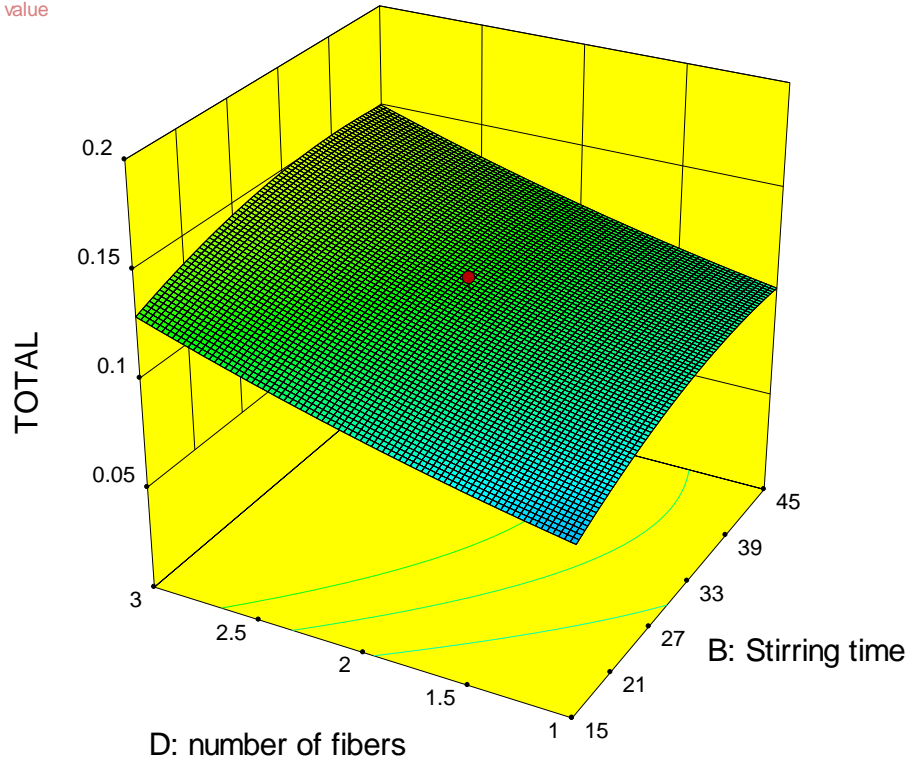


Figure 35: Plot of number of fibers- stirring time

**Figure 36** depicts the effect of number of fibers and stirring rate on the extraction efficiency. For 300 rpm stirring rate, increasing the number of fibers increased the extraction efficiency. For one fiber, the total response increased with the increase in stirring time.

Design-Expert® Software

Factor Coding: Actual

TOTAL

● Design points above predicted value

● Design points below predicted value

0.190876

0.0563735

X1 = C: Stirring rate

X2 = D: number of fibers

Actual Factors

A: Volume = 52.5

B: Stirring time = 30

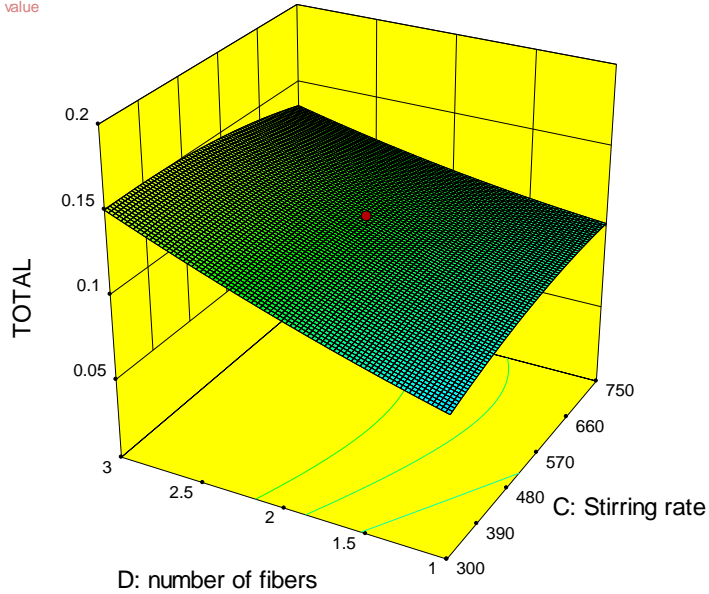


**Figure 36:** Plot of number of fibers- stirring rate

Those findings suggest that the optimal values for the multivariate experiment are:

- sample volume of 70 mL
- stirring rate of 500 rpm
- 3 fibers
- 35 min of stirring

The calibration curve experiments as well as the real sample analyses were conducted under optimal conditions. The mechanisms of interactions between the analytes and the material are explained in section [1.3.7](#). The ionic interactions are governed by the pH. The  $pK_a$  values of most of the analytes are around 7, so at the optimal pH of 7.5 they will be slightly negatively charged. As such, electrostatic Lewis acid-base interactions between a positively charged defect (a spot where the absence of a Ligand reveals a positively charged Fe cavity) are possible. (Perera et al. 2023) The aromatic rings that are present in NH<sub>2</sub>-MIL-88B and the analytes suggest that  $\pi$ - $\pi$  and hydrophobic interactions are possible. Finally, Van der Waals forces and hydrogen bonds contribute to the adsorption as well.

### 3.5 Calibration curves

Calibration curves are plotted as a means of establishing a relationship between the concentration of an analyte and the response of the instrument. By using a series of standard solutions with known concentrations and meticulously subjecting them to the optimized experimental procedure we developed, we calculate the responses received from the PDA detector of the chromatographic system. We use these responses to plot a calibration curve that provides a mathematical function that allows the precise determination of unknown sample concentrations. The areas of the chromatographic peaks were taken in the optimal wavelength of each corresponding analyte. The responses of the benzophenones and 2NP were taken at 285 nm, paraben responses were taken at 254 nm and the 3Me-4NP response was taken at 315 nm. In the following calibration curves the responses for 0.2  $\mu\text{g/mL}$  and 0.08  $\mu\text{g/mL}$  have been excluded for better fit.

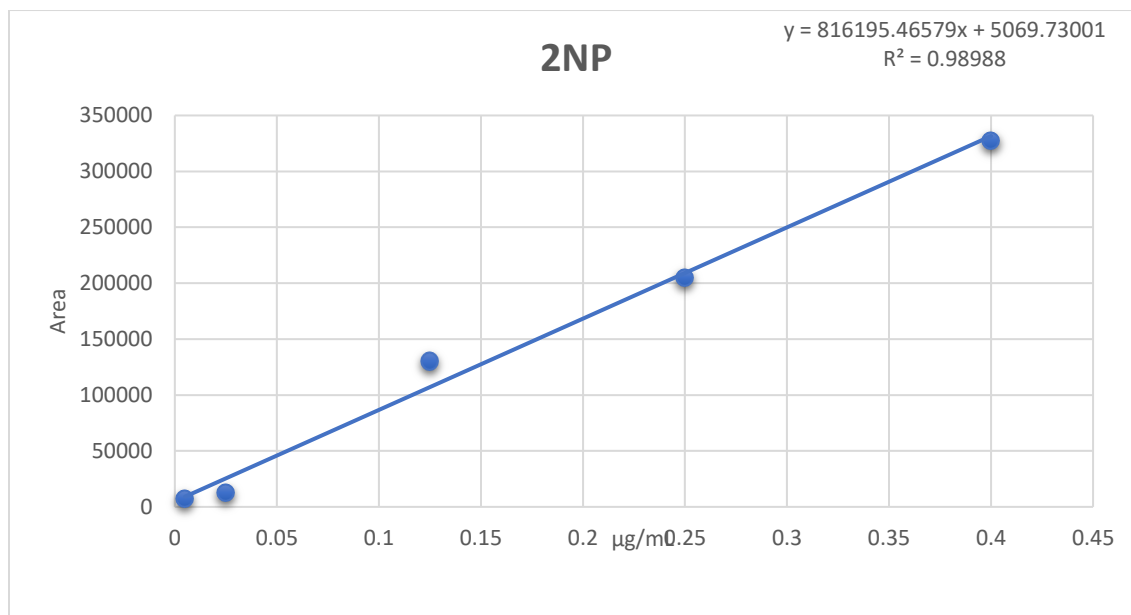


**Figure 37:** Calibration curve for 2NP. The chromatographic areas were received at 285 nm.

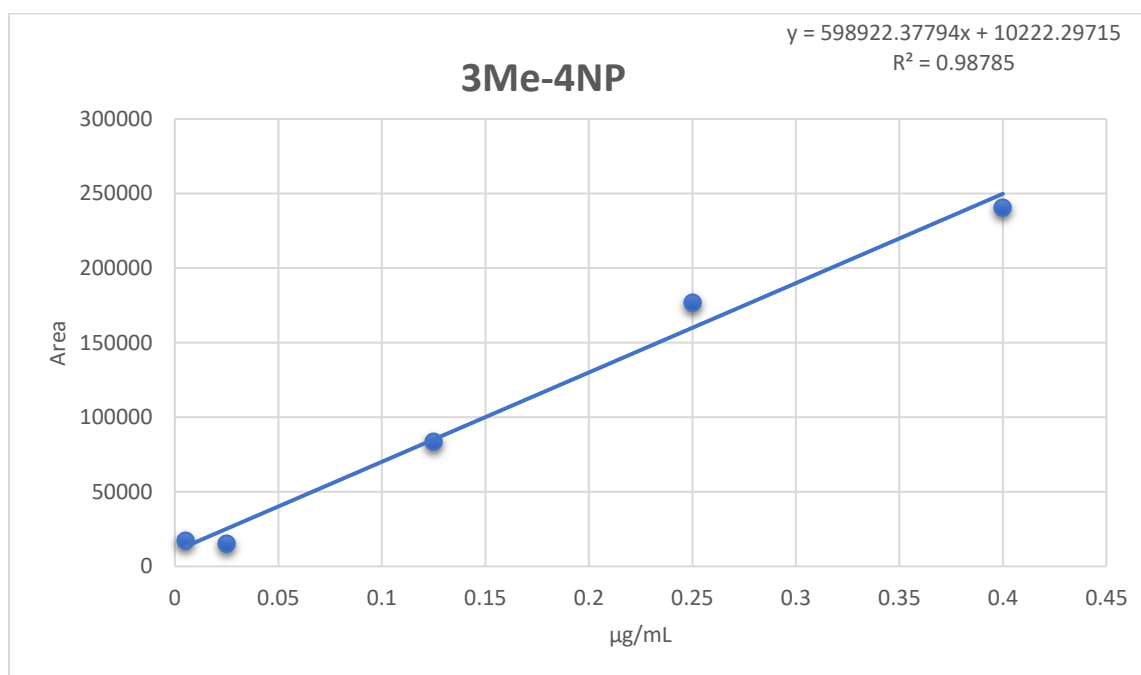


**Figure 38:** Calibration curve for 3Me-4NP. The chromatographic areas were received at 315 nm.

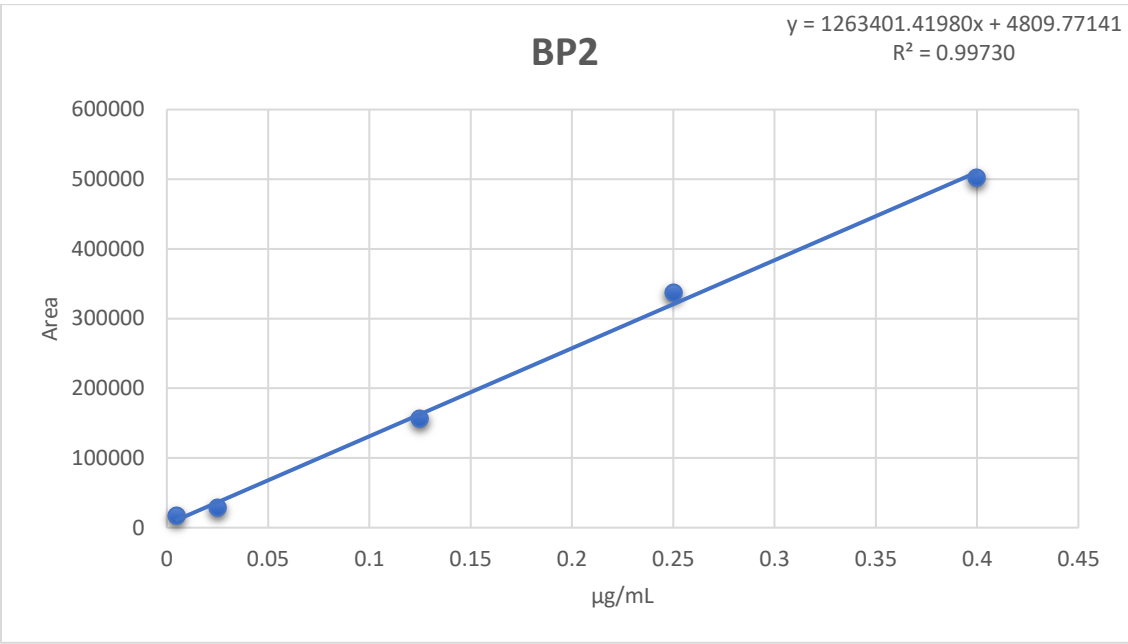


**Figure 39:** Calibration curve for BP2. The chromatographic areas were received at 285 nm.

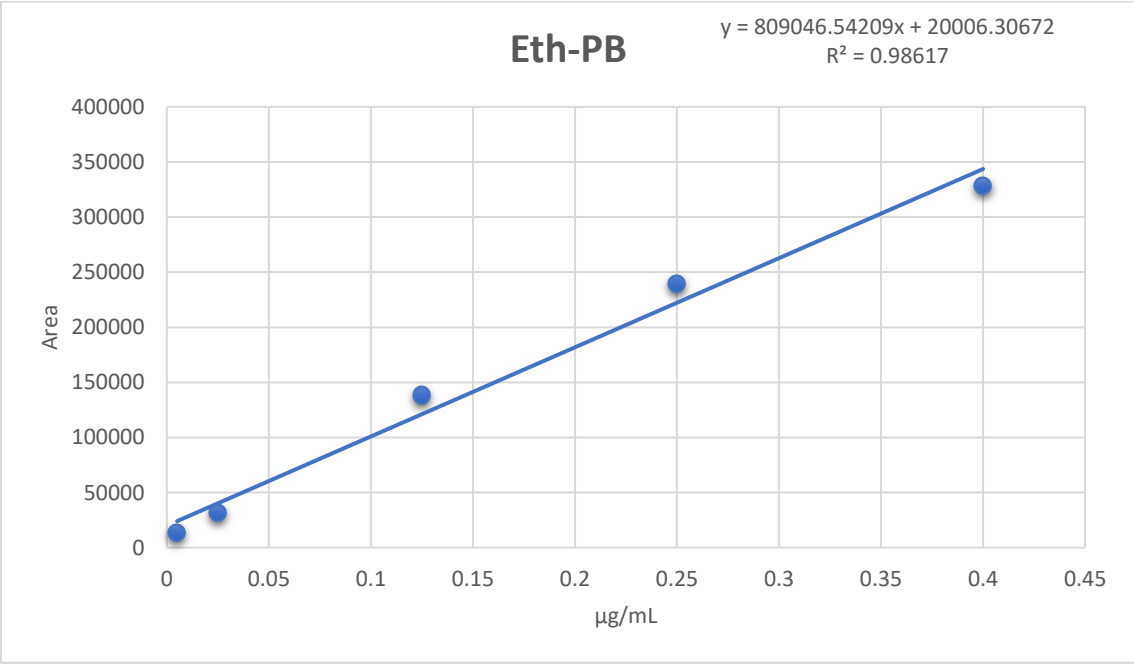


**Figure 40:** Calibration curve for Eth-PB. The chromatographic areas were received at 254 nm.

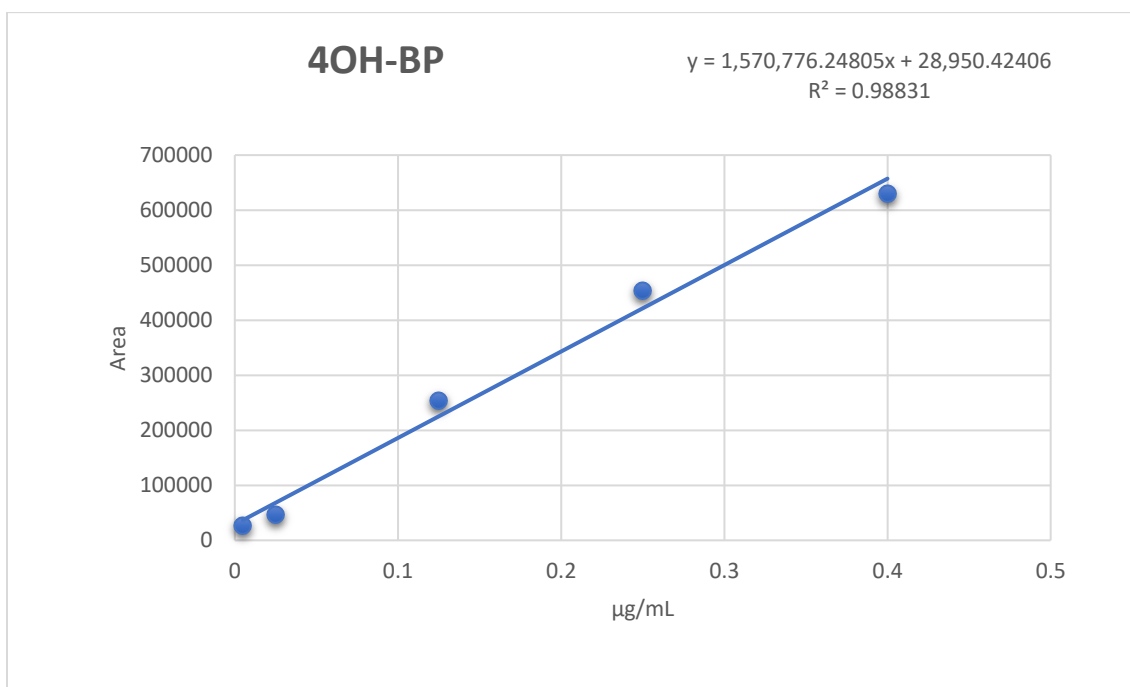


**Figure 41:** Calibration curve for 4OH-BP. The chromatographic areas were received at 285 nm.

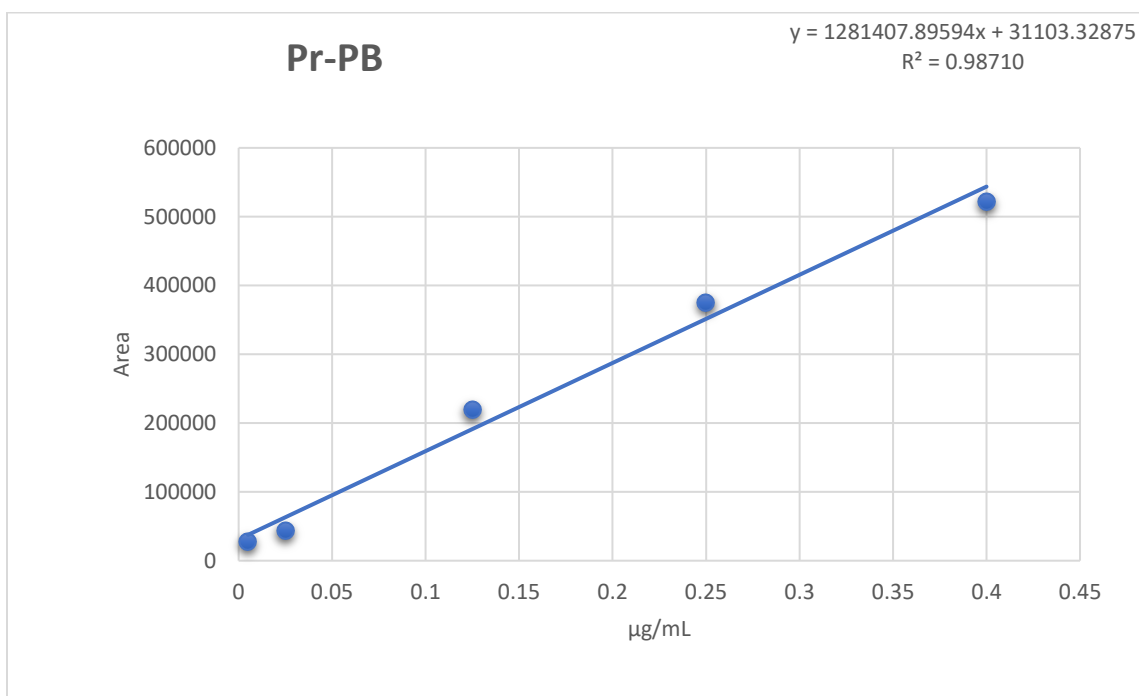


**Figure 42:** Calibration curve for Pr-PB. The chromatographic areas were received at 254 nm.

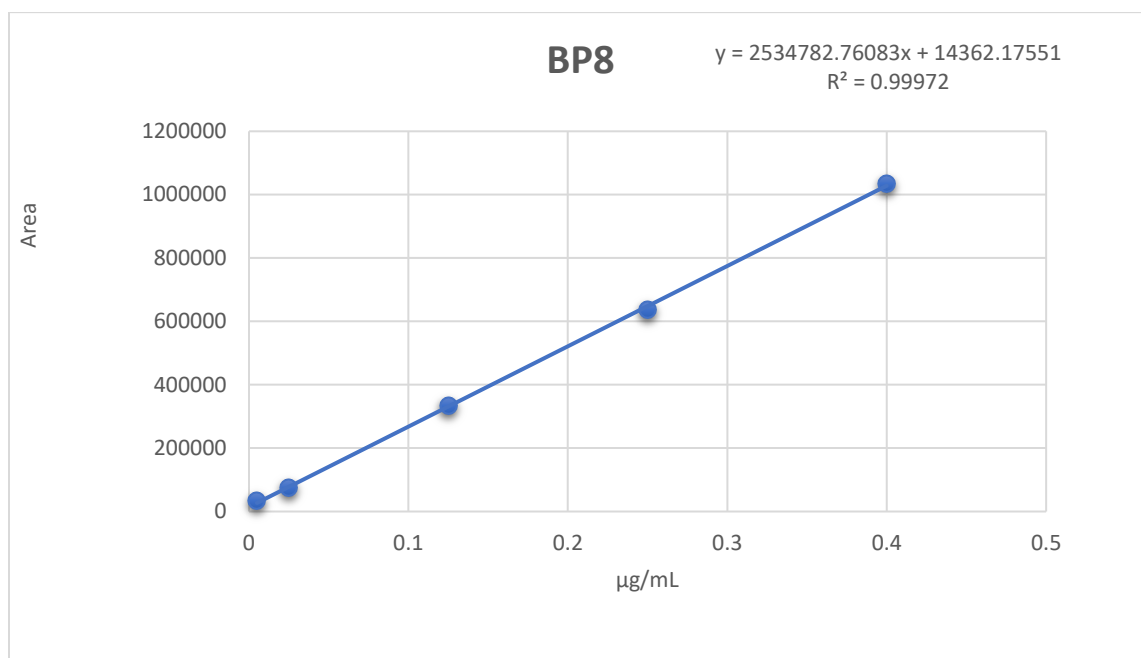


**Figure 43:** Calibration curve for BP8. The chromatographic areas were received at 285 nm.

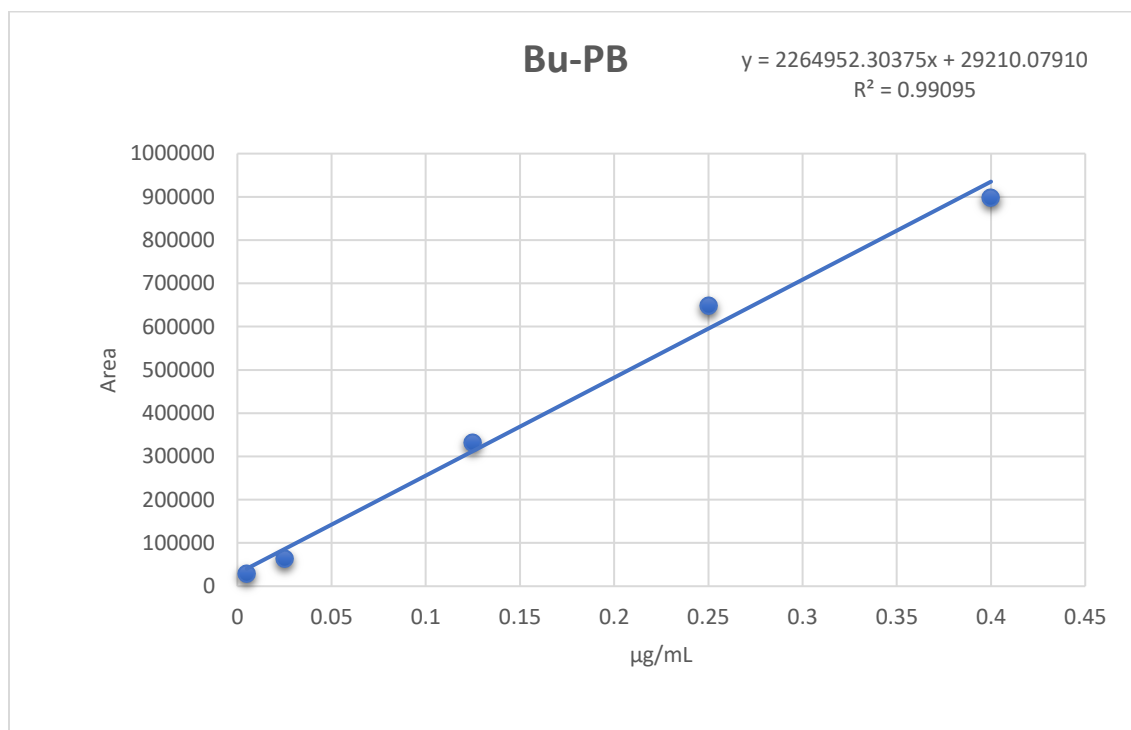


**Figure 44:** Calibration curve for Bu-PB. The chromatographic areas were received at 254 nm.

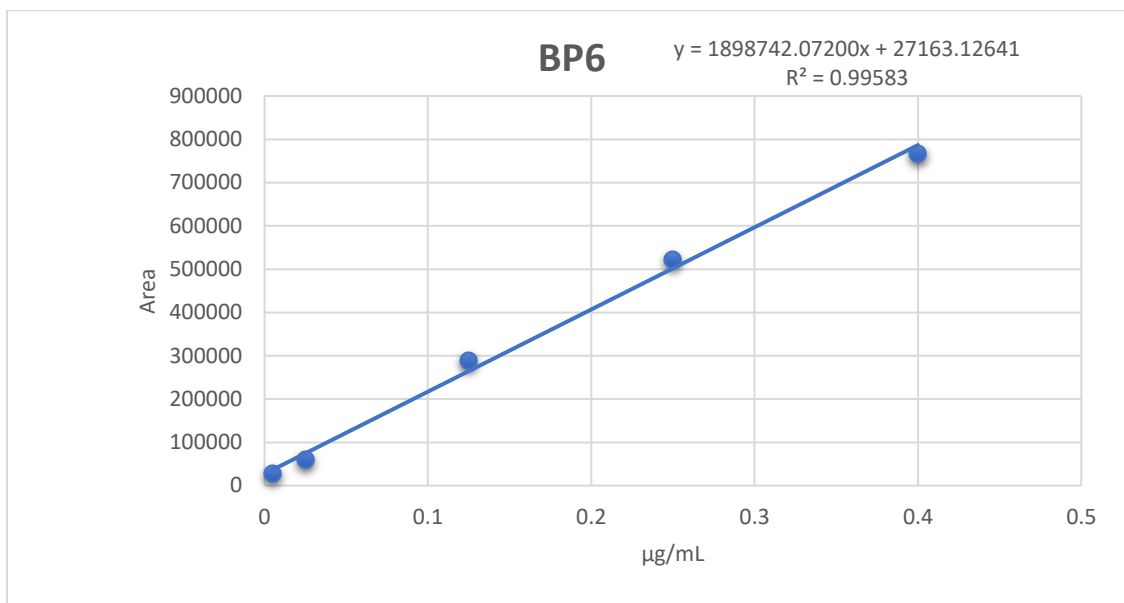


**Figure 45:** Calibration curve for BP6. The chromatographic areas were received at 285 nm.

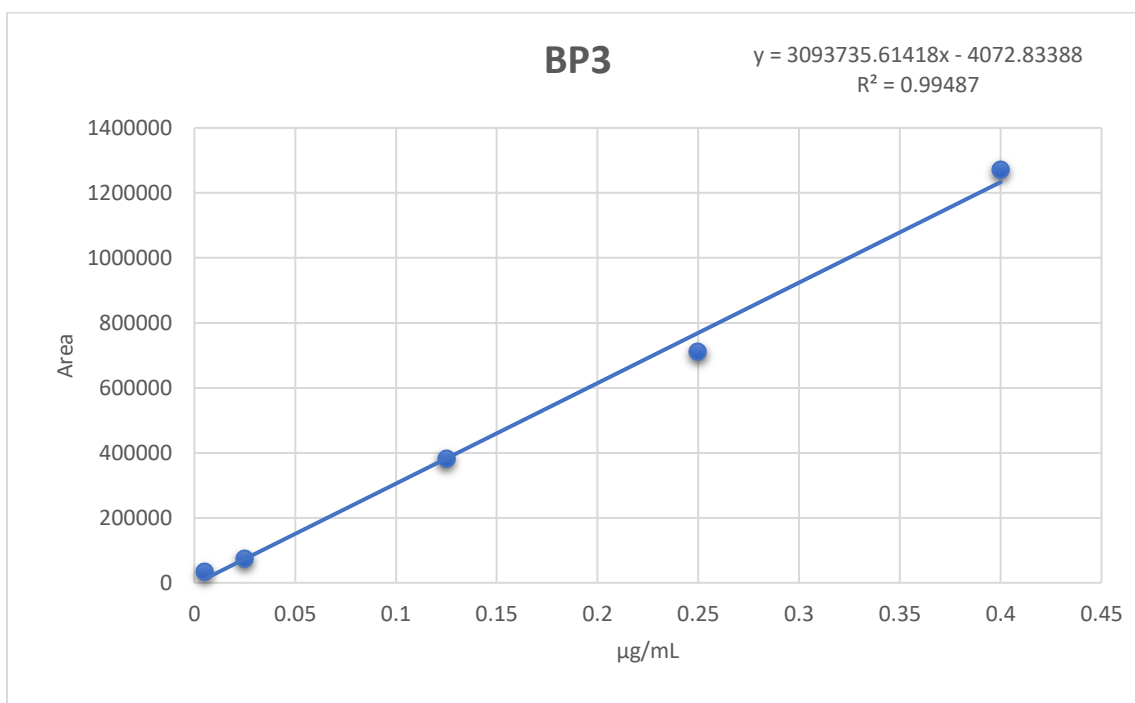


**Figure 46:** Calibration curve for BP. The chromatographic areas were received at 285 nm.

### 3.6 Real sample analysis

Unlike standard solutions, real samples are complex matrices that may contain various interferences, impurities, and co-eluting compounds. Sample treatment methods aim to ensure sufficient sensitivity and maintain selectivity in the extraction and preconcentration, even in complex matrices. In order to validate the applicability of the present analytical methodology, real samples of lake water (taken from Lake Pamvotis, Ioannina, Greece), seawater (taken from Lefkada, Greece), and treated wastewater (taken from the biological treatment plant in Ioannina, Greece). These matrices were spiked with all analytes in question in two concentration levels, 0.025  $\mu\text{g/mL}$  and 0.05  $\mu\text{g/mL}$  and the spiking-recovery results can be seen in **Table 13**.

In **Figure 47** and **Figure 48** we see the chromatograms of the matrices of lakewater, seawater, and treated wastewater superimposed on each other, and compared with a blank and a spiked sample for reference. **Figure 47** depicts the chromatograms taken in 285 nm, where the benzophenones and nitrophenols have the optimal absorption peaks, while **Figure 48** depicts the same chromatograms in 254 nm, the optimal absorption wavelength for parabens. In the case of the lake-water, small peaks of BP2 and 4OH-BP can be identified, while peaks corresponding to BP8, BP6, and BP3 are more clearly present.

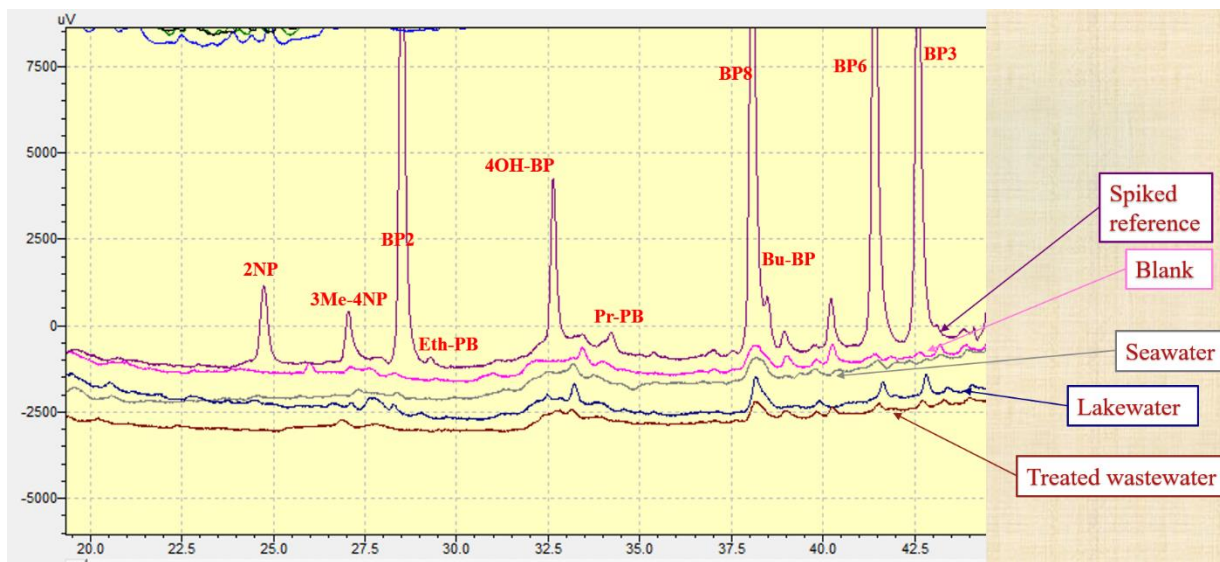


**Figure 47:** Chromatograms of treated lakewater (blue), seawater (grey), and wastewater (brown) at 285 nm superimposed on each other and compared with a blank (pink) and a spiked sample (purple) for reference.

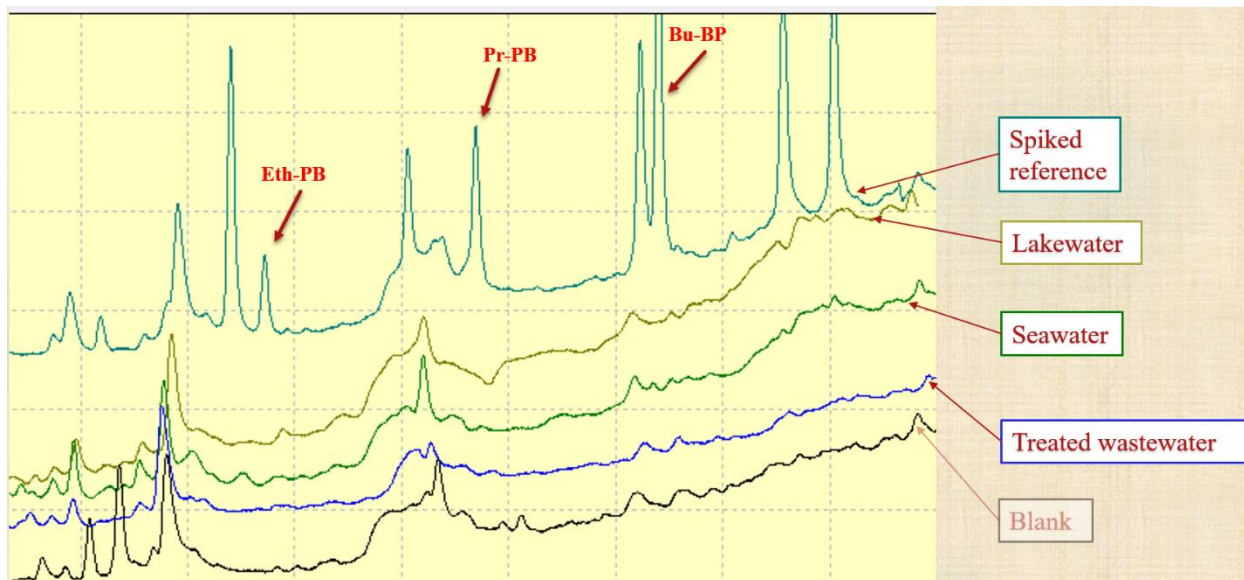


**Figure 48:** Chromatograms of treated lake-water (mustard), seawater (green), and wastewater (blue) at 254 nm superimposed on each other, and compared with a blank (black) and a spiked sample (teal) for reference.

Spiking-recovery tests that were performed in lake-water, seawater, and treated wastewater and the resulting recoveries% can be seen in the **Table 13**. Furthermore, **Table 14** showcases the enrichment factors for all the analytes in question. The enrichment factors were calculated as the ratios of the concentrations of the analytes in the condensed extract (160 $\mu$ L) to the concentration of the initial sample.

**Table 13:** Spiking-recovery tests on the lake-water, seawater, and treated wastewater matrices at two different spiking levels.

		<i>Analyte</i>										
		2NP	3Me- 4NP	BP2	Eth- PB	4OH- BP	Pr- PB	BP8	Bu- PB	BP6	BP3	
<i>Spiking-recoveries (%)</i>	0.025 $\mu$ g/mL	lakewater	70	67	80.3	67.7	65.7	61.7	103	89.0	110.3	111
		Seawater	73.2	69.7	87.3	68	69	62	85	90	93.5	95
	Spiking level	Treated	69	70.5	85	70.2	73.2	61.2	87	88	92.1	95.8
		wastewater										
	0.05 $\mu$ g/mL	lakewater	83	71.2	87	76	77.3	76	115	97	118.1	118.8
		Seawater	79.2	73	88	77.7	73	77.7	99	98.4	99.7	99.5
Spiking level	Treated	75.7	69.9	89	76.9	75	76.9	101.1	99.1	100.1	103	
	wastewater											

**Table 14:** The enrichment factors, calculated as the ratios of the concentrations of the analytes in the condensed extract (160 $\mu$ L) to the concentration of the initial sample.

		<i>Analyte</i>									
		2NP	3Me- 4NP	BP2	Eth- PB	4OH- BP	Pr- PB	BP8	Bu- PB	BP6	BP3
<i>Enrichment factor</i>		183	197	240	227	256	261	357	370	411	405

### 3.7 Other figures of merit

From the chromatograms we calculated the limits of detection of the analytes in question, the highest being 0.003  $\mu\text{g/mL}$  in the case of 2NP and BP2 and lowest being 0.01  $\mu\text{g/mL}$  in the case of BP6 and BP3. The results can be seen in the **Table 15**. The Limits of quantification (LOQ) were calculated as 3 times the LOD. Furthermore, **Table 16** shows the repeatability and reproducibility of the analytical procedure in relative standard deviation%.

**Table 15:** Limits of detection and limits of quantification in  $\mu\text{g/mL}$

	2NP	3Me4NP	BP2	Eth-PB	4OH-BP	Pr-PB	BP8	Bu-PB	BP6	BP3
LOD	0.003	0.0025	0.003	0.0025	0.002	0.0025	0.002	0.002	0.001	0.001
LOQ (3x LOD)	0.009	0.0075	0.009	0.0075	0.006	0.0075	0.006	0.006	0.003	0.003

**Table 16:** Repeatability and reproducibility.

	<i>Analyte</i>									
	2NP	3Me4NP	BP2	Eth-PB	4OH-BP	Pr-PB	BP8	Bu-PB	BP6	BP3
<i>Repeatability (Relative Standard Deviation %)</i>	7.8	6.3	6.5	5	5.2	4.5	4	4.2	3.8	3.1
<i>Reproducibility (Relative Standard Deviation %)</i>	11.1	13.2	10.8	10.1	9.0	10.1	8.9	9.1	8.7	8

### 3.8 Conclusions

This study developed a pretreatment method for target analytes, with ease of use, low cost, and greener practices in mind. Metal organic frameworks, materials that are prevalent in a plethora of applications spanning from drug delivery and the development of sensors to the development of chromatographic columns and extraction devices. An extraction device was developed in our case. The material of choice was a Material of the Institute Lavoisier codenamed NH<sub>2</sub>-MIL-88B, and the study revealed the unique features of the NH<sub>2</sub>-MIL-88B MOF as a promising material that can be utilized as a modification for PPHFs. It resisted removal from their surface even during vigorous stirring in aqueous solutions and was used for extraction in a wide pH range and optimally at initial pH 7.5. The as-prepared NH<sub>2</sub>-MIL-88B PPHFs can be used for on-site adsorption and preconcentration, providing detection of a diverse pool of potentially hazardous analytes. The results show a satisfactory response for all analytes, with BP3 and BP6 particularly noteworthy for achieving the lowest LODs. Potential interfering substances, such as humic acids did not affect the extractability, and tests on three gradually more complex matrices revealed the great applicability for real sample analysis. Further work could be undertaken to extend the applicability of the developed method to other matrices.

### REFERENCES

- Adel M, Yu RB, Quirino JP (2023) Trends in Analytical Chemistry Recent developments in open tubular liquid chromatography and electrochromatography from 2019 e 2021. Trends Anal Chem 164:117045. <https://doi.org/10.1016/j.trac.2023.117045>
- Ahmad R, Wong-Foy AG, Matzger AJ (2009) Microporous coordination polymers as selective sorbents for liquid chromatography. Langmuir 25:11977–11979. <https://doi.org/10.1021/la902276a>
- Alaerts L, Séguin E, Poelman H, et al (2006) Probing the lewis acidity and catalytic activity of the metal-organic framework [Cu<sub>3</sub>(btc)<sub>2</sub>] (BTC = Benzene-1,3,5-tricarboxylate). Chem - A Eur J 12:7353–7363.

<https://doi.org/10.1002/chem.200600220>

Aprea C, Colosio C, Mammone T, et al (2002) Biological monitoring of pesticide exposure: A review of analytical methods. *J Chromatogr B Anal Technol Biomed Life Sci* 769:191–219.

[https://doi.org/10.1016/S1570-0232\(02\)00044-2](https://doi.org/10.1016/S1570-0232(02)00044-2)

Atlanta, GA: U.S. Department of Health and Human Services PHS (2022) Toxicological Profile for Nitrophenols (Draft for Public Comment). Agency Toxic Subst Dis Regist

Azenha MA, Nogueira PJ, Silva AF (2006) Unbreakable solid-phase microextraction fibers obtained by sol-gel deposition on titanium wire. *Anal Chem* 78:2071–2074. <https://doi.org/10.1021/ac0521246>

Balmer ME, Buser HR, Müller MD, Poiger T (2005) Occurrence of some organic UV filters in wastewater, in surface waters, and in fish from Swiss lakes. *Environ Sci Technol* 39:953–962.

<https://doi.org/10.1021/es040055r>

Bauer S, Serre C, Devic T, et al (2008) High-Throughput Assisted Rationalization of the Formation Iron ( III ) Aminoterephthalate Solvothermal System. *Inorg Chem* 9:7568–7576

Bavykina A, Kolobov N, Khan IS, et al (2019) Metal – Organic Frameworks in Heterogeneous Catalysis : Recent Progress , New Trends , and Future Perspectives.

<https://doi.org/10.1021/acs.chemrev.9b00685>

Bello-López MÁ, Ramos-Payán M, Ocaña-González JA, et al (2012) Analytical Applications of Hollow Fiber Liquid Phase Microextraction (HF-LPME): A Review. *Anal Lett* 45:804–830.

<https://doi.org/10.1080/00032719.2012.655676>

Bouaziz L, Si-Ahmed K, Özacar M, et al (2022) Sensor prospect of iodine-doped ZnO materials for ethyl paraben detection. *Microchem J* 183:. <https://doi.org/10.1016/j.microc.2022.108132>

Burtch NC, Jasuja H, Walton KS (2014) Water stability and adsorption in metal-organic frameworks. *Chem Rev* 114:10575–10612. <https://doi.org/10.1021/cr5002589>

Carasek E, Scur R, Bernardi G (2023) Advances in Sample Preparation High-throughput analytical methods employing microextraction techniques : Towards fast analyses lasting a few seconds. *Adv Sample Prep* 8:100095. <https://doi.org/10.1016/j.sampre.2023.100095>

Chatzimitakos T, Vasilas A, Stalikas C (2022) Layered Double Hydroxide/Graphene Quantum Dots as a

- New Sorbent for the Dispersive Solid-Phase Microextraction of Selected Benzophenones, Phenols, and Parabens. *Molecules* 27:. <https://doi.org/10.3390/molecules27238388>
- Chen J-Q, Sharifzadeh Z, Bigdeli F, et al (2023) MOF composites as high potential materials for hazardous organic contaminants removal in aqueous environments. *J Environ Chem Eng* 11:109469. <https://doi.org/10.1016/j.jece.2023.109469>
- Chen M, Lu T, Long L, et al (2022a) NH<sub>2</sub>-Fe-MILs for effective adsorption and Fenton-like degradation of imidacloprid: Removal performance and mechanism investigation. 0–2
- Chen T, Zhao D (2023) Post-synthetic modification of metal-organic framework-based membranes for enhanced molecular separations. *Coord Chem Rev* 491:215259. <https://doi.org/10.1016/j.ccr.2023.215259>
- Chen X, Sun D, Wu W, et al (2022b) Boosting the electrochemical activity of Fe-MIL-101 via acid modulators for highly sensitive detection of o-nitrophenol. *Microchem J* 183:108076. <https://doi.org/10.1016/j.microc.2022.108076>
- Cheng L, Huang K, Cui H, et al (2020) Coiled molecularly imprinted polymer layer open-tubular capillary tube for detection of parabens in personal care and cosmetic products. *Sci Total Environ* 706:135961. <https://doi.org/10.1016/j.scitotenv.2019.135961>
- Daniel M, Mathew G, Anpo M, Neppolian B (2022) MOF based electrochemical sensors for the detection of physiologically relevant biomolecules: An overview. *Coord Chem Rev* 468:214627. <https://doi.org/10.1016/j.ccr.2022.214627>
- Darbre PD, Aljarrah A, Miller WR, et al (2004) Concentrations of Parabens in human breast tumours. *J Appl Toxicol* 24:5–13. <https://doi.org/10.1002/jat.958>
- Davidson PM (2005) Parabens. *Antimicrob Food, Third Ed* 291–303. <https://doi.org/10.2165/00128415-200410160-00047>
- De Decker J, De Clercq J, De Canck E, Van Der Voort P (2015) Metal-Organic Frameworks in the Field of Liquid Adsorption: Recovery of Rare Earths With Functionalized MIL-101(Cr). Elsevier Inc.
- Dhaka S, Kumar R, Deep A, et al (2019) Metal-organic frameworks (MOFs) for the removal of emerging contaminants from aquatic environments. *Coord Chem Rev* 380:330–352. <https://doi.org/10.1016/j.ccr.2018.10.003>

- Díaz-Cruz MS, Barceló D (2009) Chemical analysis and ecotoxicological effects of organic UV-absorbing compounds in aquatic ecosystems. *TrAC - Trends Anal Chem* 28:708–717.  
<https://doi.org/10.1016/j.trac.2009.03.010>
- Dobbins LL, Usenko S, Brain RA, Brooks BW (2009) Probabilistic ecological hazard assessment of parabens using *Daphnia magna* and *Pimephales promelas*. *Environ Toxicol Chem* 28:2744–2753.  
<https://doi.org/10.1897/08-523.1>
- Duan N, Yang W, Wu S, et al (2020) A Visual and Sensitive Detection of *Escherichia coli* Based on Aptamer and Peroxidase-like Mimics of Copper-Metal Organic Framework Nanoparticles. *Food Anal Methods* 13:1433–1441. <https://doi.org/10.1007/s12161-020-01765-9>
- Elghobashy MR, Bebawy LI, Shokry RF, Abbas SS (2016) Successive ratio subtraction coupled with constant multiplication spectrophotometric method for determination of hydroquinone in complex mixture with its degradation products, tretinoin and methyl paraben. *Spectrochim Acta - Part A Mol Biomol Spectrosc* 157:116–123. <https://doi.org/10.1016/j.saa.2015.12.019>
- Elwy HM, Sherif RS, Amer SM, Sedik GA (2020) Modification of carbon paste electrode with MWCNTs and Benzethonium chloride and its application as a novel sensor for determination of Benzophenone-4 in cosmetic preparations. *Int J Electrochem Sci* 15:4308–4325.  
<https://doi.org/10.20964/2020.05.21>
- Fanjul-Bolado P, González-García MB, Costa-García A (2006) Flow screen-printed amperometric detection of p-nitrophenol in alkaline phosphatase-based assays. *Anal Bioanal Chem* 385:1202–1208.  
<https://doi.org/10.1007/s00216-006-0367-8>
- Fatehah MO, Aziz HA, Stoll S (2015) Nanoparticle Properties, Behavior, Fate in Aquatic Systems and Characterization Methods. *J Colloid Sci Biotechnol* 3:111–140. <https://doi.org/10.1166/jcsb.2014.1090>
- Fent K, Zenker A, Rapp M (2010) Widespread occurrence of estrogenic UV-filters in aquatic ecosystems in Switzerland. *Environ Pollut* 158:1817–1824. <https://doi.org/10.1016/j.envpol.2009.11.005>
- Férey C, Mellot-Draznieks C, Serre C, et al (2005) Chemistry: A chromium terephthalate-based solid with unusually large pore volumes and surface area. *Science (80- )* 309:2040–2042.  
<https://doi.org/10.1126/science.1116275>
- Firooz SK, Armstrong DW (2022) *Analytica Chimica Acta Metal-organic frameworks in separations : A*

- review. *Anal Chim Acta* 1234:340208. <https://doi.org/10.1016/j.aca.2022.340208>
- Fonseca J, Gong T, Jiao L, Jiang HL (2021) Metal-organic frameworks (MOFs) beyond crystallinity: amorphous MOFs, MOF liquids and MOF glasses. *J Mater Chem A* 9:10562–10611. <https://doi.org/10.1039/d1ta01043c>
- Fu L, Yang Z, Wang Y, et al (2021) Construction of Metal-Organic Frameworks (MOFs)-Based Membranes and Their Ion Transport Applications. *Small Sci* 1:2000035. <https://doi.org/10.1002/smsc.202000035>
- Furukawa H, Cordova KE, O’Keeffe M, Yaghi OM (2013) The chemistry and applications of metal-organic frameworks. *Science* (80- ) 341:. <https://doi.org/10.1126/science.1230444>
- Gavrila AA, Dasteridis IS, Tzimas AA, et al (2023) Benzophenones in the Environment: Occurrence, Fate and Sample Preparation in the Analysis. *Molecules* 28:. <https://doi.org/10.3390/molecules28031229>
- Ghorbani M, Aghamohammadhassan M, Chamsaz M, et al (2019) Dispersive solid phase microextraction. *TrAC - Trends Anal Chem* 118:793–809. <https://doi.org/10.1016/j.trac.2019.07.012>
- Gu Z, Yang C, Chang NA, Yan X (2011) Metal À Organic Frameworks for Analytical Chemistry : From Sample Collection to. XXX:
- Guo H, Niu B, Wu X, et al (2019) Effective removal of 2,4,6-trinitrophenol over hexagonal metal–organic framework NH<sub>2</sub>-MIL-88B(Fe). *Appl Organomet Chem* 33:1–11. <https://doi.org/10.1002/aoc.4580>
- Hajian A, Ghodsi J, Afraz A, et al (2015) Development of a novel biosensor for nanomolar detection of methylparaben. *Procedia Eng* 120:552–555. <https://doi.org/10.1016/j.proeng.2015.08.714>
- Haman C, Dauchy X, Rosin C, Munoz JF (2015) Occurrence, fate and behavior of parabens in aquatic environments: A review. *Water Res* 68:1–11. <https://doi.org/10.1016/j.watres.2014.09.030>
- Hamisu AM, Ariffin A, Wibowo AC (2020) Cation exchange in metal-organic frameworks (MOFs): The hard-soft acid-base (HSAB) principle appraisal. *Inorganica Chim Acta* 511:119801. <https://doi.org/10.1016/j.ica.2020.119801>
- Han C, Xia B, Chen X, et al (2016) Determination of four paraben-type preservatives and three benzophenone-type ultraviolet light filters in seafoods by LC-QqLIT-MS/MS. *Food Chem* 194:1199–1207. <https://doi.org/10.1016/j.foodchem.2015.08.093>

- Han Y, Wang Y, Zhang H, et al (2023) Facile synthesis of yellow-green fluorescent silicon nanoparticles and their application in detection of nitrophenol isomers. *Talanta* 257:124347.  
<https://doi.org/10.1016/j.talanta.2023.124347>
- Han Y, Zhang S, Wang Z, et al (2018) Toxicological effects of 3-methyl-4-nitrophenol on mouse ovarian and testicular cell proliferation, apoptosis and oocyte maturation. *Reprod Toxicol* 82:94–102.  
<https://doi.org/10.1016/j.reprotox.2018.10.005>
- He J, Yu XY, Yu ZC, et al (2022) Facile fluorescent detection of o-nitrophenol by a cucurbit[8]uril-based supramolecular assembly in aqueous media. *Anal Chim Acta* 1226:340262.  
<https://doi.org/10.1016/j.aca.2022.340262>
- He S, Wu L, Li X, et al (2021) Metal-organic frameworks for advanced drug delivery. 11:.  
<https://doi.org/10.1016/j.apsb.2021.03.019>
- Hostert L, Blanc C, Zarbin AJG, et al (2021) SERS detection and comprehensive study of p-nitrophenol: Towards pesticide sensing. *New J Chem* 45:3886–3891. <https://doi.org/10.1039/d0nj05933a>
- House JE (2013) Composition and Stability of Complexes. *Inorg Chem* 643–664.  
<https://doi.org/10.1016/b978-0-12-385110-9.00019-4>
- Huang YF, Chang JP, Chen HC, Huang YM (2021) Simultaneous trace analysis of 10 benzophenone-type ultraviolet filters in fish through liquid chromatography–tandem mass spectrometry. *Environ Pollut* 286:117306. <https://doi.org/10.1016/j.envpol.2021.117306>
- Huo W, Cai P, Chen M, et al (2016) The relationship between prenatal exposure to BP-3 and Hirschsprung's disease. *Chemosphere* 144:1091–1097.  
<https://doi.org/10.1016/j.chemosphere.2015.09.019>
- Janiak C, Vieth JK (2010) MOFs, MILs and more: Concepts, properties and applications for porous coordination networks (PCNs). *New J Chem* 34:2366–2388. <https://doi.org/10.1039/c0nj00275e>
- Kajal N, Singh V, Gupta R, Gautam S (2022) Metal organic frameworks for electrochemical sensor applications: A review. *Environ Res* 204:112320. <https://doi.org/10.1016/j.envres.2021.112320>
- Kajornkavinkul S, Punrat E, Siangproh W, et al (2016) Graphene/polyvinylpyrrolidone/polyaniline nanocomposite-modified electrode for simultaneous determination of parabens by high performance liquid chromatography. *Talanta* 148:655–660.

<https://doi.org/10.1016/j.talanta.2015.05.044>

Keshta BE, Yu H, Wang L (2023) MIL series-based MOFs as effective adsorbents for removing hazardous organic pollutants from water. *Sep Purif Technol* 322:124301.

<https://doi.org/10.1016/j.seppur.2023.124301>

Kotova AA, Thiebaut D, Vial J, et al (2022) Metal-organic frameworks as stationary phases for chromatography and solid phase extraction: A review. *Coord Chem Rev* 455:214364.

<https://doi.org/10.1016/j.ccr.2021.214364>

Kraševc I, Prosen H (2021) Determination of polar benzotriazoles in aqueous environmental samples by hollow-fibre microextraction method with LC-MS/MS and its comparison to a conventional solid-phase extraction method. *Microchem J* 166:106191. <https://doi.org/10.1016/j.microc.2021.106191>

Lawson HD, Walton SP, Chan C (2021) Metal – Organic Frameworks for Drug Delivery: A Design Perspective. <https://doi.org/10.1021/acsami.1c01089>

Li H, Guan H, Dai H, et al (2012) An amperometric sensor for the determination of benzophenone in food packaging materials based on the electropolymerized molecularly imprinted poly-o-phenylenediamine film. *Talanta* 99:811–815. <https://doi.org/10.1016/j.talanta.2012.07.033>

Li L, Meng T, Zhang W, et al (2020) Selective and colorimetric detection of p-nitrophenol based on inverse opal polymeric photonic crystals. *Polymers (Basel)* 12:. <https://doi.org/10.3390/polym12010083>

Li X, Li C, Suzuki AK, et al (2009) Endocrine disruptive effect of 3-Methyl-4-nitrophenol Isolated from diesel exhaust particles in hershberger assay using castrated immature rats. *Biosci Biotechnol Biochem* 73:2018–2021. <https://doi.org/10.1271/bbb.90204>

Li X, Yu Z, Shao L, et al (2021) Self-cleaning photocatalytic PVDF membrane loaded with NH<sub>2</sub>-MIL-88B/CDs and Graphene oxide for MB separation and degradation. *Opt Mater (Amst)* 119:111368. <https://doi.org/10.1016/j.optmat.2021.111368>

Liang J, Zulki MYB, Choy S, et al (2020) Metal – Organic Framework – Plant Nanobiohybrids as Living Sensors for On-Site Environmental Pollutant Detection. <https://doi.org/10.1021/acs.est.0c04688>

Lin F, Song S, Liu L, et al (2011) Development of the detection of benzophenone in recycled paper packaging materials by ELISA. *Food Agric Immunol* 22:39–46. <https://doi.org/10.1080/09540105.2010.523781>

- Lincho J, Martins RC, Gomes J (2021) Paraben compounds—part i: An overview of their characteristics, detection, and impacts. *Appl Sci* 11:1–38. <https://doi.org/10.3390/app11052307>
- Liu Y, Fan Y, Hou C, et al (2021) Highly Selective Chloromethanes Detection Based on Quartz Crystal Microbalance Gas Sensors with Ba-MOFs. *Inorg Chem* 60:16370–16377. <https://doi.org/10.1021/acs.inorgchem.1c02185>
- Liu Z, Zhou W, Hong Y, et al (2022) Covalent organic framework-V modified porous polypropylene hollow fiber with detachable dumbbell-shaped structure for stir bar sorptive extraction of benzophenones. *J Chromatogr A* 1664:462798. <https://doi.org/10.1016/j.chroma.2021.462798>
- Lord H, Pawliszyn J (2000) Microextraction of drugs. *J Chromatogr A* 902:17–63. [https://doi.org/10.1016/S0021-9673\(00\)00836-0](https://doi.org/10.1016/S0021-9673(00)00836-0)
- Lucas-Sánchez S, Abad-Gil L, Isabel-Cabrera C, et al (2022) Disposable screen-printed carbon-based electrodes in amperometric detection for simultaneous determination of parabens in complex-matrix personal care products by HPLC. *Talanta* 245:. <https://doi.org/10.1016/j.talanta.2022.123459>
- Luo K, Luo X, Wu Y, et al (2023) Synthesis of graphene quantum dots with temperature-sensitive properties from sea rice for rapid and highly selective detection of 4-nitrophenol. *Diam Relat Mater* 135:109849. <https://doi.org/10.1016/j.diamond.2023.109849>
- Luo P, Liu J, Li Y, et al (2012) Voltammetric Determination of Methylparaban in Cosmetics Using a Multi-Wall Carbon Nanotubes/Nafion Composite Modified Glassy Carbon Electrode. *Anal Lett* 45:2445–2454. <https://doi.org/10.1080/00032719.2012.691589>
- Ma B, Lu G, Liu F, et al (2016) Organic UV Filters in the Surface Water of Nanjing, China: Occurrence, Distribution and Ecological Risk Assessment. *Bull Environ Contam Toxicol* 96:530–535. <https://doi.org/10.1007/s00128-015-1725-z>
- Ma M, Noei H, Mienert B, et al (2013) Iron metal-organic frameworks MIL-88B and NH<sub>2</sub>-MIL-88B for the loading and delivery of the gasotransmitter carbon monoxide. *Chem - A Eur J* 19:6785–6790. <https://doi.org/10.1002/chem.201201743>
- Ma Z, Li Y, Lu Z, et al (2023) A novel biosensor-based method for the detection of p-nitrophenol in agricultural soil. *Chemosphere* 313:137306. <https://doi.org/10.1016/j.chemosphere.2022.137306>
- Maceira A, Marcé RM, Borrull F (2020) Analytical methods for determining organic compounds present

- in the particulate matter from outdoor air. *TrAC - Trends Anal Chem* 122:.  
<https://doi.org/10.1016/j.trac.2019.115707>
- Majeed Khorsheed Ahmed A, Salim Khazaal A, Hussain Ahmed A (2016) Spectrophotometric Determination of Methyl Paraben in Pharmaceutical Formulations by Oxidative Coupling Reaction. *Tikrit J Pure Sci* 21:2415–1726
- Mao F, He Y, Gin KYH (2019) Occurrence and fate of benzophenone-type UV filters in aquatic environments: A review. *Environ Sci Water Res Technol* 5:209–223.  
<https://doi.org/10.1039/c8ew00539g>
- Maya F, Palomino Cabello C, Frizzarin RM, et al (2017) Magnetic solid-phase extraction using metal-organic frameworks (MOFs) and their derived carbons. *TrAC - Trends Anal Chem* 90:142–152.  
<https://doi.org/10.1016/j.trac.2017.03.004>
- Mertens F, Tony B, Chemie P, Straße L (2015) Microporous and Mesoporous Materials Two isorecticular pillared-layer frameworks as stationary phases for gas chromatographic applications e Unusual peak broadening in size exclusion chromatography , determination of thermodynamic and kinetic data. 216:82–91. <https://doi.org/10.1016/j.micromeso.2015.03.019>
- Michałowicz J, Duda W (2007) Phenols - Sources and toxicity. *Polish J Environ Stud* 16:347–362
- Min J, Wang B, Hu X (2017) Effect of inoculation of Burkholderia sp. strain SJ98 on bacterial community dynamics and para-nitrophenol, 3-methyl-4-nitrophenol, and 2-chloro-4-nitrophenol degradation in soil. *Sci Rep* 7:1–9. <https://doi.org/10.1038/s41598-017-06436-0>
- Mohan B, Kamboj A, Virender, et al (2023) Metal-organic frameworks (MOFs) materials for pesticides, heavy metals, and drugs removal: Environmental safety. *Sep Purif Technol* 310:123175.  
<https://doi.org/10.1016/j.seppur.2023.123175>
- Muthaiah S, Bhatia A, Kannan M (2020) Stability of Metal Complexes. *Stab Appl Coord Compd* 1–18.  
<https://doi.org/10.5772/intechopen.90894>
- Mutić S, Anojčić J, Vraneš M, et al (2024) Voltammetric determination of organic UV filters by carbon paste electrodes modified with pyridinium-based ionic liquids. *Talanta* 266:.  
<https://doi.org/10.1016/j.talanta.2023.125103>
- Narloch I, Wejnerowska G (2021) An overview of the analytical methods for the determination of organic

- ultraviolet filters in cosmetic products and human samples. *Molecules* 26:  
<https://doi.org/10.3390/molecules26164780>
- Ocaña-González JA, Villar-Navarro M, Ramos-Payán M, et al (2015) New developments in the extraction and determination of parabens in cosmetics and environmental samples. A review. *Anal Chim Acta* 858:1–15. <https://doi.org/10.1016/j.aca.2014.07.002>
- Öhrström L (2015) Let's talk about MOFs—Topology and terminology of metal-organic frameworks and why we need them. *Crystals* 5:154–162. <https://doi.org/10.3390/cryst5010154>
- Okubo T, Yokoyama Y, Kano K, Kano I (2001) ER-dependent estrogenic activity of parabens assessed by proliferation of human breast cancer MCF-7 cells and expression of ER $\alpha$  and PR. *Food Chem Toxicol* 39:1225–1232. [https://doi.org/10.1016/S0278-6915\(01\)00073-4](https://doi.org/10.1016/S0278-6915(01)00073-4)
- Oubahmane M, Mihucz VG, Vasanits A (2023) Recent trends in the determination of organic UV filters by gas chromatography-mass spectrometry in environmental samples. *TrAC - Trends Anal Chem* 161:  
<https://doi.org/10.1016/j.trac.2023.116995>
- Parada H, Gammon MD, Ettore HL, et al (2019) Urinary concentrations of environmental phenols and their associations with breast cancer incidence and mortality following breast cancer. *Environ Int* 130:  
<https://doi.org/10.1016/j.envint.2019.05.084>
- Pastor-Belda M, Sánchez-López MJ, Campillo N, et al (2018) Determination of nitrophenols in environmental samples using stir bar sorptive extraction coupled to thermal desorption gas chromatography-mass spectrometry. *Talanta* 189:543–549.  
<https://doi.org/10.1016/j.talanta.2018.07.043>
- Perera AAPR, Madhushani KAU, Kumar A, Gupta RK (2023) Metal-organic frameworks for wastewater treatment: Recent developments, challenges, and future prospects. *Chemosphere* 139713.  
<https://doi.org/10.1016/J.CHEMOSPHERE.2023.139713>
- Pezhhanfar S, Farajzadeh MA, Mohsen Daraei N, et al (2022) Introduction of an exclusive, highly linear, and matrix-effectless analytical method based on dispersive micro solid phase extraction using MIL-88B(Fe) followed by dispersive liquid–liquid microextraction specialized for the analysis of pesticides in cele. *Microchem J* 183:107967. <https://doi.org/10.1016/j.microc.2022.107967>
- Piao C, Chen L, Wang Y (2014) A review of the extraction and chromatographic determination methods

- for the analysis of parabens. *J Chromatogr B Anal Technol Biomed Life Sci* 969:139–148.  
<https://doi.org/10.1016/j.jchromb.2014.08.015>
- Pramanik B, Sahoo R, Das MC (2023) pH-stable MOFs : Design principles and applications. *Coord Chem Rev* 493:215301. <https://doi.org/10.1016/j.ccr.2023.215301>
- Prapainop K, Mekseriwattana W, Siangproh W, et al (2019) Successive detection of benzoic acid and total parabens in foodstuffs using mercaptosuccinic acid capped cadmium telluride quantum dots. *Food Control* 96:508–516. <https://doi.org/10.1016/j.foodcont.2018.10.009>
- Ricardo IA, Paniagua CES, Alberto EA, et al (2022) A critical review of trends in advanced oxidation processes for the removal of benzophenone-3, fipronil, and propylparaben from aqueous matrices: Pathways and toxicity changes. *J Water Process Eng* 49:. <https://doi.org/10.1016/j.jwpe.2022.102973>
- Saikia M, Bhuyan D, Saikia L (2015) Facile synthesis of Fe<sub>3</sub>O<sub>4</sub> nanoparticles on metal organic framework MIL-101(Cr): Characterization and catalytic activity. *New J Chem* 39:.  
<https://doi.org/10.1039/c4nj01312c>
- Sanganyado E, Kajau TA (2022) The fate of emerging pollutants in aquatic systems: An overview. Elsevier Inc.
- Schlecht C, Klammer H, Jarry H, Wuttke W (2004) Effects of estradiol, benzophenone-2 and benzophenone-3 on the expression pattern of the estrogen receptors (ER) alpha and beta, the estrogen receptor-related receptor 1 (ERR1) and the aryl hydrocarbon receptor (AhR) in adult ovariectomized rats. *Toxicology* 205:123–130. <https://doi.org/10.1016/j.tox.2004.06.044>
- Schlumpf M, Cotton B, Conscience M, et al (2001) In vitro and in vivo estrogenicity of UV screens. *Environ Health Perspect* 109:239–244. <https://doi.org/10.1289/ehp.01109239>
- Seidlová-Wuttke D, Jarry H, Wuttke W (2004) Pure estrogenic effect of benzophenone-2 (BP2) but not of bisphenol a (BPA) and dibutylphthalate (DBP) in uterus, vagina and bone. *Toxicology* 205:103–112.  
<https://doi.org/10.1016/j.tox.2004.06.042>
- Services H (2002) Toxicological Profile for Nitrophenols. ATSDR's Toxicol Profiles.  
[https://doi.org/10.1201/9781420061888\\_ch125](https://doi.org/10.1201/9781420061888_ch125)
- Sethunathan N (1973) Degradation of Parathion in Flooded Acid Soils. *J Agric Food Chem* 21:602–604.  
<https://doi.org/10.1021/jf60188a042>

- Shubhangi, Nandi I, Rai SK, Chandra P (2024) MOF-based nanocomposites as transduction matrices for optical and electrochemical sensing. *Talanta* 266:125124. <https://doi.org/10.1016/j.talanta.2023.125124>
- Si T, Lu X, Zhang H, et al (2022) Metal-organic framework-based core-shell composites for chromatographic stationary phases. *TrAC - Trends Anal Chem* 149:116545. <https://doi.org/10.1016/j.trac.2022.116545>
- Soysal M (2021) An Electrochemical Sensor Based on Molecularly Imprinted Polymer for Methyl Paraben Recognition and Detection. *J Anal Chem* 76:381–389. <https://doi.org/10.1134/S1061934821030114>
- Sun H, Cong S, Zheng Z, et al (2018a) Metal–Organic Frameworks as Surface Enhanced Raman Scattering Substrates with High Tailorability. *J Am Chem Soc* 141:870–878. <https://doi.org/10.1021/jacs.8b09414>
- Sun X, Jiao X yue, Li J, Xu L (2018b) A miniaturized sorbent phase-based extraction device in the form of syringe filter holder using molecularly imprinted polymer as sorbent and its application to extract benzophenones. *J Chromatogr A* 1543:1–13. <https://doi.org/10.1016/j.chroma.2018.02.039>
- Tanaka M, Takano H, Fujitani Y, et al (2013) Effects of exposure to nanoparticle-rich diesel exhaust on 8-OHdG synthesis in the mouse asthmatic lung. *Exp Ther Med* 6:703–706. <https://doi.org/10.3892/etm.2013.1198>
- Tang Y, Yin M, Yang W, et al (2019) Emerging pollutants in water environment: Occurrence, monitoring, fate, and risk assessment. *Water Environ Res* 91:984–991. <https://doi.org/10.1002/wer.1163>
- Tran LT, Dang HTM, Tran H V., et al (2023a) MIL-88B(Fe)-NH<sub>2</sub>: an amine-functionalized metal-organic framework for application in a sensitive electrochemical sensor for Cd<sup>2+</sup>, Pb<sup>2+</sup>, and Cu<sup>2+</sup> ion detection. *RSC Adv* 13:21861–21872. <https://doi.org/10.1039/d3ra02828c>
- Tran LT, Dang HTM, Tran H V, et al (2023b) MIL-88B(Fe)-NH<sub>2</sub>: an amine-functionalized metal–organic framework for application in a sensitive electrochemical sensor for Cd<sup>2+</sup>, Pb<sup>2+</sup>, and Cu<sup>2+</sup> ion detection. 21861–21872. <https://doi.org/10.1039/d3ra02828c>
- Uflyand IE, Zhinzhilo VA, Nikolaevskaya VO, et al (2021) Recent strategies to improve MOF performance in solid phase extraction of organic dyes. *Microchem J* 168:. <https://doi.org/10.1016/j.microc.2021.106387>
- Ullah S, Bustam MA, Assiri MA, et al (2019) Synthesis, and characterization of metal-organic frameworks -177 for static and dynamic adsorption behavior of CO<sub>2</sub> and CH<sub>4</sub>. *Microporous Mesoporous Mater*

288:109569. <https://doi.org/10.1016/j.micromeso.2019.109569>

Vale F, Sousa CA, Sousa H, et al (2022) Parabens as emerging contaminants: Environmental persistence, current practices and treatment processes. *J Clean Prod* 347:.

<https://doi.org/10.1016/j.jclepro.2022.131244>

Vuckovic D (2013) microextraction in multi-well-plate format. *Trends Anal Chem* 45:136–153.

<https://doi.org/10.1016/j.trac.2013.01.004>

W. Zhang, A. Bu , Q. Ji , L. Min, S. Zhao, Y. Wang JC (2019) - Directed Incorporation of Phosphonates into MOF-808 via Ligand Exchange: Stability and Adsorption Properties for Uranium. *Technol Desalin Technol New Energy*. <https://doi.org/10.1021/acsami.9b10920>

Wang C, Liu X, Keser Demir N, et al (2016) Applications of water stable metal-organic frameworks. *Chem Soc Rev* 45:5107–5134. <https://doi.org/10.1039/c6cs00362a>

Wang C, Luan J, Wu C (2019a) Metal-organic frameworks for aquatic arsenic removal. *Water Res* 158:370–382. <https://doi.org/10.1016/j.watres.2019.04.043>

Wang K, Tan L, Zhang Y, et al (2023a) A molecular imprinted fluorescence sensor based on carbon quantum dots for selective detection of 4-nitrophenol in aqueous environments. *Mar Pollut Bull* 187:114587. <https://doi.org/10.1016/j.marpolbul.2023.114587>

Wang L, Li X, Yang B, et al (2022) The chemical stability of metal-organic frameworks in water treatments: Fundamentals, effect of water matrix and judging methods. *Chem Eng J* 450:138215. <https://doi.org/10.1016/j.cej.2022.138215>

Wang Q, Chen L, Cui X, et al (2023b) Determination of trace bisphenols in milk based on Fe<sub>3</sub>O<sub>4</sub>@NH<sub>2</sub>-MIL-88(Fe)@TpPa magnetic solid-phase extraction coupled with HPLC. *Talanta* 256:124268. <https://doi.org/10.1016/j.talanta.2023.124268>

Wang X, Chen X, Alcântara CCJ, et al (2019b) MOFBOTS : Metal – Organic-Framework-Based Biomedical Microrobots. 1901592:2–8. <https://doi.org/10.1002/adma.201901592>

Wejnerowska G, Narloch I (2021) Determination of benzophenones in water and cosmetics samples: A comparison of solid-phase extraction and microextraction by packed sorbent methods. *Molecules* 26:.. <https://doi.org/10.3390/molecules26226896>

- Wen J, Fang Y, Zeng G (2018) Progress and prospect of adsorptive removal of heavy metal ions from aqueous solution using metal–organic frameworks: A review of studies from the last decade. *Chemosphere* 201:627–643. <https://doi.org/10.1016/j.chemosphere.2018.03.047>
- Wu YY, Yang CX, Yan XP (2014) Fabrication of metal-organic framework MIL-88B films on stainless steel fibers for solid-phase microextraction of polychlorinated biphenyls. *J Chromatogr A* 1334:1–8. <https://doi.org/10.1016/j.chroma.2014.01.079>
- Xin T, Chen M, Liu Z, et al (2023) Highly efficient separation of glucose and fructose by pore exclusion of zirconium-based metal – organic frameworks isomers. *Sep Purif Technol* 319:124038. <https://doi.org/10.1016/j.seppur.2023.124038>
- Yang L, Ma S, Wan Y, et al (2016) In vitro effect of 4-pentylphenol and 3-methyl-4-nitrophenol on murine splenic lymphocyte populations and cytokine/granzyme production. *J Immunotoxicol* 13:548–556. <https://doi.org/10.3109/1547691X.2016.1140853>
- Yang Y, Chen J, Shi YP (2015) Recent developments in modifying polypropylene hollow fibers for sample preparation. *TrAC - Trends Anal Chem* 64:109–117. <https://doi.org/10.1016/j.trac.2014.08.016>
- You Y, Li SN, Zou J, et al (2023) Ultrasonic-assisted self-assembly of a neodymium vanadate and hydroxylated multi-walled carbon nanotubes composite for electrochemical detection of p-nitrophenol. *Process Saf Environ Prot* 175:834–844. <https://doi.org/10.1016/j.psep.2023.05.092>
- Yuan R, Yue C, Qiu J, et al (2019) Highly efficient sunlight-driven reduction of Cr(VI) by TiO<sub>2</sub>@NH<sub>2</sub>-MIL-88B(Fe) heterostructures under neutral conditions. *Appl Catal B Environ* 251:229–239. <https://doi.org/10.1016/j.apcatb.2019.03.068>
- Yücebaşı BB, Yaman YT, Bolat G, et al (2020) Molecular imprinted polymer based electrochemical sensor for selective detection of paraben. *Sensors Actuators, B Chem* 305:. <https://doi.org/10.1016/j.snb.2019.127368>
- Zang X, Chang Q, Li H, et al (2023) Construction of a ringent multi-shelled hollow MIL-88B as the solid-phase microextraction fiber coating for the extraction of organochlorine pesticides. *Sep Purif Technol* 304:122350. <https://doi.org/10.1016/j.seppur.2022.122350>
- Zayed SMAD, Mahdy F (2008) Decomposition of 14C-fenitrothion under the influence of UV and sunlight under tropical and subtropical conditions. *Chemosphere* 70:1653–1659.

<https://doi.org/10.1016/j.chemosphere.2007.07.063>

Zhang H, Hu X, Li T, et al (2022a) MIL series of metal organic frameworks (MOFs) as novel adsorbents for heavy metals in water: A review. *J Hazard Mater* 429:128271.

<https://doi.org/10.1016/j.jhazmat.2022.128271>

Zhang S, Yang Q, Li Z, et al (2018) Solid phase microextraction of phthalic acid esters from vegetable oils using iron (III)-based metal-organic framework/graphene oxide coating. *Food Chem* 263:258–264.

<https://doi.org/10.1016/j.foodchem.2018.04.132>

Zhang X, Li X, Ding T, et al (2023) Post-synthetic functionalization of Zn-CP by Tb<sup>3+</sup> ions: a ratiometric luminescent sensor for the ultraviolet filter benzophenone. *Dalt Trans* 52:.

<https://doi.org/10.1039/d3dt00392b>

Zhang YB, Furukawa H, Ko N, et al (2015) Introduction of functionality, selection of topology, and enhancement of gas adsorption in multivariate metal-organic framework-177. *J Am Chem Soc* 137:2641–2650.

<https://doi.org/10.1021/ja512311a>

Zhang Z, Yu Y, Xi H, Zhou Y (2022b) Inhibitory effect of individual and mixtures of nitrophenols on anaerobic toxicity assay of anaerobic systems: Metabolism and evaluation modeling. *J Environ Manage* 304:114237.

<https://doi.org/10.1016/j.jenvman.2021.114237>

Zhou YN, Zhao SJ, Leng WX, et al (2023) Dual-Functional Eu-Metal-Organic Framework with Ratiometric Fluorescent Broad-Spectrum Sensing of Benzophenone-like Ultraviolet Filters and High Proton

Conduction. *Inorg Chem* 62:12730–12740. <https://doi.org/10.1021/acs.inorgchem.3c01224>

Zhu W, Xiang G, Shang J, et al (2018) Versatile Surface Functionalization of Metal–Organic Frameworks through Direct Metal Coordination with a Phenolic Lipid Enables Diverse Applications. *Adv Funct Mater* 28:1–12.

<https://doi.org/10.1002/adfm.201705274>